

University of Kentucky

UKnowledge

---

Theses and Dissertations--Electrical and  
Computer Engineering

Electrical and Computer Engineering

---

2024

## Optimal Control and Evaluation of Shipboard Power Systems

Musharrat Sabah

*University of Kentucky*, [musharrat.sabah@gmail.com](mailto:musharrat.sabah@gmail.com)

Author ORCID Identifier:

<https://orcid.org/0009-0009-5749-0366>

Digital Object Identifier: <https://doi.org/10.13023/etd.2024.279>

[Right click to open a feedback form in a new tab to let us know how this document benefits you.](#)

### Recommended Citation

Sabah, Musharrat, "Optimal Control and Evaluation of Shipboard Power Systems" (2024). *Theses and Dissertations--Electrical and Computer Engineering*. 205.

[https://uknowledge.uky.edu/ece\\_etds/205](https://uknowledge.uky.edu/ece_etds/205)

This Doctoral Dissertation is brought to you for free and open access by the Electrical and Computer Engineering at UKnowledge. It has been accepted for inclusion in Theses and Dissertations--Electrical and Computer Engineering by an authorized administrator of UKnowledge. For more information, please contact [UKnowledge@lsv.uky.edu](mailto:UKnowledge@lsv.uky.edu), [rs\\_kbnotifs-acl@uky.edu](mailto:rs_kbnotifs-acl@uky.edu).

## **STUDENT AGREEMENT:**

I represent that my thesis or dissertation and abstract are my original work. Proper attribution has been given to all outside sources. I understand that I am solely responsible for obtaining any needed copyright permissions. I have obtained needed written permission statement(s) from the owner(s) of each third-party copyrighted matter to be included in my work, allowing electronic distribution (if such use is not permitted by the fair use doctrine) which will be submitted to UKnowledge as Additional File.

I hereby grant to The University of Kentucky and its agents the irrevocable, non-exclusive, and royalty-free license to archive and make accessible my work in whole or in part in all forms of media, now or hereafter known. I agree that the document mentioned above may be made available immediately for worldwide access unless an embargo applies.

I retain all other ownership rights to the copyright of my work. I also retain the right to use in future works (such as articles or books) all or part of my work. I understand that I am free to register the copyright to my work.

## **REVIEW, APPROVAL AND ACCEPTANCE**

The document mentioned above has been reviewed and accepted by the student's advisor, on behalf of the advisory committee, and by the Director of Graduate Studies (DGS), on behalf of the program; we verify that this is the final, approved version of the student's thesis including all changes required by the advisory committee. The undersigned agree to abide by the statements above.

Musharrat Sabah, Student

Aaron M. Cramer, Major Professor

Daniel Lau, Director of Graduate Studies

OPTIMAL CONTROL AND EVALUATION OF SHIPBOARD POWER  
SYSTEMS

---

DISSERTATION

---

A dissertation submitted in partial  
fulfillment of the requirements for  
the degree of Doctor of Philosophy  
in the College of Engineering at the  
University of Kentucky

By  
Musharrat Sabah  
Lexington, Kentucky

Director: Dr. Aaron M. Cramer, Professor of Electrical and Computer Engineering  
Lexington, Kentucky 2024

Copyright© Musharrat Sabah 2024

## ABSTRACT OF DISSERTATION

### OPTIMAL CONTROL AND EVALUATION OF SHIPBOARD POWER SYSTEMS

Electric warships are involved in complex missions consisting of multiple simultaneous operations. In order to ensure mission success, future ships must be designed in a way that optimizes their performance in the presence of complex mission loads. The focus of this research is an effort to optimally control the performance of shipboard systems during missions involving multiple scenarios or vignettes. The evaluation of the performance of mission-oriented power systems is based on the degree to which these systems deliver power to the loads required to perform the mission at hand. The performance of such systems involves a dynamic interplay between the power systems, the mission, and the loads required to perform the mission. Evaluating the performance is fundamental in the design of such systems for future use, and this evaluation is advanced by formulating the evaluation as an optimal control problem. This formulation allows the dynamic interaction between the system and the mission to be considered directly and is a natural evolution of existing simulation-based methods. In this work, the proposed approach is demonstrated using a notional, but representative, set of system implementations and missions. Furthermore, examples of the types of system trade offs that can be considered using this approach are presented and discussed. In addition, the optimal control problem can be implemented using market-based control. Market-based control is an approach which can be used when the system becomes difficult to control and maintain using centralized approaches such as Markov decision process-based optimization. A key feature of market-based control is that it reduces a global optimization problem into a series of smaller local optimization problems (i.e., profit maximization) combined with finding the market clearing prices that result in market equilibrium (i.e., quantity supplied is equal to quantity demanded). The market clearing price is the price which results in an equilibrium between demanded and supplied resources. Finding the globally coordinating market-clearing prices is a root-finding problem. It is known that under sufficient conditions the market-clearing problem is equivalent to solving the global optimization problem. To enable market-based control of such systems, it is necessary that appropriate market-clearing algorithms exist that can locate the market-clearing prices that allow the system to operate at equilibrium. This work



examines the numerical challenges of solving the root-finding problem of finding the market-clearing prices using traditional algorithms. A method has been proposed for solving the market clearing problem and its performance has been compared with the performances of traditional root-finding algorithms. Finally, the connection between various optimization approaches has been explored and validated with results.

KEYWORDS: Operability, mission, Markov decision process, market-based control, price, dynamic programming, simulation

Author's signature: Musharrat Sabah

Date: July 29, 2024

OPTIMAL CONTROL AND EVALUATION OF SHIPBOARD POWER  
SYSTEMS

By  
Musharrat Sabah

Director of Dissertation: Aaron M. Cramer

Director of Graduate Studies: Daniel Lau

Date: July 29, 2024

## ACKNOWLEDGMENTS

The years I have dedicated to my Ph.D. have been immensely rewarding and enlightening. I have received profound support, guidance, encouragement, and love, which has inspired me to be more thankful and humble about my position in life.

This dissertation owes its primary scholarly debt to my advisor, Dr. Aaron Cramer, whose enthusiasm and encouragement were instrumental in completing this project. Thank you very much for your patience, calm demeanor, and guidance.

I wish to acknowledge the support of my research from the Office of Naval Research (ONR) of the United States Navy through research grants N00014-20-1-2816 and N00014-23-1-2824. Special thanks to the program officers, Mr. Joseph Borraccini and Mr. Nathan Spivey. Their support and sponsorship have been crucial in completing my research work.

I am deeply grateful to my committee members, Dr. Yuan Liao, Dr. Jiangbiao He and Dr. Joseph Sottile, and outside examiner, Dr. David Murrugarra, for their insightful feedback, constructive criticism, and invaluable suggestions, which have enriched the quality of this research. I am incredibly thankful to the Department of Electrical and Computer Engineering for supporting me throughout my time here.

I extend my gratitude to my former colleagues, Dr. Isuje Ojo and Dr. Pranoy Roy, for their guidance, support, and encouragement. Additionally, I am thankful to all my other colleagues in the Power and Energy Lab for creating a strong and supportive community, which made this journey less challenging.

I would like to thank my Bangladeshi community in Lexington (Bangladeshi Student Association), who made this place feel remarkably close to home. Without their support, company, and love, this life-changing journey would not have felt as seamless

and comfortable. I also thank my extended family in the United States for guiding me, warmly welcoming me, and taking care of my needs.

I am deeply grateful to all my teachers, starting from preschool all the way to graduate school, for playing a vital role in this ‘almost’ lifelong journey of being a student. Thank you very much for shaping me into who I am today. I express my heartfelt appreciation to my extended family members in Bangladesh, particularly my paternal aunts, for their love, motivation, and prayers. Thanks to my friends, particularly ‘SaMuSaZ’ for supporting me in various ways, offering encouragement, sharing ideas, and providing much-needed laughter along the way.

Lastly, and most importantly, I owe a debt of gratitude to my father, Dr. Sabah Uddin Ahmed, my mother, Dr. Maherun Nessa, and my sister, Dr. Munjarin Sabah. Despite their own hardships, they have constantly given me strength, motivation, and prayers, ensuring I stayed focused on my goals throughout this challenging journey. My parents deserve a special credit for always believing in me and supporting my decisions. I would never have been even close to where I am if I did not have the support and encouragement from them. Thanks to my husband, Al Mazedur Rahman, for providing me with valuable suggestions, guiding me through the transition to professional life, encouraging me, and understanding me. I hope I would be able to give you the same support and motivation as you embark towards the finish line of your Ph.D. journey.

This dissertation is a culmination of the collective efforts, support, and encouragement of all those who have crossed my path. While their names may not all be mentioned here, their contributions are deeply appreciated and will forever be cherished. Thank you all.

## TABLE OF CONTENTS

Acknowledgments . . . . .	iii
Table of Contents . . . . .	v
List of Figures . . . . .	viii
List of Tables . . . . .	xiv
Chapter 1 Introduction . . . . .	1
1.1 Introduction . . . . .	1
1.2 Contributions of the Dissertation . . . . .	3
1.3 Organization of the Dissertation . . . . .	3
Chapter 2 Background and Literature Review . . . . .	5
2.1 Introduction . . . . .	5
2.2 Overview of Various Metrics . . . . .	5
2.3 Operability Metric . . . . .	6
2.4 Beginnings of Operability as a Performance Metric . . . . .	7
2.5 Evolution of Operability . . . . .	8
2.6 Markov Chains . . . . .	9
2.7 Markov Decision Process . . . . .	10
2.8 Value Function Iteration . . . . .	10
2.9 Conclusion . . . . .	11
Chapter 3 Optimal Control-Based Performance Evaluation . . . . .	12
3.1 Introduction . . . . .	12
3.2 Current State of Operability . . . . .	12
3.3 State of Optimal Control-based Evaluation using MDP . . . . .	12
3.4 Notional Problem . . . . .	13
3.4.1 Mission 1 . . . . .	14
3.4.2 Mission 2 . . . . .	16
3.4.3 Mission 3 . . . . .	17
3.4.4 Aggregate Mission Performance . . . . .	17
3.4.5 System State . . . . .	18
3.5 Results . . . . .	18
3.5.1 System 1 (Shared) . . . . .	18
3.5.2 System 2 (Dedicated) . . . . .	18
3.5.3 System 3 (Distributed) . . . . .	19
3.5.4 Comparison of Systems . . . . .	19
3.6 Conclusion . . . . .	21

Chapter 4	Optimal Control-Based Performance Evaluation in the Presence of Energy Magazines . . . . .	23
4.1	Introduction . . . . .	23
4.2	System Description . . . . .	24
4.3	Operability Formulation . . . . .	26
4.4	Mission Scenario . . . . .	26
4.4.1	Fixed-Duration Model . . . . .	27
4.4.2	Probabilistic Model . . . . .	28
4.5	Solution Algorithm . . . . .	29
4.6	Results and Discussion . . . . .	30
4.6.1	Relationship between Operability and Value Function . . . . .	30
4.6.2	Results for the Two Models . . . . .	31
4.7	Conclusion . . . . .	33
Chapter 5	Robust Optimal Control-Based Evaluation Considering System Trade-offs . . . . .	35
5.1	Introduction . . . . .	35
5.2	Problem Formulation . . . . .	37
5.3	Notional System And Missions . . . . .	37
5.3.1	Mission 1 (Search and Destroy) . . . . .	38
5.3.2	Mission 2 (Contested Transit) . . . . .	40
5.3.3	Mission 3 (Fight or Flight) . . . . .	42
5.4	System Implementations . . . . .	43
5.4.1	System 1 (Shared) . . . . .	43
5.4.2	System 2 (Dedicated) . . . . .	44
5.4.3	System 3 (Distributed) . . . . .	45
5.5	Solution Algorithm . . . . .	46
5.6	Results and Discussion . . . . .	47
5.6.1	Problem Solutions . . . . .	48
5.6.2	Overall Performance . . . . .	50
5.6.3	Comparison of Systems . . . . .	55
5.6.4	Distribution System Unavailability . . . . .	58
5.6.5	Mission Sensitivity . . . . .	60
5.7	Conclusion . . . . .	63
Chapter 6	Market-Based Control in Power Electronics-Based Power Distribution Systems and its Challenges . . . . .	66
6.1	Introduction . . . . .	66
6.2	Problem Formulation . . . . .	67
6.3	Decision Functions . . . . .	69
6.3.1	Generator . . . . .	69
6.3.2	Converter . . . . .	70
6.3.3	Interconnect . . . . .	71
6.3.4	Load . . . . .	71
6.4	Numerical Algorithms for Market Clearing . . . . .	72

6.5	Example System and Scenarios . . . . .	72
6.6	Results . . . . .	74
6.7	Application in a Notional MVDC System . . . . .	76
6.8	Conclusion . . . . .	78
Chapter 7	Numerical Algorithm for Solving Market Clearing Problem in Power Electronics-Based Power Distribution Systems . . . . .	80
7.1	Introduction . . . . .	80
7.2	Problem Formulation . . . . .	80
7.3	Proposed Algorithm for Solving the Market Clearing Problem . . . . .	81
7.4	Reference Algorithms . . . . .	84
7.4.1	Broyden's Method . . . . .	84
7.4.2	Newton-Raphson Method . . . . .	85
7.4.3	Fsolve Method . . . . .	85
7.5	Example Systems . . . . .	85
7.5.1	Representative System . . . . .	85
7.5.2	Simplified Systems . . . . .	86
7.5.3	Operating Scenarios . . . . .	89
7.6	Convergence of the Proposed Algorithm and Reference Algorithms . . . . .	90
7.7	Dynamic Simulation of Representative System . . . . .	93
7.8	Conclusion . . . . .	97
Chapter 8	Equivalence of Dynamic Programming Problem and Sequence of Static Optimizations . . . . .	99
8.1	Introduction . . . . .	99
8.2	Problem Equivalence . . . . .	101
8.3	Demonstration Problem . . . . .	102
8.4	Demonstration Problem with Fixed Weights for Discharging . . . . .	106
8.5	Demonstration Problem with Varying Weights for Discharging . . . . .	108
8.6	Conclusion . . . . .	109
Chapter 9	Summary and Opportunities for Future Developments . . . . .	111
9.1	Introduction . . . . .	111
9.2	Future Developments . . . . .	112
Appendices	. . . . .	114
Appendix A:	Figures for Chapter 5 . . . . .	114
Appendix B:	Figures for Chapter 6 . . . . .	117
Appendix C:	Figures for Chapter 7 . . . . .	124
Bibliography	. . . . .	132
Vita	. . . . .	141

## LIST OF FIGURES

2.1	Markov chain illustrating transition from one state to another. . . . .	11
3.1	System 1 (Shared). This is an idealized system in which stored energy is freely available throughout the system. . . . .	14
3.2	System 2 (Dedicated). Energy in system is allocated to a specific actuator and cannot be repurposed. . . . .	15
3.3	System 3 (Distributed). Energy is allocated to specific actuators but can be moved with limited power through distribution system. . . . .	15
3.4	Variation of mission performance for System 1 (Shared) . . . . .	19
3.5	Variation of mission performance for System 2 (Dedicated) . . . . .	20
3.6	Variation of mission performance for System 3 (Distributed) . . . . .	20
3.7	Performance comparison of System 1 (Shared), System 2 (Dedicated), and System 3 (Distributed). Energy for System 2 (Dedicated) and System 3 (Distributed) is allocated optimally between the two actuators. . . . .	21
3.8	Performance comparison showing overlap between System 1 (Shared) and System 3 (Distributed) . . . . .	22
4.1	Diagram of the simplified representation of the notional system. Symmetry is used to aggregate generation, energy magazines, and propulsion, service, and mission loads. . . . .	25
4.2	State transition diagram for the fixed-duration model. . . . .	27
4.3	State transition diagram for the probabilistic model. . . . .	29
4.4	Temporal discounting factor $\hat{\alpha}$ with transition probability $p$ with $\alpha = 1$ and $N = 12$ . . . . .	30
4.5	Performance of notional system for fixed-duration model. . . . .	31
4.6	Variation of rms error between fixed-duration and probabilistic model with transition probability, $p$ . The relatively low values of error indicate that the two types of modeling yield almost identical results. There is little variation amongst each of the errors indicating that it is not dependent on the combination of transition probability $p$ and discounting parameter $\hat{\alpha}$ . . . . .	32
4.7	Performance of notional system for probabilistic model when transition probability $p = 0$ and discounting parameter $\hat{\alpha} = 0.9167$ . . . . .	33
4.8	Performance of notional system for probabilistic model when transition probability $p = \frac{1}{N}$ and discounting parameter $\hat{\alpha} = 1$ . . . . .	34
5.1	Probability of maintaining track on target versus tracking power. Power rating of tracking actuator is vertical line. . . . .	39
5.2	State transition diagram for Mission 1 (Search and Destroy). . . . .	40
5.3	State transition diagram for Mission 2 (Contested Transit). . . . .	41
5.4	State transition diagram for Mission 3 (Fight or Flight). . . . .	42



5.5	System 1 (Shared). This is an idealized system in which stored energy is freely available throughout system. . . . .	43
5.6	System 2 (Dedicated). Energy in system is allocated to a specific actuator and cannot be repurposed. . . . .	44
5.7	System 3 (Distributed). Energy allocated to specific actuators but can be moved with limited power through distribution system. . . . .	45
5.8	Expected performance for Mission 1 (Search and Destroy) with System 1 (Shared). Higher initial allocation of energy results in higher expected performance. . . . .	48
5.9	Expected performance for Mission 1 (Search and Destroy) with System 2 (Dedicated). Higher initial energy for either actuator results in higher expected performance. However, if very low energy is available for either actuator, the performance is low, even if the energy available for the other actuator is high. . . . .	49
5.10	Expected performance for Mission 1 (Search and Destroy) with System 3 (Distributed). The performance is higher when higher energy is available for tracking, attacking, and moving. The vertical spread represents initial energy allocations that are not optimal with respect to this mission. Unlike System 2 (Dedicated), the performance is not zero unless no energy is available. If the initial energy allocation is not optimal, energy can be moved through the distribution system. . . . .	50
5.11	Expected performance for Mission 2 (Contested Transit) with System 3 (Distributed). The performance is higher when higher energy is available for tracking, attacking, and moving. The vertical spread represents initial energy allocations that are not optimal with respect to this mission. . . .	51
5.12	Expected performance for Mission 3 (Fight or Flight) with System 3 (Distributed). The performance is higher when higher energy is available for tracking, attacking, and moving. . . . .	52
5.13	Overall mission performance for System 1 (Shared). Similar to individual mission performances for this system, higher allocation of energy results in higher expected performance. . . . .	53
5.14	Overall mission performance for System 2 (Dedicated). Similar to individual mission performances for this system, higher allocation of energy results in higher expected performance. The wide vertical spread indicates high sensitivity to initial allocation of energy. The optimal curve indicates overall performance when energy is initially optimally allocated among actuators. . . . .	54
5.15	Optimal split of energy among three actuators for System 2 (Dedicated). For lower amounts of energy, energy is only allocated to moving, but ratio changes as total energy increases. . . . .	55

5.16	Overall mission performance for System 3 (Distributed). Similar to the individual mission performances for this system, higher allocation of energy results in higher expected performance. Narrow vertical spread indicates low sensitivity to initial allocation of energy. The optimal curve indicates overall performance when energy is initially optimally allocated among actuators. . . . .	56
5.17	Optimal split of energy among three actuators for System 3 (Distributed). There is considerably smaller range of energy for which energy is only allocated to one actuator (attack). . . . .	57
5.18	Performance comparison of systems. Energy for the System 2 (Dedicated) and System 3 (Distributed) is optimally allocated among three actuators. System 1 (Shared) is an idealized system and represents an upper bound on available performance. The performance penalty is computed by comparison of more practical systems with idealized System 1 (Shared). System 3 (Distributed) generally performs better for given amount of energy and requires lesser energy to achieve same performance as System 2 (Dedicated).	58
5.19	Distribution of distance traveled at each time period for Mission 2 (Contested Transit) with System 2 (Dedicated). Starting from optimally allocated 30 pu of energy, 500 sample trajectories are simulated for 100 periods. The range (with outliers excluded) and the lower and upper quartiles are shown. . . . .	59
5.20	Distribution of distance traveled at each time period for Mission 2 (Contested Transit) with System 3 (Distributed). Starting from optimally allocated 30 pu of energy, 500 sample trajectories are simulated for 100 periods. The range (with outliers excluded) and the lower and upper quartiles are shown. . . . .	60
5.21	Performance comparison of systems with possibility of unavailable distribution system when there is no hedging against unavailability. System 3 (Distributed) outperforms System 2 (Dedicated) when distribution system is available, but System 2 (Dedicated) outperforms System 3 (Distributed) when it is unavailable. . . . .	61
5.22	Performance comparison of systems with 10% probability of unavailable distribution system. Expected performance of System 3 (Distributed) is slightly lower than performance when distribution system is available. Expected performance remains significantly greater than System 2 (Dedicated).	62
5.23	Performance comparison of systems with possibility of unavailable distribution system when there is hedging against unavailability. System 3 (Distributed) outperforms System 2 (Dedicated) when distribution system is available, but System 2 (Dedicated) outperforms System 3 (Distributed) when it is unavailable. However, range of energy for which System 2 (Dedicated) outperforms System 3 (Distributed) when distribution system is unavailable is significantly smaller than when no hedging is performed. .	63

5.24	Performance comparison of systems considering the probability of distribution system unavailability. Expected performance of System 3 (Distributed) with hedging is essentially identical to expected performance without hedging and significantly better than System 2 (Dedicated), but hedging performance is generally better when distribution system is unavailable. . . . .	64
5.25	Performance comparison of systems under real mission distribution when designed considering real mission distribution or assumed mission distribution. There is small performance decrease associated with design using assumed distribution instead of real distribution. Difference is labeled sensitivity. System 2 (Dedicated) has higher sensitivity than System 3 (Distributed). . . . .	65
6.1	Generator output power as a function of bus price and mechanical state. The parameter $\epsilon$ is artificially much larger than used herein to emphasize the high-slope regions. . . . .	70
6.2	Representative System 1 with one bus, two generators, and a load. . . . .	73
6.3	Representative System 2 with two buses, two generators, an interconnect, and a load. . . . .	73
6.4	Representative System 3 with three buses, two generators, an interconnect, a converter, and a load. . . . .	74
6.5	Price convergence probability for System 1 in Scenario 1 (Scarcity). Similar figures emerge for the other systems and scenarios. . . . .	75
6.6	Average starting Jacobian rank for System 1 in Scenario 1 (Scarcity). . . . .	76
6.7	Notional MVDC system. MTG signifies main turbine generator, ATG signifies auxiliary turbine generator, PMD signifies propulsion motor drive, CM signifies converter module, R signifies radar, and ZL signifies zonal load [1]. The small black squares are used to separate the four zones in the horizontal direction, and the upper and lower zones in the vertical direction. . . . .	77
6.8	Price convergence probability for MVDC system . . . . .	78
7.1	Root finding for a single dimensional problem . . . . .	82
7.2	Diagram illustrating a complex, representative power system (System 4). It consists of two main generators on the inner zones (MG 1 and MG 2), two auxiliary generators on the outer zones (AG 3 and AG 4), four propulsion loads (P), mission loads (M) fed through converter module (C), service loads (L), and interconnects (I) to connect between buses (B). . . . .	87
7.3	Diagram illustrating System 1. The main generator (MG), auxiliary generator (AG), service load (L), mission load (M), and propulsion load (P) are all connected to a single bus (B). . . . .	88
7.4	Diagram illustrating System 2. The main generator (MG) supplies power to the propulsion load (P) through one bus (B 1) since a higher rated load requires a higher rated generator. The mission load (M) and service load (L) are supplied power by the auxiliary generator (AG) through another bus (B 2). The two buses are connected via an interconnect (I). . . . .	89

7.5	Diagram illustrating System 3. The main generator (MG) supplies power to the propulsion load (P) through one bus (B 1) since it has higher rating. The mission load (M) and service load (L) are supplied power by the auxiliary generator (AG) through another bus (B 2). The two buses are connected via an interconnect (I). The mission load (M) is connected to a converter module (C) via a separate bus (B 3). . . . .	90
7.6	Monte Carlo sampling of starting prices. . . . .	91
7.7	Price convergence probability for System 1 in Scenario 1 (Scarcity). Similar figures emerge for the other systems and scenarios. The arrow points to the plot for the proposed algorithm. . . . .	93
7.8	Bus prices for dynamic simulation. Bus 9 is the bus for main generator 1 and bus 17 is the bus for mission load 1. During the time interval between 20 s and 21.1 s, both prices decrease to approximately $-\$20/\text{s}/\text{pu}$ (an overabundance condition). . . . .	95
7.9	Generator output power for dynamic simulation. . . . .	96
7.10	Load input power for dynamic simulation. . . . .	96
7.11	Converter output power for dynamic simulation. . . . .	97
8.1	Relationship between optimization concepts. . . . .	101
8.2	Diagram of representation of the notional system showing the power flows. . . . .	102
8.3	State transition diagram. . . . .	104
8.4	Performance comparison between MDP-based optimal control and sequence of static optimization for fixed discharging weights. The plot on the bottom indicates that slightly lower performance is obtained with sequence of static optimizations. . . . .	107
8.5	Variation of discharging weight. . . . .	109
8.6	Performance comparison between MDP-based optimal control and sequence of static optimization for variable discharging weights. The two plots are comparable indicating the equivalence of the two optimization approaches. The slight differences are due to sampling errors. . . . .	110
9.1	Relationship between optimization concepts. . . . .	113
1	Expected performance for Mission 2 (Contested Transit) with System 1 (Shared). . . . .	114
2	Expected performance for Mission 2 (Contested Transit) with System 2 (Dedicated). . . . .	115
3	Expected performance for Mission 3 (Fight or Flight) with System 2 (Dedicated). . . . .	116
4	Price convergence probability for System 2 in Scenario 1 (Scarcity). . . . .	117
5	Price convergence probability for System 3 in Scenario 1 (Scarcity). . . . .	118
6	Price convergence probability for System 1 in Scenario 2 (Sufficiency). . . . .	118
7	Price convergence probability for System 2 in Scenario 2 (Sufficiency). . . . .	119
8	Price convergence probability for System 3 in Scenario 2 (Sufficiency). . . . .	120
9	Price convergence probability for System 1 in Scenario 3 (Overabundance). . . . .	121

10	Price convergence probability for System 2 in Scenario 3 (Overabundance).	122
11	Price convergence probability for System 3 in Scenario 3 (Overabundance).	123
12	Price convergence probability for System 1 in Scenario 2 (Sufficiency). . .	124
13	Price convergence probability for System 1 in Scenario 3 (Overabundance).	125
14	Price convergence probability for System 2 in Scenario 1 (Scarcity). . . .	126
15	Price convergence probability for System 2 in Scenario 2 (Sufficiency). . .	127
16	Price convergence probability for System 2 in Scenario 3 (Overabundance).	128
17	Price convergence probability for System 3 in Scenario 1 (Scarcity). . . .	129
18	Price convergence probability for System 3 in Scenario 2 (Sufficiency). . .	130
19	Price convergence probability for System 3 in Scenario 3 (Overabundance).	131

## LIST OF TABLES

3.1	Notional Parameter Values . . . . .	14
4.1	Ratings of System Components . . . . .	25
4.2	Mission Parameters . . . . .	26
5.1	Notional Problem Parameter Values . . . . .	38
5.2	Grids for Notional Problems . . . . .	47
5.3	Notional Mission Probabilities . . . . .	52
5.4	Assumed Mission Probabilities . . . . .	61
6.1	System Parameters . . . . .	72
6.2	Scenario Parameters . . . . .	73
6.3	Equilibrium Prices for Systems under Scenarios . . . . .	74
6.4	Maximum Range of Starting Prices . . . . .	75
6.5	Parameters of Notional MVDC System . . . . .	77
7.1	Parameters of Representative System (System 4) . . . . .	86
7.2	Parameters of Simplified Systems (Systems 1–3) . . . . .	88
7.3	Scenario Parameters for All Systems (Systems 1–4) . . . . .	90
7.4	Equilibrium Prices for Systems under Scenarios . . . . .	92
7.5	Maximum Range of Starting Prices . . . . .	94
8.1	System Parameters . . . . .	103
8.2	Discretization Parameters . . . . .	103
8.3	<b>H</b> matrix parameters and values . . . . .	105
8.4	Monte Carlo Simulation Parameter Values . . . . .	106

## Chapter 1 Introduction

### 1.1 Introduction

Mission-oriented power systems are designed to support the performance of specific missions. These missions may involve dynamic use of different loads during missions of varying duration. The value of power delivered to different loads will depend on the specific mission or even the particular point in the mission's progress. Such systems include shipboard power systems [2, 3], aerospace systems [4, 5], uncrewed electric vehicles [6, 7], and other power-electronic-based power systems [8, 9].

The power system of an electric warship provides electric power to loads involved in missions in a way that they continue operating even after sustaining damage. It differs from traditional power systems as it is not entirely focused on maintaining system reliability and stability at all times; rather, it aims to deliver power dynamically during missions of relatively short durations or operational vignettes. Unlike conventional power systems, loads are not generally relatively equal in importance. Power quality metrics used in these systems must consider the value of the power system in performing the mission at hand. Specifically, to evaluate the potential performance of such systems, it is necessary to understand how they will help complete the mission when controlled optimally across a range of vignettes.

Various metrics such as survivability [10–12], operability [13], etc. have been used for this evaluation. Some performance metrics can also be derived from the metrics mentioned herein. Metrics such as susceptibility, vulnerability, and recoverability can be derived from the survivability metrics [14] whereas metrics derived from operability are dependability, average system dependability, minimum system dependability, etc. [13, 15]. Traditionally, survivability and its associated metrics have been used in shipboard power system evaluation. With the emergence of shipboard systems with dynamic loads, it is assumed that the ship would physically survive and continue the mission. In such case, a more dynamic evaluation of performance is needed. The metric operability can play a major role in this assessment. The ability to continue a mission and the performance during the mission can be assessed using the metric operability and metrics derived from it.

An evolution in mission-oriented power system evaluation was necessary. In particular, to develop a reasonable understanding of the potential performance of such systems, it is necessary to consider the dynamic interplay between mission and system because there is an intrinsic connection to mission performance. This resulted in a break from evaluation using static load profiles and weights, and served as an improved basis for system evaluation, as the basis for system control development, and as a framework for better understanding the role of mission requirements in power system design. This evolution, initial steps of which are described in [16, 17], involves transforming the evaluation problem into an optimal control problem, the solution of which can reveal the potential performance of a power system implementation.

This approach of modeling the combined system and mission as a hybrid dis-

crete/continuous, stochastic/deterministic dynamic system and combining with mission-specific rewards to be optimized is naturally represented as a Markov decision process (MDP). The applications of MDP-based modeling vary across literature, but the common goal is to solve an optimization problem to achieve the maximum reward (e.g. in the form of maximum performance or minimum costs), given some constraints in the system and its dynamics.

In case of power electronics-based power systems, generally, the control objective involves directing power to specific loads as required under the current conditions. This can typically be formulated as a mathematical optimization problem. If the overall system structure and condition, including the statuses and internal characteristics of each component, are known globally, it is possible to develop a centralized control system that is able to control the system by solving the global optimization problem. However, it is recognized that this approach may be brittle (i.e., sensitive to changes in system configuration and design) and dependent on data that may not be centrally available about individual components and their statuses in certain conditions. An alternative to a centralized control system is market-based control.

Market-based control is a control approach in which an artificial market is created for resources within the system, and the forces of supply and demand guide the system toward equilibrium states. The operation of each component can be represented as a profit-maximizing firm. In a perfectly competitive market, resource distribution is guided by the market forces to the most productive (in this sense, maximizing the control objective above). If system conditions shift, a shortage or surplus arises, causing prices to rise or fall, respectively, components change their behavior, and a new equilibrium emerges.

A key feature of market-based control is that it reduces a global optimization problem into a series of smaller local optimization problems (i.e., profit maximization) combined with finding the market-clearing prices that result in market equilibrium (i.e., quantity supplied is equal to quantity demanded). Finding the globally coordinating market-clearing prices is a root-finding problem. It is known that under sufficient conditions the market-clearing problem is equivalent to solving the global optimization problem (e.g., [17]).

To enable market-based control of such systems, it is necessary that appropriate market-clearing algorithms exist that can locate the market-clearing prices that allow the system to operate at equilibrium. Power-electronics-based power distribution systems exhibit some features that can complicate market-based control. For example, the systems are typically efficient, resulting in relatively small variations in losses with operating conditions. They tend to operate relatively similarly across their operating ranges, except at their operating limits, which can create sharp discontinuities in their operating profiles. The numerical challenges of solving the root-finding problem of finding the market-clearing prices in these systems is explored in this work. In addition, an algorithm has been proposed to solve the market clearing problem.

The decision functions of various components in the system are used to optimize the controller to solve for the market clearing price. On the other hand, the optimal control solution can also be determined using the state variables and actions to evaluate the expected performance of the system. Hence, both MDP-based optimal



control and market-based control optimize a controller under certain constraints. The dynamic optimal control problem can also be represented by solving a sequence of static optimizations, where each step's solution informs the next, ensuring that the overall control strategy is optimized over the entire planning horizon. Thus, sequence of static optimizations also optimize a controller under certain constraints. Hence, a connection among these three optimization approaches can be established, which will be explored in this work.

## 1.2 Contributions of the Dissertation

With the advancement in modeling of power systems and power electronics-based systems, the current state of performance evaluation can be represented using MDP-based dynamic optimal control, market-based control, and sequence of static optimizations of the dynamic problem. This way, the effect of the power system performance on the dynamic mission performance can be represented. Namely, the major contributions of this work are-

1. The evaluation of mission-oriented power system performance as an optimal control problem has been articulated, allowing the dynamic interaction between the system and the mission to be considered. This involves demonstrating the optimal-control-based approach to evaluation in a notional, but representative, set of system implementations and missions. In addition, the types of system trade offs that can be considered using this approach has been illustrated.
2. The numerical challenges of market-based control has been explored. An algorithm has been proposed that solves the market clearing price under constraints and it has been demonstrated that the proposed algorithm is efficient in clearing the market. This has also been validated using dynamic simulation.
3. In addition, the equivalence of sequence of static optimizations to dynamic optimal control problem has been explored, and validated with results. This has bridged the connection among various optimization approaches- market-based control, sequence of static optimizations, and MDP-based dynamic optimal control.

## 1.3 Organization of the Dissertation

This dissertation shows how optimal control and performance evaluation of ship-board power system has evolved, how it is currently being performed and how it can be improved. The organization of the report is as follows. In Chapter 2, an insight on previous work on optimal control-based evaluation has been given along with a background on important concepts used in the dissertation. In Chapter 3, optimal control-based evaluation using Markov decision process (MDP) is introduced using a notional problem. In Chapter 4, the application of MDP-based modeling has been applied on a system consisting of energy magazines. It has also been shown how

MDP-based optimal control is similar to the traditional performance evaluation metric ‘*operability*’. In Chapter 5, the current state of optimal control has been described for mission-oriented power systems. Various system trade offs and sensitivity of performance to initial assumptions are considered. Chapter 6 introduces market-based control approach and discusses the computational difficulty of solving the market clearing price using traditional root-finding algorithms. In Chapter 7, an algorithm has been proposed for solving the market clearing problem, and determining the market clearing price for systems with various constraints. The efficiency of the proposed approach has been verified using dynamic simulation. In Chapter 8, the equivalence of dynamic optimal control and sequence of static optimizations has been discussed and established. Finally, in Chapter 9, the current research has been summarized and opportunities for future developments to this research has been discussed.

## Chapter 2 Background and Literature Review

### 2.1 Introduction

The use of various metrics have varied across literature for the evaluation of performance of mission-oriented power systems. In this chapter, the evolution of these metrics and performance evaluation techniques will be discussed. This will be followed by a discussion of the current approach of solving optimal control-based problems.

### 2.2 Overview of Various Metrics

In traditional shipboard systems, the evaluation of performance involved the use of the survivability metric [18–21]. Survivability can be expressed mathematically as the probability of survival,  $P_S$ . It can be described by the equation below:

$$P_S = 1 - (P_H * P_{K/H}) * (1 - P_R), \quad (2.1)$$

where  $P_H$  is the probability of being hit, or susceptibility,  $P_{K/H}$  is the probability of being killed, given a hit, or vulnerability, and  $P_R$  is the probability of recovery, or recoverability.

In addition to survivability, traditional shipboard power systems focused on Quality of Service (QOS) metric [22, 23]. This metric determines how reliable the power system is in providing electrical power to loads. In [23], a two-level topology design and architecture for a shipboard power system has been presented. The system ensures QOS and survivability in case of an interruption [24, 25]. Survivability and QOS can be characterized as primary design criteria that ensures reliability. Survivability measures the ability of the power system to support system during damage. On the other hand, QOS measures the ability to provide continued service during peacetime or normal operations.

To ensure survivability, zonal architectures are sought that prohibit the spread of a fault to undamaged zones of the SPS [15, 26–28]. As for the peacetime operations, service interruptions are most often caused by the failures of individual components within the distribution system. The reliability during peacetime operations is characterized using QOS metrics. In the literature, the metrics for calculating peacetime QOS in SPS have been established [1], [16] and applied to designing SPS with a primary focus on equipment design choices and control interfaces. The approach to quantify distribution system reliability as a function of system topology has also been explored [2, 4, 29, 30].

However, the metric QOS does not indicate a way to measure the performance of electric warships. This is particularly true in case of damaged systems where the shipboard power system must continue the mission even after sustaining damage. In other words, the mission must be continued even when there is lack of survivability

and reliability. The metric operability provides a useful measure of performance in such a situation.

The application of operability and reliability metrics is not only limited to ship-board electrical systems. The control and mechanics of aerospace vehicles affect these metrics, particularly operability [31]. The evaluation of operability has also been conducted in the control of systems in chemical engineering. An index, dynamic operability (dOI) has been defined for performance assessment of dynamic systems over a range of desired outputs [32, 33].

### 2.3 Operability Metric

Operability can generally be thought of as the ability of a system to perform during a single scenario (or vignette). The earliest examples of operability were calculated based on scenarios involving battle damage [13, 15, 26], but this was extended to challenging load profiles [27], cyber disruptions [28], and other situations. It was understood that, given an accepted definition of operability, metrics could be derived from operability that characterized the system performance in different ways. Metrics based on expected and worst-case values of operability were considered initially [13, 26]. Later, histograms of operability were presented along with probabilities of failing to attain a given level of operability [16, 28]. The recent conception of operability of a control system as being a factored metric normalized by the underlying capability of the platform is a method of attempting to attribute the ability of the overall system to various elements.

Previous approaches to operability formulation have been based on integrating an instantaneous reward function in continuous time [1, 13, 26, 27] or summing such a function in discrete time [2, 4, 29, 30]. In both cases, it has been possible to include temporal discounting (potentially necessary for convergence if the time interval is unbounded). The reward function in previous approaches has been based on power flow, which is attractive from a power systems standpoint (power flow is well understood), but it may not represent the mission value of the power flow. More recent discussions of load elasticity as a nonlinear relationship between the applied power and/or energy and the mission effectiveness of that application represent a shift from a purely load-oriented operability metric toward a mission-oriented operability metric [16].

Operability was previously evaluated based on static load profiles (perhaps randomly drawn in some way). The load profile did not vary based on the ability of the system to satisfy the given load demand. Combined with these challenges was the question of how to represent control action during the evaluation of operability. Each previous conception of operability involved the evaluation of a time-domain-based performance metric [34]. The control of the system has a significant influence on the evaluated operability of the system. The earliest studies of operability involved simplistic representation of local distributed controllers.

In this chapter, the evolution of ship platforms from a load-oriented system to a mission-oriented system is discussed. A trajectory leading towards current optimal-control-based approaches emerges, and the current state of such approaches is demonstrated in a notional problem in the next chapter.

## 2.4 Beginnings of Operability as a Performance Metric

In [13,26], the metric operability was introduced to determine how effective the power system is at responding to mission loads. It measures the degree to which the performance of the power system contributes to mission effectiveness in a particular scenario. Operability was initially represented as an integral of weighted power flows to loads:

$$O = \frac{\int_{t_0}^{t_{end}} \sum_{i=1}^I w_i P_i(t) dt}{\int_{t_0}^{t_{end}} \sum_{i=1}^I w_i P_{max,i}(t) dt}, \quad (2.2)$$

where  $I$  is the number of loads in the system,  $P_i(t)$  is the power consumption of load  $i$  at time  $t$ ,  $P_{max,i}(t)$  is the maximum (or demanded) power of load  $i$  at time  $t$ , and  $w_i$  is a mission-specific, potentially time-varying weighting function indicating the relative importance of load  $i$ . The interval of time considered is  $[t_0, t_{end}]$  and the weighting functions might be exponentially decaying to place specific value on performance early during the scenario.

Depending on the modeling and simulation methodology employed, it may be convenient to express the operability metric in discrete-time form as

$$O = \frac{\sum_{k=k_1}^{k_{end}} \sum_{i=1}^I w_i P_i(k)}{\sum_{k=k_1}^{k_{end}} \sum_{i=1}^I w_i P_{max,i}(k)}, \quad (2.3)$$

where  $k$  indicates the period (of time) as an integer from  $k_0$  to  $k_{end}$ .

The operability metrics above are intended to convey the value of the power system performance to the mission being performed in a given operational scenario. Given an accepted definition of operability as such a measure of mission performance, other metrics can be derived from the operability metric. One such metric is dependability [13,26]. Average system dependability is the expected value of the operability over a distribution of events that the power system could face:

$$\bar{D}_s = E[O]. \quad (2.4)$$

In the same way, the minimum system dependability can be used as a metric of worst-case performance:

$$D_{s,min} = \min[O]. \quad (2.5)$$

Other derived metrics (e.g., the probability of operability exceeding a given threshold value) have also been considered [35].

One of the features of these metrics is that they are evaluated via time-domain simulation. To do this, variable loading should be represented. The load demands of different ships in a mission vary depending on a ship's intended operational use and operational speeds. A ship can move at various speeds, and its load demands vary in time depending on mission.

In addition to variable loading conditions being represented, it is necessary to represent the control of the power system. The manner in which the system is controlled has a strong influence on the performance of the overall system, and this becomes

particularly important in situations in which there is scarcity, i.e., systems in which the allocation of power to various purposes is constrained by the physical limits of the systems. This specifically includes the types of challenging operational scenarios for which operability is intended to quantify performance. The earliest approaches to modeling the control systems in time-domain simulation involved simplistic local control systems that avoided physically unacceptable solutions. Loads operated when local conditions suggested it was physically plausible. This baseline representation permitted evaluation of time-domain performance metrics, but it did not represent a more sophisticated control system.

## 2.5 Evolution of Operability

While the earliest applications of operability involved performance of damaged power systems, the loading of these systems was relatively static, but realistic load profiles are necessarily dynamic [36]. The next step happened in [27, 28]. In these works, two approaches for generating dynamic load profiles were presented. In [37, 38], a generative approach for producing load profiles based on a statistical representation of a given mission narrative was presented. In [28], a Markov-chain-based approach for producing load profiles was presented in which a mission profile could be conceived as a trajectory of a Markov chain. These approaches, while superficially dissimilar, are mathematically essentially equivalent and represent a statistical approach for generating dynamic and mission-relevant load profiles.

Coupled with this evolution was an evolution in the manner in which control systems (and indeed the system physics) were represented for purposes of time-domain evaluation. Very early, it was recognized that the most important dynamics associated with operability evaluation were slower, at the same rate as the bulk load dynamics. This includes thermal phenomena, generator ramp rates, energy storage, etc. An initial first step was to represent the power system physics using a linear programming problem [37]. This idea was further developed in other mathematical programming modeling approaches [39, 40]. One of the consequences of introducing mathematical programming modeling approaches to modeling the power system physics is that these problems have objective functions; there is something the mathematical programming solver is trying to optimize. The obvious approach was to maximize the instantaneous integrand (or the summand) in the operability definition, a representation of the action of a greedy controller. In other words, the adoption of mathematical-programming-based modeling approaches also resulted in a representation of a controller that was attempting to allocate power optimally at a system level [41].

These solutions were still instantaneous solutions. They did not intrinsically consider the future or the value of future energy. They were not solving the desired optimal control problem; they approximated the optimal control problem as a sequence of static optimization problems. This idea was further extended in [2, 38] to the idea of multiperiod optimal power flow. In this approach, the optimization problems describing the physics and control objectives of the power system are carefully concatenated to form a larger optimization problem representing the complete opti-

mal control problem. This approach represented an optimal solution to the control of the power system during a potentially dynamic loading situation provided that the future is known in advance.

In the next sections, general descriptions of the terms used in this work are discussed. In the next chapter, a notional problem is presented where these general terms and notations are made more specific to the problem description.

## 2.6 Markov Chains

A Markov chain is a probabilistic sequence that adheres to the Markov property, indicating that knowledge of the present renders the past and future independent [42]. In essence, with awareness of the current state, no further historical data is necessary for optimal future predictions. This characteristic streamlines analysis by significantly reducing the parameter count.

A stochastic process  $X = X_n, n \in N$  in a countable space  $S$  is a discrete-time Markov chain if:

For all  $n \geq 0, X_n \in S$

For all  $n \geq 1$  and for all  $i_0, \dots, i_{n-1}, i_n \in S$ , we have:

$$P\{X_n = i_n \mid X_{n-1} = i_{n-1}, \dots, X_0 = i_0\} = P\{X_n = i_n \mid X_{n-1} = i_{n-1}\}$$

A transition matrix  $P_t$  for Markov chain  $\{X\}$  at time  $t$  is a matrix containing information on the probability of transitioning between states. In particular, given an ordering of a matrix's rows and columns by the state space  $S$ , the  $(i, j)$ <sup>th</sup> element of the matrix  $P_t$  is given by

$$(P_t)_{i,j} = \mathbb{P}(X_{t+1} = j \mid X_t = i). \quad (2.6)$$

This means each row of the matrix is a probability vector, and the sum of its entries is 1.

Transition matrices have the property that the product of subsequent ones describes a transition along the time interval spanned by the transition matrices. That is to say,  $P_0 \cdot P_1$  has in its  $(i, j)$ <sup>th</sup> position the probability that  $X_2 = j$  given that  $X_0 = i$ . And, in general, the  $(i, j)$ <sup>th</sup> position of  $P_t \cdot P_{t+1} \cdots P_{t+k}$  is the probability  $\mathbb{P}(X_{t+k+1} = j \mid X_t = i)$

The k-step transition matrix is  $P_t^{(k)} = P_t \cdot P_{t+1} \cdots P_{t+k-1}$  and, satisfies

$$P_t^{(k)} = \begin{pmatrix} \mathbb{P}(X_{t+k} = 1 \mid X_t = 1) & \mathbb{P}(X_{t+k} = 2 \mid X_t = 1) & \cdots & \mathbb{P}(X_{t+k} = n \mid X_t = 1) \\ \mathbb{P}(X_{t+k} = 1 \mid X_t = 2) & \mathbb{P}(X_{t+k} = 2 \mid X_t = 2) & \cdots & \mathbb{P}(X_{t+k} = n \mid X_t = 2) \\ & & \vdots & \\ \mathbb{P}(X_{t+k} = 1 \mid X_t = n) & \mathbb{P}(X_{t+k} = 2 \mid X_t = n) & \cdots & \mathbb{P}(X_{t+k} = n \mid X_t = n) \end{pmatrix} \quad (2.7)$$

## 2.7 Markov Decision Process

A Markov decision process (MDP) is defined by  $(S, A, P, R, \alpha)$ , where  $S$  are the states,  $A$  is the set of actions,  $P$  is the state-transition probability of moving from one state to another,  $R$  is the reward, and  $\alpha$  is the discounting factor [43]. The state reward  $R$  is the expected reward over all the possible states that one can transition to from state  $s_t$ . This reward is received for being at the state  $S$ . By convention, it is said that the reward is received after the agent leaves the state, and is hence regarded as  $R_{t+1}$ . Introduction to actions elicits a notion of control over the Markov process. Previously, the state transition probability and the state rewards were more or less stochastic (random). However, now the rewards and the next state also depend on what action the agent picks. Basically, the agent can control its own fate (to some extent).

The return  $G_t$  is the total discounted reward from time-step  $t$ .

$$G_t = R_{t+1} + \alpha R_{t+2} + \dots = \sum_{k=0}^{\infty} \alpha^k R_{t+k+1} \quad (2.8)$$

Rewards are temporary. Even after picking an action that gives a decent reward, there might be a greater total reward missing in the long-run. This long-term total reward is the Return. However, in practice, discounted Returns are considered.

The variable  $\alpha \in [0, 1]$  is the discounting factor. The intuition behind using a discount is that there is no certainty about the future rewards. While it is important to consider future rewards to increase the Return, it's also equally important to limit the contribution of the future rewards to the Return.

A policy  $\pi$  is a distribution over actions given states,

$$\pi(a | s) = \mathbb{P}[A_t = a | S_t = s] \quad (2.9)$$

A policy defines the thought behind making a decision (picking an action). Formally, a policy is a probability distribution over the set of actions  $a$ , given the current state  $s$ . It gives the probability of picking an action  $a$  at state  $s$ .

## 2.8 Value Function Iteration

A value function is the long-term value of a state or an action. In other words, it is the expected Return over a state or an action.

The state value function  $v_\pi(s)$  of an MDP is the expected return starting from state  $s$ , and then following the policy  $\pi$ .

$$v_\pi(s) = \mathbb{E}_\pi[G_t | S_t = s] \quad (2.10)$$

The action value function  $q_\pi(s, a)$  is the expected return starting from state  $s$ , taking the action  $a$  and then following the policy  $\pi$ .

$$q_\pi(s, a) = \mathbb{E}_\pi[G_t | S_t = s, A_t = a] \quad (2.11)$$



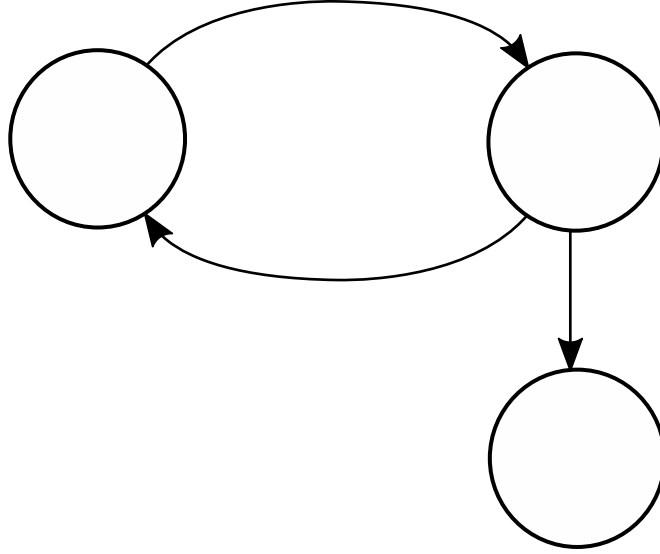


Figure 2.1: Markov chain illustrating transition from one state to another.

Since there is a state to action transition, the expected action value over all the actions needs to be taken.

And this completely satisfies the Bellman equation as the same is done for the action value function:

$$q_{\pi}(s, a) = R_s^a + \alpha \sum_{s' \in S} P_{ss'}^a v_{\pi}(s') \quad (2.12)$$

## 2.9 Conclusion

In this chapter, a background on various performance metrics has been discussed. The evolution of the metric operability over the years has been discussed in detail. This evolution directs towards the current optimal control approach of using MDP-based performance evaluation. A generalized discussion of the terms used in MDP-based evaluation has also been presented in this chapter.

## Chapter 3 Optimal Control-Based Performance Evaluation

### 3.1 Introduction

In the previous chapter, the evolution of the metric ‘*operability*’ has been discussed. This was followed by a discussion on the current optimal control approaches based on Markov Decision Process. The primary contributions of this chapter are

1. to establish the current state of optimal control-based performance evaluation, and
2. to present a notional two-function problem involving multiple missions that demonstrates the current state of optimal control-based approaches for the evaluation of power system performance.

### 3.2 Current State of Operability

Prior to the current developments in the use of operability as a performance metric for power systems, it was possible to represent dynamic loading profiles. These were drawn statically from a given statistical distribution. Importantly, they did not dynamically depend on the performance of the power system. If a load needed a certain amount of power for a certain amount of time, there was no provision for this load demand to be adjusted if the power system could only provide a fraction of that power (e.g., by demanding power for a longer period of time). Likewise, there was the capacity for representing optimal control of the power system, but this could only be done in this framework if the future was known with certainty.

The next step in the evolution of operability as a performance metric was the representation of the problem using Markov decision processes [16]. In this way, the effect of the power system performance on dynamic mission performance could be represented (i.e., in the transitions of the Markov decision process). Likewise, the uncertainty of the future could be incorporated into the problem.

### 3.3 State of Optimal Control-based Evaluation using MDP

Markov decision processes are used widely to represent optimal control problems. Notation varies, so the notation used herein is described below.

A problem is defined by a combination of mission and system implementation. The combined state of the mission and system at moment  $k$  is represented by  $\mathbf{x}_k$ . This state variable is a vector involving both continuous and discrete components. The elements can evolve deterministically or stochastically.

Given a state  $\mathbf{x}_k$ , there is a set of available actions  $\Omega(\mathbf{x}_k)$ , which is a property of both the mission and the system. The action taken at moment  $k$  is  $\mathbf{u}_k \in \Omega(\mathbf{x}_k)$  and is a vector.

The state in the next moment  $\mathbf{x}_{k+1}$  will depend on the moment  $k$ , the present state  $\mathbf{x}_k$ , and the present action  $\mathbf{u}_k$ . The state can transition deterministically or stochastically (or some combination of both) depending on the system and mission.

A functional  $V$  depending on the trajectory of the state  $(\mathbf{x}_0, \mathbf{x}_1, \dots)$  and action  $(\mathbf{u}_0, \mathbf{u}_1, \dots)$  indicates the quality of the mission performance. The functional for an infinite horizon, time-invariant problem with temporal discounting can be expressed as

$$V = \sum_{k=0}^{\infty} \alpha^k R(\mathbf{x}_k, \mathbf{u}_k, \mathbf{x}_{k+1}), \quad (3.1)$$

where  $\alpha \in (0, 1]$  is a temporal discounting factor and  $R$  is an instantaneous reward function. This is a time-invariant Markov decision process. The optimal control problem is

$$\max_{(u_0, u_1, \dots)} E[V(x_0, x_1, \dots, u_0, u_1, \dots)]. \quad (3.2)$$

The stochastic Bellman equation can be solved for the expected reward  $\bar{V}$  numerically

$$\bar{V}(\mathbf{x}_k) = \max_{\mathbf{u}_k \in \Omega(\mathbf{x}_k)} E[R(\mathbf{x}_k, \mathbf{u}_k, \mathbf{x}_{k+1}) + \alpha \bar{V}(\mathbf{x}_{k+1})]. \quad (3.3)$$

Solving the Bellman equation yields an evaluation of the expected mission performance of the system given a starting state, while also including the dynamic and potentially stochastic interdependence of the mission and system states. The value of  $\bar{V}(x_0)$  for a given starting state becomes a measure of the mission capability of the system in a given operating environment.

### 3.4 Notional Problem

A two-function notional problem is used here to illustrate the current state of optimal control-based evaluation. The system is able to allocate power to actuators to track a target and/or to attack a target based on the mission being undertaken.

In this problem, the system may have to perform one of the three missions, with given probabilities. The missions involve different applications of the system's actuators and available energy. In the missions considered, one or both the actuators are required for success.

Along with the three different missions, three different systems are considered. In System 1 (Shared), energy storage is shared between actuators as shown in Figure 3.1. In System 2 (Dedicated), energy storage is dedicated to each actuator, as shown in Figure 3.2. In System 3 (Distributed), an interconnecting distribution network provides a path for power between the two actuators. Thus, energy can be moved from one actuator to the other, as shown in Figure 3.3, but at a limited rate. The parameter values for the problem are given in Table 3.1.

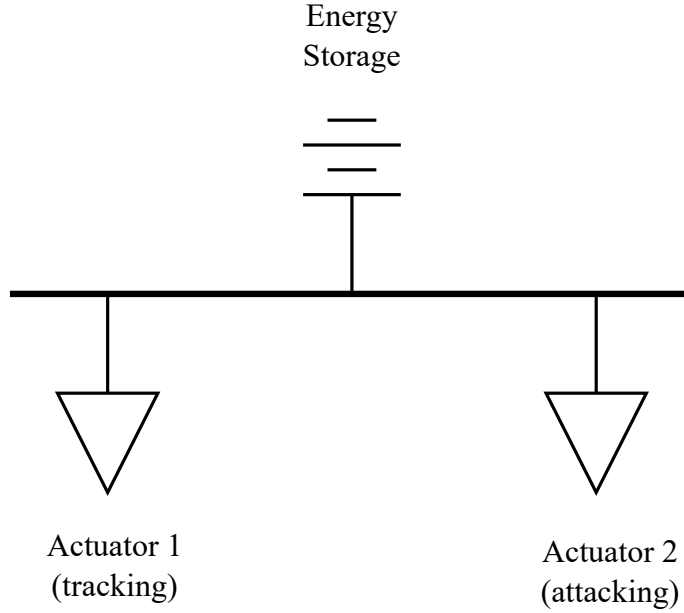


Figure 3.1: System 1 (Shared). This is an idealized system in which stored energy is freely available throughout the system.

Table 3.1: Notional Parameter Values

Parameter	Value
$p_{track,max}$	1
$p_{attack,max}$	1
$p_{dist,max}$	0.2
$p_{track,m1} = p_{track,m3}$	0.12
$\bar{p}_{track,m1} = \bar{p}_{track,m3}$	0.5
$\bar{p}_{attack,m1} = \bar{p}_{attack,m3}$	1.4
$\alpha_{m1}$	0.5
$\alpha_{m2}$	0.99
$\alpha_{m3}$	0.99
$p_{m1}$	0.3
$p_{m2}$	0.3
$p_{m3}$	0.4

### 3.4.1 Mission 1

Mission 1 involves obtaining and maintaining an adequate track on a target. The variable,  $stracked$ , indicates whether the target is being tracked adequately and is initially false. The action consists of the variable,  $p_{track} \in [0, p_{track,max}]$ , which is the normalized energy expended in tracking during the current period. The probability

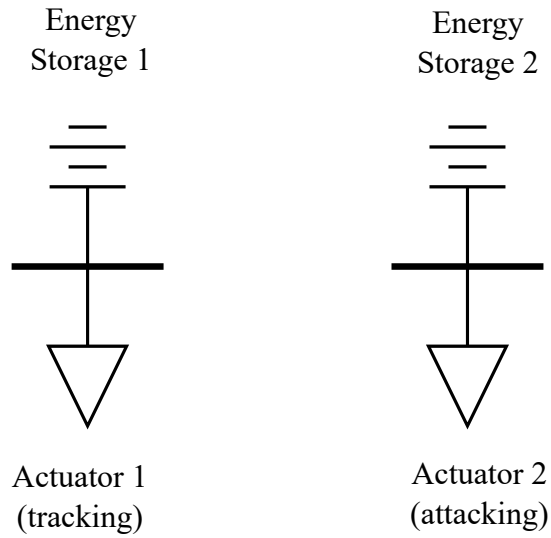


Figure 3.2: System 2 (Dedicated). Energy in system is allocated to a specific actuator and cannot be repurposed.

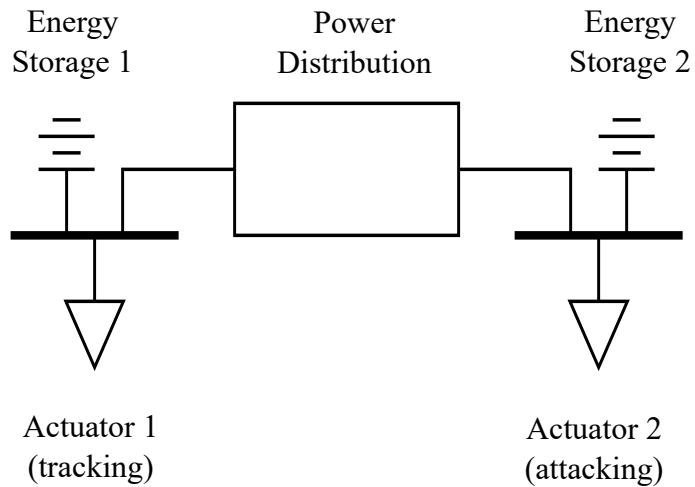


Figure 3.3: System 3 (Distributed). Energy is allocated to specific actuators but can be moved with limited power through distribution system.

of the target being tracked adequately in the next period is modeled as

$$P[s_{tracked,k+1}] = \begin{cases} 1 - e^{-\frac{p_{track}}{p_{track,m1}}} & s_{tracked,k} \\ 1 - e^{-\frac{p_{track}}{\bar{p}_{track,m1}}} & \bar{s}_{tracked,k}, \end{cases} \quad (3.4)$$

where  $p_{track,m1} > 0$  and  $\bar{p}_{track,m1} > 0$  are parameters that represent the difficulty of maintaining and obtaining an adequate track, respectively. Greater values of these parameters indicate that the task requires more energy to achieve a high probability of success. Generally,  $p_{track,m1} \leq \bar{p}_{track,m1}$ .

The functional representing the performance of a system for Mission 1 is given by

$$V_{m1}(x_0) = \frac{1 - \alpha_{m1}}{\alpha_{m1}^2} \sum_{k=0}^{\infty} \alpha_{m1}^k s_{tracked,k}, \quad (3.5)$$

where  $\alpha_{m1} \in (0, 1)$  is a parameter that represents temporal discounting. A greater value of this parameter indicates that the future is given greater weight (i.e., is discounted less with respect to the present). This functional represents the ability of the system to track the target continuously.

### 3.4.2 Mission 2

Mission 2 involves using energy to neutralize a target. The variable,  $s_{neut}$ , indicates whether the target has been neutralized and is initially false. The action consists of the variable,  $p_{attack} \in [0, p_{attack,max}]$ , which is the normalized energy expended in attacking during the current period.

The probability of the target being neutralized in the next period is described by

$$P[s_{neut,k+1}] = \begin{cases} 1 & s_{neut,k} \\ 1 - e^{-\frac{p_{attack}}{\bar{p}_{attack,m2}}} & \bar{s}_{neut,k}, \end{cases} \quad (3.6)$$

where  $\bar{p}_{attack,m2} > 0$  is a parameter that represents the difficulty of neutralizing the target. A greater value of this parameter indicates that the task requires more energy to achieve a high probability of success. The functional representing the performance of a system for Mission 2 is given by

$$V_{m2}(x_0) = \frac{1 - \alpha_{m2}}{\alpha_{m2}^2} \sum_{k=0}^{\infty} \alpha_{m2}^k s_{neut,k}, \quad (3.7)$$

where  $\alpha_{m2} \in (0, 1)$  is a parameter that represents temporal discounting. A greater value of this parameter indicates that the future is given greater weight (i.e., is discounted less with respect to the present). This functional represents the ability of the system to neutralize the target quickly.

### 3.4.3 Mission 3

Mission 3 involves obtaining and maintaining an adequate track on a target, and then using energy to neutralize it. The mission state involves two discrete state variables. The variable,  $s_{tracked}$ , indicates whether the target is being tracked adequately and is initially false. The second,  $s_{neut}$ , indicates whether the target has been neutralized and is also initially false. The action consists of two variables. The first,  $p_{track} \in [0, p_{track,max}]$ , is the normalized energy expended in tracking during the current period. The second,  $p_{attack} \in [0, p_{attack,max}]$ , is the normalized energy expended in attacking during the current period. The probability of the target being tracked adequately in the next period is modeled as

$$P[s_{tracked,k+1}] = \begin{cases} 1 - e^{-\frac{p_{track}}{p_{track,m3}}} & s_{tracked,k} \\ 1 - e^{-\frac{p_{track}}{\bar{p}_{track,m3}}} & \bar{s}_{tracked,k}, \end{cases} \quad (3.8)$$

where  $p_{track,m3} > 0$  and  $\bar{p}_{track,m3} > 0$  are parameters that represent the difficulty of maintaining and obtaining an adequate track, respectively. Greater values of these parameters indicate that the task requires more energy to achieve a high probability of success. Generally,  $p_{track,m3} \leq \bar{p}_{track,m3}$ . The probability of the target being neutralized in the next period is described by

$$P[s_{neut,k+1}] = \begin{cases} 1 & s_{neut,k} \\ s_{tracked,k} \left( 1 - e^{-\frac{p_{attack}}{\bar{p}_{attack,m3}}} \right) & \bar{s}_{neut,k}, \end{cases} \quad (3.9)$$

where  $\bar{p}_{attack,m3} > 0$  is a parameter that represents the difficulty of neutralizing the target. A greater value of this parameter indicates that the task requires more energy to achieve a high probability of success. Significantly, it is impossible to neutralize the target without obtaining an adequate track first. The functional representing the performance of a system for Mission 3 is given by

$$V_{m3}(x_0) = \frac{1 - \alpha_{m3}}{\alpha_{m3}^2} \sum_{k=0}^{\infty} \alpha_{m3}^k s_{neut,k}, \quad (3.10)$$

where  $\alpha_{m3} \in (0, 1)$  is a parameter that represents temporal discounting. A greater value of this parameter indicates that the future is given greater weight (i.e., is discounted less with respect to the present). This functional represents the ability of the system to track and then neutralize the target quickly.

### 3.4.4 Aggregate Mission Performance

The combined value of a given mission and system state is given by the weighted combination of these three value functionals:

$$V(x_0) = \sum_{n=1}^3 P_{mn} V_{mn}(x_0), \quad (3.11)$$

where  $P_{m1} \geq 0$ ,  $P_{m2} \geq 0$ , and  $P_{m3} \geq 0$  are the probabilities of performing Missions 1, 2, and 3, respectively, with  $P_{m1} + P_{m2} + P_{m3} = 1$ .

### 3.4.5 System State

The system state in each system is modeled differently. In System 1 (Shared), which has shared energy storage, the system state is a scalar,  $e$ , that represents the normalized stored energy. The energy stored in the next period is described by

$$e_{k+1} = e_k - p_{track,k} - p_{attack,k}. \quad (3.12)$$

In System 2 (Dedicated), there are two state variables,  $e_{track}$  and  $e_{attack}$ , which represent the normalized stored energy associated with each actuator. The energy stored in the next period is described by

$$e_{track,k+1} = e_{track,k} - p_{track,k} \quad (3.13)$$

$$e_{attack,k+1} = e_{attack,k} - p_{attack,k}. \quad (3.14)$$

In System 3 (Distributed), there are two additional action variables,  $p_{track,t,k}$  and  $p_{attack,t,k}$  that represent the flow of normalized energy from each actuator to the distribution system and by conservation of power

$$p_{track,t,k} + p_{attack,t,k} = 0. \quad (3.15)$$

These actions are constrained by the limits of the distribution system such that  $-p_{dist,max} \leq p_{track,t,k} \leq p_{dist,max}$  and  $-p_{dist,max} \leq p_{attack,t,k} \leq p_{dist,max}$ , where  $p_{dist,max}$  is the maximum normalized flow of energy through the distribution system in a period.

## 3.5 Results

For each configuration, the individual results from each mission were combined using the probabilities of each mission to obtain the aggregate expected performance of the system.

### 3.5.1 System 1 (Shared)

By solving the optimization problem, it can be seen how the mission performance varies with the initial normalized energy storage as shown in Figure 3.4. As expected, a higher available energy results in a higher expected performance.

### 3.5.2 System 2 (Dedicated)

Similar to System 1 (Shared), the probability of success is higher when higher energy is available for both tracking and attacking. This is visualized in Figure 3.5. However, if insufficient energy is available for either operation (tracking or attacking), the aggregate expected performance will be low, even if energy available for the other task is high. In such a system, it is necessary to maintain an appropriate balance between the available energy storage dedicated to each action. For example, it is possible to find the configuration of initial available energy that results in the highest aggregate expected performance by dividing a fixed amount of energy between the two actuators.



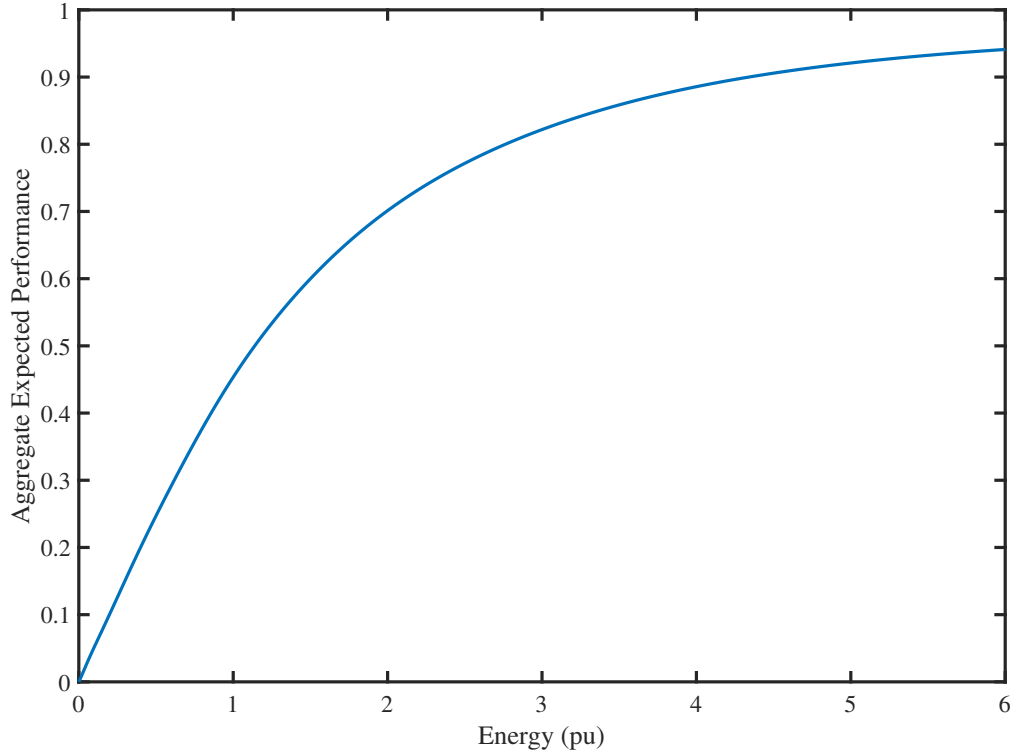


Figure 3.4: Variation of mission performance for System 1 (Shared)

### 3.5.3 System 3 (Distributed)

Similar to the previous configurations, the aggregate expected performance is higher when higher energy is available for both tracking and attacking. If insufficient energy is available for either tracking or attacking, the system can move energy through the power distribution system to achieve the given mission. This transfer is power limited, but it results in performance that is less sensitive to the initial allocation of energy than System 2 (Dedicated). Nonetheless, it is also possible to find the configuration of initial available energy that results in the highest aggregate expected performance by dividing a fixed amount of energy between the two actuators.

### 3.5.4 Comparison of Systems

When a given amount of energy is optimally allocated between the two actuators for both the dedicated and distributed energy storage systems, it is possible to compare the three systems on the basis of their aggregate expected performances. This comparison is shown in Figure 3.7. In this figure, it can be seen that the flexibility of the shared energy storage system results in higher expected performance regardless of the initial amount of available energy than the dedicated energy storage system. However, it can also be seen that, with a distribution system that is capable of handling 20% of the maximum load power and optimally allocated initial energy, the distributed energy storage system is capable of matching the performance of the shared energy

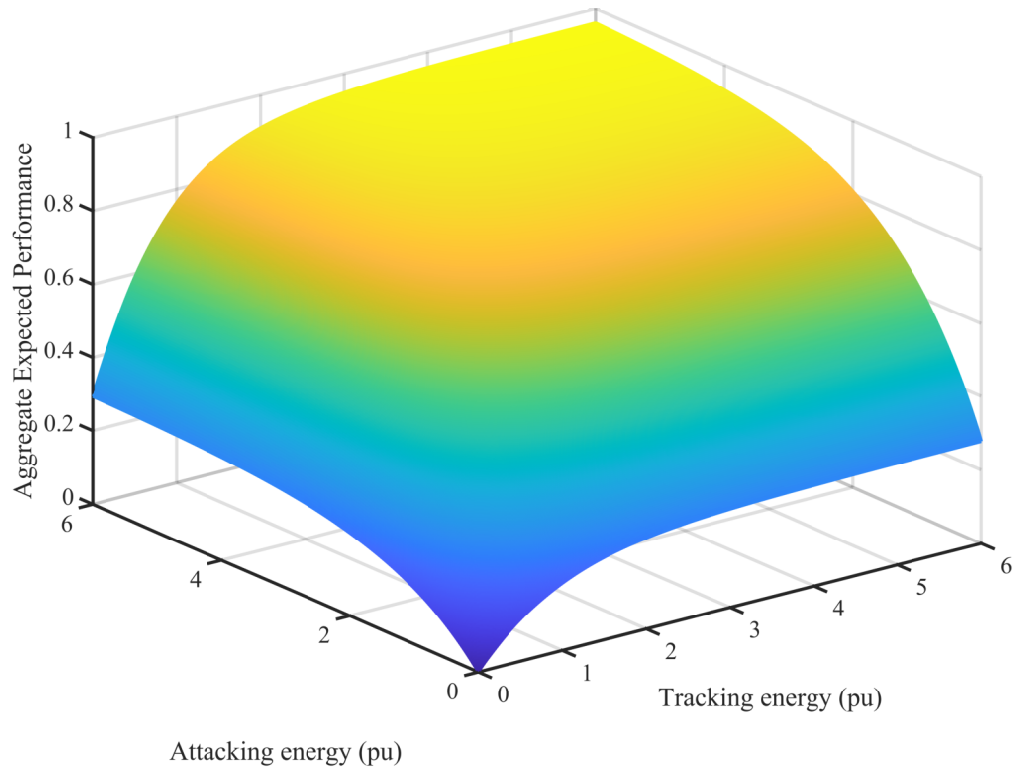


Figure 3.5: Variation of mission performance for System 2 (Dedicated)

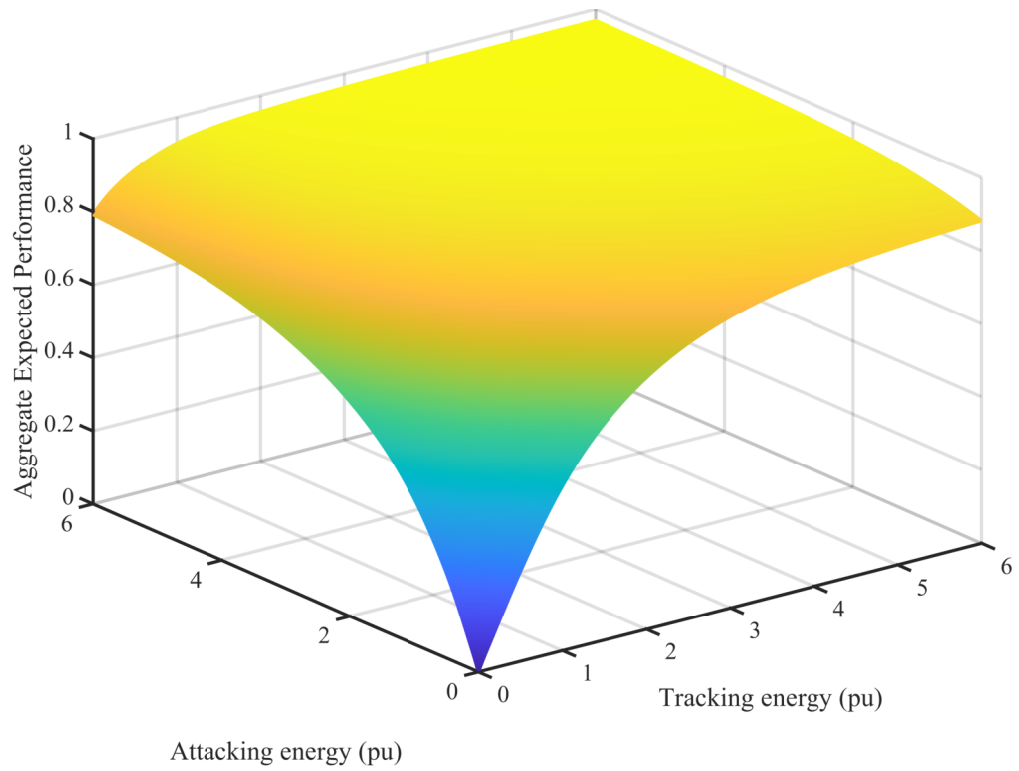


Figure 3.6: Variation of mission performance for System 3 (Distributed)

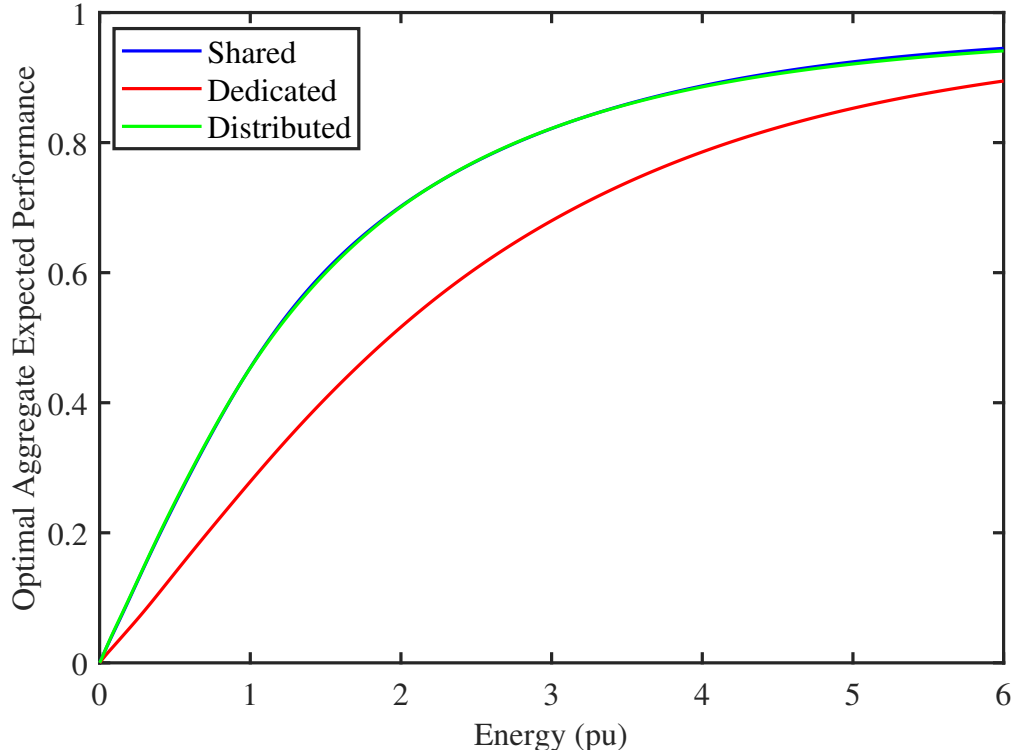


Figure 3.7: Performance comparison of System 1 (Shared), System 2 (Dedicated), and System 3 (Distributed). Energy for System 2 (Dedicated) and System 3 (Distributed) is allocated optimally between the two actuators.

storage system. This overlap between shared and dedicated energy storage systems is shown in Figure 3.8.

### 3.6 Conclusion

In this chapter, mission-based systems are considered more carefully from a mission perspective, as opposed to the earlier approaches involving fixed loads. Current optimal-control-based approaches represent dynamic interaction between the system and the mission. The results obtained using three different system arrangements are presented and compared. In more realistic scenarios, a ship might involve several more types of mission functions. Expansion to higher orders of system and mission nature is explored in the upcoming chapters along with sensitivity analysis to understand how much resolution in modeling system-mission interactions is needed to obtain useful performance measures.

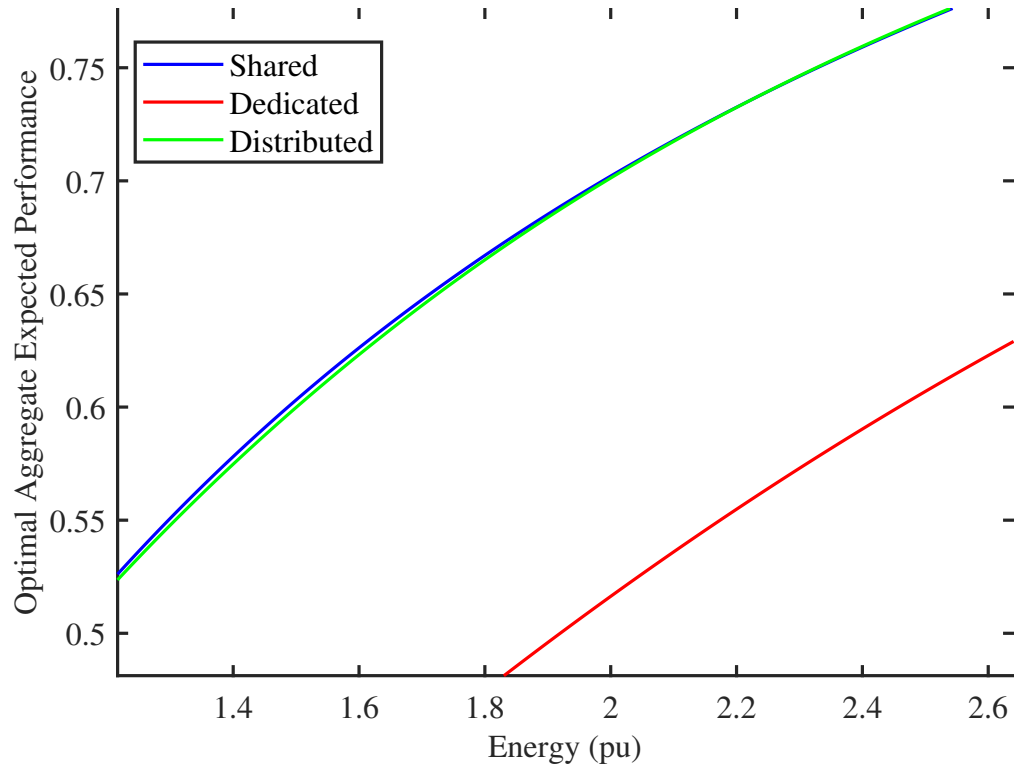


Figure 3.8: Performance comparison showing overlap between System 1 (Shared) and System 3 (Distributed)

## Chapter 4 Optimal Control-Based Performance Evaluation in the Presence of Energy Magazines

### 4.1 Introduction

In the current era of mission-oriented power systems, the optimal control and performance evaluation is done in the presence of dynamic loads based on the initial allocation of energy storage. In this chapter, the optimal performance of mission-based systems is evaluated in the presence of both dynamic loads which are involved in missions, and regular loads which are not involved in missions. The evaluation takes place in the presence of energy magazines which essentially involves a power converter with energy storage that is connected to one or more load. Such evaluation is essential because it helps in the understanding of allocation of energy to vital and non-vital loads, as opposed to a system which only considers mission loads. The optimization problem can be solved using Markov decision process (MDP) where state-space models can be used to represent missions and the systems to determine the maximum performance during missions.

The system considered in the previous chapter is fairly simple, but it represented a transformation of operability to a more mission-oriented perspective. Herein, this approach to operability evaluation is applied to a more conventional operability problem, allowing this work to bridge from conventional to mission-focused concepts of operability.

MDP-based approaches have widely been used across various areas to solve mission-oriented problems [44–47]. The application of MDP-based modeling has varied across different domains, but the common goal has always been to solve an optimization problem to achieve the maximum reward (e.g. in the form of maximum performance or minimum costs), given some constraints in the system.

In [48], MDP has been used to solve optimal power generation scheduling for shipboard power systems with and without energy storage. The goal was to minimize average fuel consumption in a system that is dynamic in nature. With the increase of renewable distributed generation, operating distribution systems has become a challenge due to the uncertainties in the system [49]. Therein, MDP-based modeling was used to minimize load curtailments and load sheddings given the uncertainties as system constraints. In [50], MDPs have been applied for the allocation of power in the hybrid energy storage system in electric vehicle. Optimal power allocation can ensure optimal performance by reducing energy loss and increasing battery life. The constraint is the fluctuation of power and the reward depends on the stored energy and the loss of energy.

Although the above mentioned works apply MDP-based modeling in systems with some form of energy storage, the systems are relatively static in nature but modeled as dynamic systems due to the system uncertainties. They are largely concerned with minimizing energy loss or maximizing the amount of stored energy. In other words, they do not consider how the system uses the stored energy to approach dynamic

mission power requirements.

How energy stored in a shipboard power system (e.g., in an energy magazine) is optimally applied to dynamic missions and how such systems are evaluated is considered herein. One of the first mentions about the concept of energy magazines in power systems was in [51]. In [52], the history and future trends in electric ships were discussed. Therein, it was mentioned that energy magazines need to be developed in power systems to provide support for pulse power loads, improved system stability, backup power, and integration with existing distribution voltages on multiple platforms. Energy magazines are used in systems of intermittent, pulsed, or dynamic nature. The concept of energy magazines was studied in [53] where the performance of three different types of energy storage was evaluated for integrating pulsed laser loads on electric ships. The energy magazines provide support to the power system by recharging during downtimes. In this way, the challenges posed by the intermittent nature of pulsed loads were overcome. Similarly, in [54], energy magazines were integrated in a pulsed power system which was modeled using a digital twin. Energy magazines were considered as a solution for shipboard power systems in the presence of high power and dynamic loads in [55]. The resources were managed based on the priorities of loads in a constrained power system.

The primary contributions of this chapter are

1. to extend optimal-control-based evaluation to practical shipboard systems, including systems with considerable energy storage used to serve mission loads, and
2. to align conventional and optimal-control-based operability concepts to demonstrate the connection between and the evolution of these concepts.

## 4.2 System Description

A notional integrated power and energy system has been developed. The system consists of two main gas turbine generators and two auxiliary gas turbine generators with proportional power sharing controls. The loads are propulsion motor modules, service loads, and mission loads. Propulsion motor modules comprise the largest loads in the system. In this system, there are four propulsion loads. Ship service loads are supplied from eight low voltage ac load centers. There are four dc mission loads in the system which are interfaced to the medium voltage ac system through eight energy magazines. The energy magazines are sized to be able to supply the full power demand for a designated amount of time. The system has four zones, with the outer zones 1 and 4 having the same energy magazine ratings and the inner zones 2 and 3 having the same energy magazine ratings. This symmetry as well as the bilateral symmetry is exploited in the studies presented herein. The ratings of each of the components is given in Table 4.1

A representation of the notional integrated power and energy system is considered in this study to understand the effect of energy magazines. This representation exploits the symmetry of the notional system. It consists of inner zone of same rating

Table 4.1: Ratings of System Components

Component name	Rating (MW)
Main turbine generator	$2 \times 35$
Auxiliary turbine generator	$2 \times 4.5$
Propulsion motor module	$4 \times 15$
Outer zone mission	$2 \times 2.0$
Inner zone mission load inner	$2 \times 1.0$
Outer zone energy magazine	$4 \times 2.0$
Inner zone energy magazine	$4 \times 1.0$
Outer zone service load	$4 \times 1.0$
Inner zone service load	$4 \times 1.0$

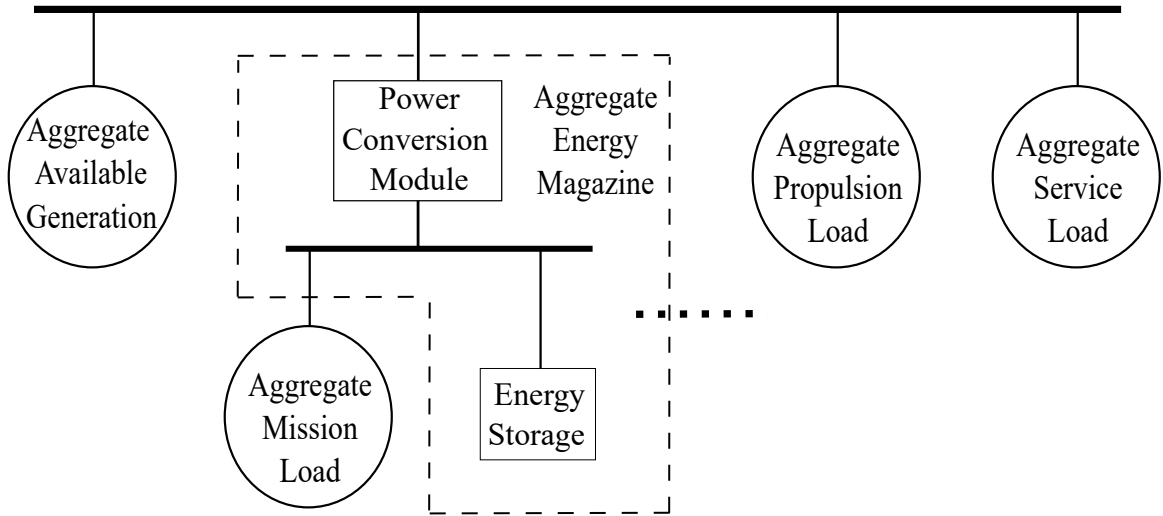


Figure 4.1: Diagram of the simplified representation of the notional system. Symmetry is used to aggregate generation, energy magazines, and propulsion, service, and mission loads.

aggregated together and outer zone components of same rating aggregated together. There are auxiliary turbine generators, energy magazines, missions loads, propulsion loads, and service loads. The main turbine generators are not used in this simplified representation. The auxiliary turbine generators provide power to all the loads and the energy magazines. Four energy magazines of the same rating are on the inner zone and four energy magazines of a different rating are on the outer zone. The four energy magazines on each zone are connected to two mission loads of the same rating. In addition, there are two other loads- service loads and propulsion motor module. The four energy magazines and two mission loads of the same rating (on the same zone) are aggregated together to be treated as a single energy magazine and a single mission load. The overall system has been illustrated in Figure 4.1. The total ratings of each of the components is given in Table 4.2.

Table 4.2: Mission Parameters

Parameter	Value
Total available generation	9 MW
Total outer zone energy magazine power rating	8 MW
Total inner zone energy magazines power rating	4 MW
Total outer zone mission load demand	3.2 MW
Total inner zone mission load demand	1.6 MW
Total propulsion load demand	1.25 MW
Total service load demand	6.4 MW
Weight of mission load	2
Weight of propulsion load	0.75
Weight of service load	1

### 4.3 Operability Formulation

The metric operability was defined in the previous chapter and in [13, 26] to determine the effectiveness of power systems in responding to mission loads. This metric measures the degree to which the performance of the power system contributes to mission effectiveness in a particular scenario. Initially, operability was equivalent to a weighted sum of power flows to loads:

$$O = \frac{\sum_{k=k_0}^{k_{end}} \sum_{i=1}^I w_i P_i(k)}{\sum_{k=k_0}^{k_{end}} \sum_{i=1}^I w_i P_{max,i}(k)}, \quad (4.1)$$

where  $I$  is the number of loads in the system,  $P_i(k)$  is the power consumption of load  $i$  at discrete period (of time)  $k$ ,  $P_{max,i}(k)$  is the maximum (or demanded) power of load  $i$  at period  $k$ , and  $w_i$  is a mission-specific, potentially time-varying weighting function indicating the relative importance of load  $i$ . The period of time considered is  $k_0, \dots, k_{end}$ .

Operability is therefore the sum of weighted power flows of all loads in a system with respect to the sum of weighted maximum power flows of the loads, and it is a widely adopted means of evaluating system performance. The connection between this formulation of operability and MDPs is explored in the following section.

### 4.4 Mission Scenario

The mission state consists of a discrete state variable  $s$ , which indicates the progress. A mission involving a sudden engagement in which the generator lineup is insufficient to meet the system's loads is considered. The system must deliver power while additional generation is brought online. This situation is modeled in two ways: fixed-duration and probabilistic. The system state is the energy stored in each of the aggregate energy magazines.



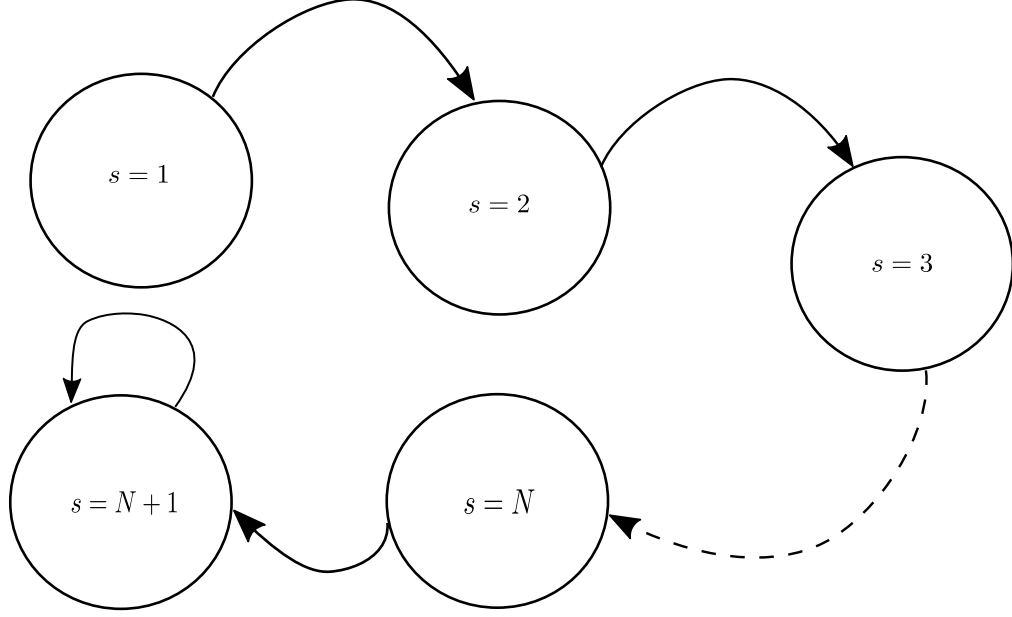


Figure 4.2: State transition diagram for the fixed-duration model.

#### 4.4.1 Fixed-Duration Model

In the fixed-duration model, there are  $N + 1$  discrete states. The mission transitions from state 1 to state  $N + 1$  in  $N$  steps. Rewards are accumulated on the transitions from  $s = 1$  to  $s = N + 1$ . The possible state transitions of the fixed-duration model are illustrated in Figure 4.2. The action consists of four variables. The first,  $p_{ml1} \in [0, p_{ml,max1}]$ , is the power applied to the outer zone mission loads during the current period. The second,  $p_{ml2} \in [0, p_{ml,max2}]$ , is the power applied to the inner zone mission loads during the current period. The third,  $p_{em1} \in [0, p_{em,max1}]$ , is the power applied to the outer zone energy magazines during the current period. The fourth,  $p_{em2} \in [0, p_{em,max2}]$ , is the power applied to the inner zone energy magazines during the current period.

The actions are constrained such that the total power flowing each energy storage is limited by the available energy, and the total power flow from the generation is limited by the available power:

$$(p_{ml1} - p_{em1})\Delta t \leq e_{em1} \quad (4.2)$$

$$(p_{ml2} - p_{em2})\Delta t \leq e_{em2} \quad (4.3)$$

$$p_{lc} + p_{pl} + p_{em1} + p_{em2} \leq p_{g,max}, \quad (4.4)$$

where  $\Delta t$  is the time step,  $e_{em1}$  represents energy stored in outer zone energy magazines,  $e_{em2}$  represents energy stored in inner zone energy magazines,  $p_{lc}$  represents service load power,  $p_{pl}$  represents propulsion power, and  $p_{g,max}$  represents the maximum generator power available.

The instantaneous reward for the mission is given by the ratio

$$R = \frac{1}{V_{norm}} \frac{(w_{ml}(p_{ml1} + p_{ml2}) + w_{lc}p_{lc} + w_{pl}p_{pl})}{(w_{ml}(p_{ml,max1} + p_{ml,max2}) + w_{lc}p_{lc,max} + w_{pl}p_{pl,max})}, \quad (4.5)$$

where  $w_{ml}$  is the weight of mission load,  $w_{lc}$  is the weight of service load,  $w_{pl}$  is the weight of propulsion load,  $p_{lc,max}$  is the maximum service load demand,  $p_{pl,max}$  is the maximum propulsion load demand, and

$$V_{norm} = \frac{1 - \alpha^N}{1 - \alpha}, \quad (4.6)$$

with this value approaching  $N$  in limit if  $\alpha = 1$ .

The reward is normalized so the maximum value of the value function  $V$  is one if all load demands are satisfied.

#### 4.4.2 Probabilistic Model

In the probabilistic model, there are two discrete states. The first state represents the period of time in which the system operates with insufficient available generation, and the second state represents the time when the system has sufficient generation. Rather than modeling the interval of time required to transition between these states deterministically as represented in the fixed-duration model, it is represented stochastically. The system can transition from state 1 to state 2 in one step with a given probability.

The probability of transition from one state to another is  $p$  which is a function of  $\hat{\alpha}$  and the total number of states,  $N$ . The probability of remaining in current state is  $1 - p$ . This is illustrated in Figure 4.3. The action consists of the four variables as discussed above. The instantaneous reward function for the system is given by (4.5). The temporal discounting parameter  $\hat{\alpha} \in (0, 1]$  may be different than the value  $\alpha$  used in the fixed-duration model.

Using the fixed-duration model, a system with all load demands satisfied will have a performance of

$$V_{fixed} = \sum_{k=0}^{N-1} \alpha^k \frac{1}{V_{norm}}, \quad (4.7)$$

which is unity due to the normalization factor  $V_{norm}$ .

For the probabilistic model, the expected reward for a system with all load demands satisfied is

$$V_{prob} = \sum_{j=0}^{\infty} p(1-p)^{j-1} \frac{1}{V_{norm}} \left( \frac{1 - \hat{\alpha}^j}{1 - \hat{\alpha}} \right) \quad (4.8)$$

$$= \frac{1}{V_{norm}} \frac{1}{1 - (1-p)\hat{\alpha}}, \quad (4.9)$$

and this is an expected value rather than a deterministic value because the number of steps required to reach the final state is random. To ensure that the fixed-duration

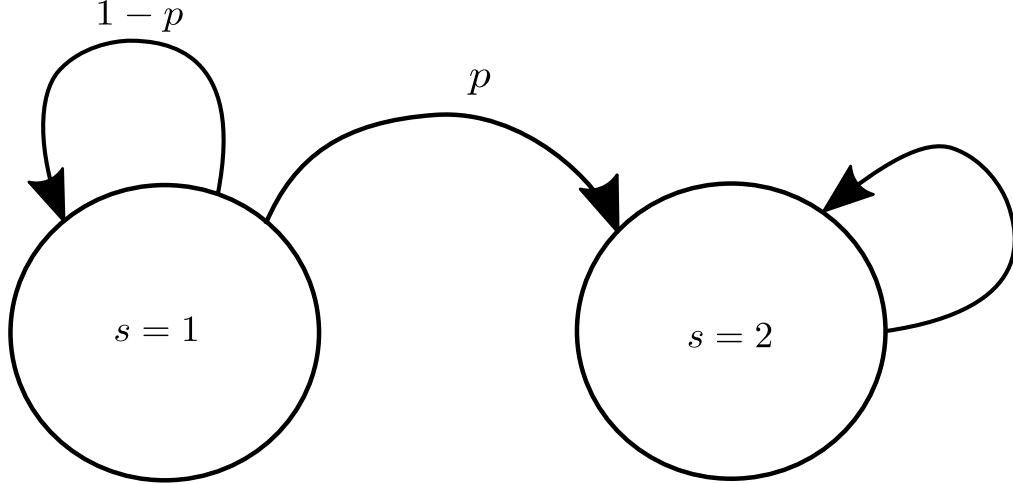


Figure 4.3: State transition diagram for the probabilistic model.

and probabilistic models are normalized equivalently,  $V_{prob} = 1$ , or

$$(1 - p)\hat{\alpha} = 1 - \frac{1}{V_{norm}}. \quad (4.10)$$

This creates a degree of freedom in representing the fixed-duration scenario with a probabilistic model. This relationship between the temporal discounting parameter and the transition probability is illustrated in Figure 4.4.

Modeling stochastically using one state transition reduces solution run time and complexity. It is also possible that the probabilistic model more accurately represents some of the problem uncertainty. The degree to which the probabilistic model matches the fixed-duration model for different configurations is considered below.

#### 4.5 Solution Algorithm

The optimization problem is solved using value function iteration. The non-linear optimization method `fmincon` in MATLAB is used with the constraints described in the earlier section. Using `fmincon`, the solution is stored each time, which is later used as the starting guess for the next iteration. In this way, a total of 100 iterations is performed to converge to a final solution. This problem is two-dimensional for two aggregate energy magazines. To solve the problem, the number of points in each dimension is arbitrarily considered as 11, ranging linearly from 0 MJ to 400 MJ. In this way, a representation of the performance,  $V$  is solved by using a specific number of grid points for the problem.

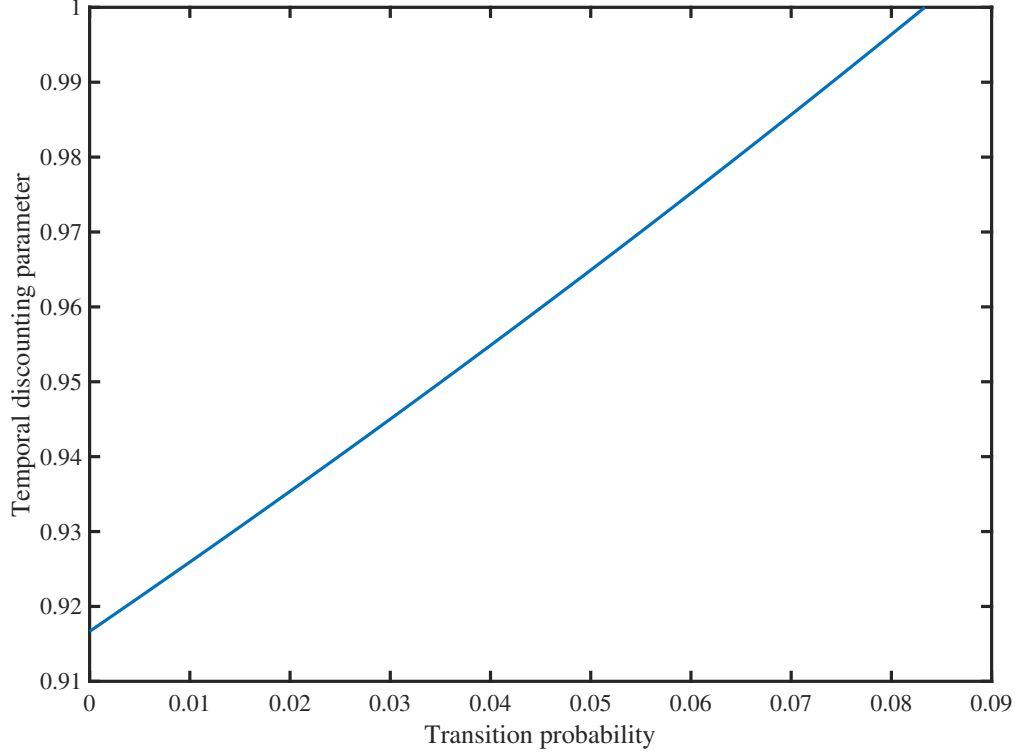


Figure 4.4: Temporal discounting factor  $\hat{\alpha}$  with transition probability  $p$  with  $\alpha = 1$  and  $N = 12$ .

## 4.6 Results and Discussion

### 4.6.1 Relationship between Operability and Value Function

In Section 4.3, the operability metric was discussed as means of evaluating system performance. In Section 4.4, the expected reward  $V$  was defined, and it was mentioned that the two metrics are similar. In the modeling with fixed duration presented in this paper, the discounting factor  $\alpha = 1$ , time step  $\Delta t = 10$  and the number of steps  $N = 12$ . The weights and load demands, i.e., the terms in the denominators of both the operability and value functions, are constant. Hence, the operability can be expressed as

$$\begin{aligned}
 O &= \frac{\sum_k \sum_i w_i P_i(k)}{\sum_k \sum_i w_i P_{max,i}} \\
 &= \frac{1}{N \sum_i w_i P_{max,i}} \sum_k \sum_i w_i P_i(k).
 \end{aligned} \tag{4.11}$$

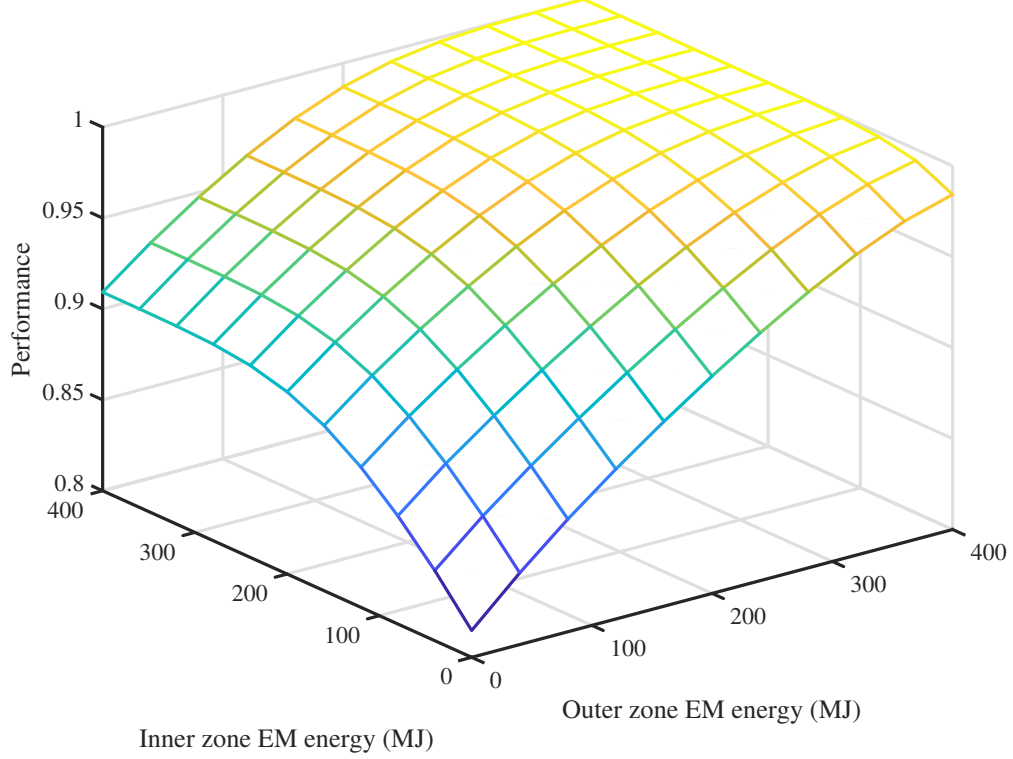


Figure 4.5: Performance of notional system for fixed-duration model.

In the same way, the value function can be expressed as

$$\begin{aligned}
 V &= \frac{1}{N} \sum_k \frac{\sum_i w_i P_i(k)}{\sum_i w_i P_{max,i}} \\
 &= \frac{1}{N \sum_i w_i P_{max,i}} \sum_k \sum_i w_i P_i(k).
 \end{aligned} \tag{4.12}$$

Thus, in the given scenario with  $\alpha = 1$  and the denominators being constant, operability is exactly equal to the value function of the MDP. In more general situations, these values may be expected to be correlated, but not necessarily identical.

#### 4.6.2 Results for the Two Models

The solution to the fixed-duration model is shown in Figure 4.5. As expected, higher initial energy in the energy magazine results in higher performance. The performance is more highly dependent on the energy stored in the outer zone energy magazines because the outer zone mission loads require more power. As long as a certain amount of energy is present in the outer and inner zones, the performance saturates because a fixed amount of energy is required to complete a fixed duration scenario.

In the probabilistic model, the problem is solved using different combinations of temporal discounting parameter and transition probability. In particular, six transition probabilities linearly distributed between 0 and  $1/N$  are selected along with

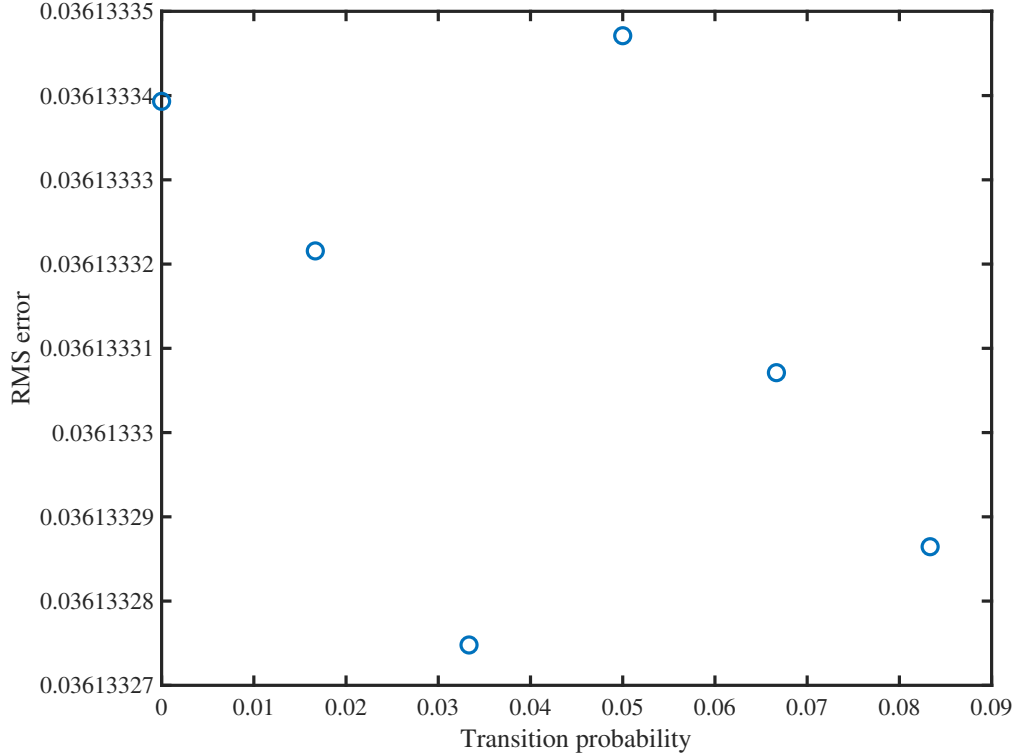


Figure 4.6: Variation of rms error between fixed-duration and probabilistic model with transition probability,  $p$ . The relatively low values of error indicate that the two types of modeling yield almost identical results. There is little variation amongst each of the errors indicating that it is not dependent on the combination of transition probability  $p$  and discounting parameter  $\hat{\alpha}$ .

the corresponding temporal discounting parameter from (4.10) (or Figure 4.4). Value function iteration was performed for each combination and the rms error with respect to the fixed-duration model was computed over the 121 grid points. This comparison is shown in Figure 4.6.

As can be seen, the error or similarity with the fixed-duration model is not dependent on the combination selected. Moreover, the solutions themselves do not appear visually distinct. In Figure 4.7, the results with  $p = 0$  and  $\hat{\alpha} = 0.9167$  are shown, and in Figure 4.8, the results with  $p = 1/N$  and  $\hat{\alpha} = 1$  are shown.

These results are visually indistinguishable, which is likely a result of the manner of ensuring consistent normalization. While the particular combination does not appear to matter, there can be algorithmic convergence differences associated with different choices of  $\hat{\alpha}$ .

As seen in the figures for the probabilistic model, the performance is higher when the initial energy in the energy magazine is higher. Similar to the fixed-duration model, it is more highly dependent on the energy stored in the outer zone energy magazines. The maximum performance is however less than that of fixed-duration model, indicating that there might be some loss in accuracy when the system is

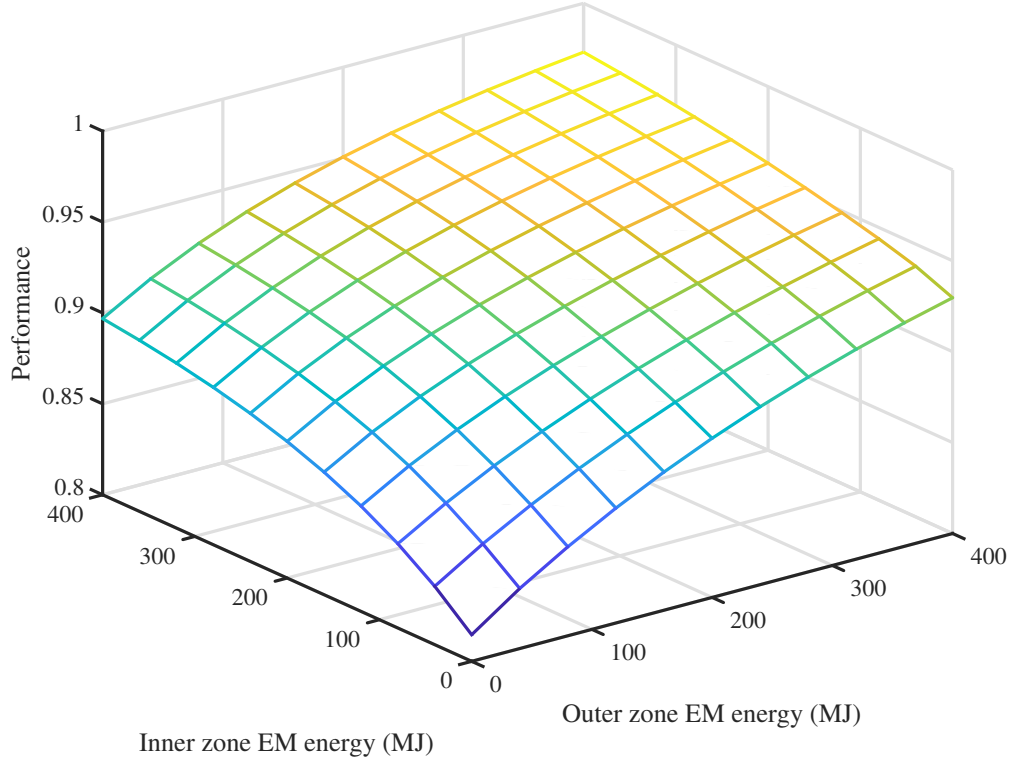


Figure 4.7: Performance of notional system for probabilistic model when transition probability  $p = 0$  and discounting parameter  $\hat{\alpha} = 0.9167$ .

modeled stochastically. Although visually similar, there are some differences in the performances as indicated by the rms errors in Figure 4.6. Hence, the choice of modeling is a compromise between solution run time and accuracy.

#### 4.7 Conclusion

In this chapter, MDP-based state-space models have been used to evaluate the optimal performance of mission-based systems in presence of regular loads and energy magazines connected to dynamic mission loads. The mission scenarios were modeled in two different ways: fixed-duration model and probabilistic model. Results for the two modeling approaches have been presented to show how the two types of modeling resemble and vary, along with a numerical comparison of the performances. The similarity between MDP-based performance evaluation using value function iteration and the widely adopted mission performance evaluation metric, operability has also been explored. In the next section, a more robust approach is considered for the evaluation of system performance using MDP-based approach.

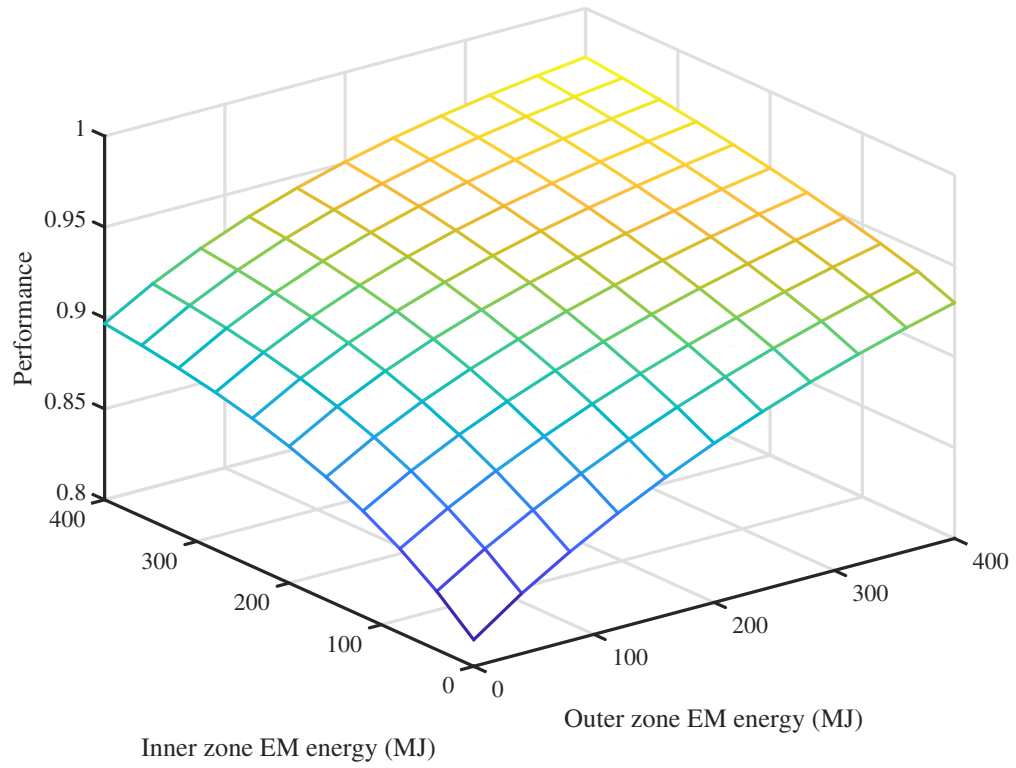


Figure 4.8: Performance of notional system for probabilistic model when transition probability  $p = \frac{1}{N}$  and discounting parameter  $\hat{\alpha} = 1$ .



## Chapter 5 Robust Optimal Control-Based Evaluation Considering System Trade-offs

### 5.1 Introduction

Mission-oriented power systems are designed to support the performance of specific missions. To evaluate the potential performance, it is necessary to understand how the system will help complete the mission when controlled optimally.

The significance of mission profile on system performance has been recognized. In [8, 9, 56, 57], the impact of mission profile on reliability of power-electronics-based systems was analyzed. Similarly, in [58], the reliability was predicted for multilevel converters, and a synchronous buck dc-dc converter was used in mission profile-based optimization of a wearable power system [59]. Mission profile-based analysis have also been used to predict the lifetime of single-phase transformerless photovoltaic inverters [60], to study the reconfiguration of hybrid shipboard power systems [61], and to study the optimal sizing of hybrid electric vehicle components [62]. In addition, the impact of mission profile on the performance of uncrewed aerial vehicles have been discussed in [6, 7, 63].

In shipboard power systems, a mission-load oriented metric called operability has been used [13, 26]. Operability has generally been described as a weighted integral of load power flows, which provides a quantitative measure of the ability of the power system to meet the demand for power under different operating conditions. The basic idea behind this approach is to evaluate the performance of the power system by considering the power flows through the system and the importance of each load in the overall mission. This can be achieved by defining a set of weighting factors that reflect the criticality of each load in achieving the mission objectives. Typically, such evaluations have either involved static load demands and weights (but perhaps physical or cyber disruptions) with weights dictating priority [13, 26, 62]. Dynamic load demands and weights have also been considered in which Markov chain or mission narrative approaches are used to construct dynamic load demands and weights, but these fixed profiles are not responsive to system performance [1, 27, 37, 38].

An evolution in mission-oriented power system evaluation is necessary. In particular, to develop a reasonable understanding of the potential performance of such systems, it is necessary to consider the dynamic interplay between mission and system because there is an intrinsic connection to mission performance. This will result in a break from evaluation using static load profiles and weights and will serve as an improved basis for system evaluation, as the basis for system control development, and as a framework for better understanding the role of mission requirements in power system design. This evolution, initial steps of which are described in [16, 17], involves transforming the evaluation problem into an optimal control problem, the solution of which can reveal the potential performance of a power system implementation.

This approach of modeling the combined system and mission as a hybrid discrete/continuous, stochastic/deterministic dynamic system and combining with mission-

specific rewards to be optimized is naturally represented as a Markov decision process (MDP). The applications of MDP-based modeling vary across literature, but the common goal is to solve an optimization problem to achieve the maximum reward (e.g. in the form of maximum performance or minimum costs), given some constraints in the system and its dynamics.

One area of application of mission or situation-based MDP is the optimal dispatch of medical evacuation assets [44]. In this work, the goal was to maximize steady-state system utility based on the number of casualties, priority level, and locations of casualty event and ambulatory helicopters. In [45], the possibility of cyber data attacks and system vulnerability was analyzed in a dynamic environment consisting of smart grids. Like before, the goal was to maximize the aggregate reward (e.g. financial benefits, system stability, etc.) based on the intruder's current actions.

MDP-based modeling is highly useful in cases where the power system needs to behave differently from traditional power systems, such as calamities and cases with load fluctuations. MDP-based strategies have been used to predict hurricane probability to minimize generation costs and load curtailments [46]. A similar goal was pursued in [47], where dynamic programming and iteration were used in the case of extreme weather events. With the increase of renewable distributed generation, operating distribution systems has become a challenge due to the uncertainties in the system [49]. Therein, MDP-based modeling was used to minimize load curtailments and load shedding given the uncertainties as system constraints. Real-time pricing can also be predicted based on the total requested energy for residential energy management (REM) in smart grids using MDP [64].

The application of MDP-based modeling can be extended to autonomous systems in aircraft and spacecraft. In [65], an autonomous spacecraft system has been modeled by solving an MDP problem. In [66], the control system in an autonomous aerial vehicle was modeled to increase flight safety and decrease mission failures to ensure that they would avoid obstacles in hostile environments. Similarly, it has been used to analyze the behavior through different stages of flight operations based on mission requirements [67] and in path planning [68, 69].

MDPs have also found utility closer to the application area considered herein. In [48], the optimal power generation scheduling for shipboard power systems with and without energy storage is solved using MDP. The goal was to minimize average fuel consumption in a system that is dynamic in nature. Allocation of energy storage has been considered in [50, 70]. The priority of charging and discharging was developed using MDP in [70]. In [50], MDPs have been applied for the allocation of power in the hybrid energy storage system of an electric vehicle. Optimal power allocation ensured optimal performance by reducing energy loss and increasing battery life. The constraint was the fluctuation of power and the reward depended on the stored energy and the loss of energy.

Herein, the fundamental objective is to advance the evaluation of mission-oriented power systems. The specific contributions of this chapter toward this objective are

1. to articulate the evaluation of mission-oriented power system performance as an optimal control problem, allowing the dynamic interaction between the system

and the mission to be considered,

2. to demonstrate the optimal-control-based approach to evaluation in a notional, but representative, set of system implementations and missions, and
3. to illustrate the types of system trade offs that can be considered using this approach.

## 5.2 Problem Formulation

The formulation of the problem has been discussed in Chapter 3 in Section 3.3.

The Bellman equation is solved to evaluate the expected mission performance of the system given a starting state. This allows for various system implementations with different component ratings or interconnections to be compared objectively on the basis of their mission performance. As a byproduct, the solution also yields the optimal control policy for the system implementations. This understanding of how to control the system optimally could be valuable in developing the system control implementation.

## 5.3 Notional System And Missions

A notional system employing various actuators for performing different types of missions is considered. Alternative implementations are considered, and their performance in a set of notional missions is evaluated.

The notional system and missions are explicitly not connected to any practical real world system, but they are intended to convey many salient features such as scarcity of resources, competing uses of resources, and multiple approaches to completing missions. Power, energy, and time are normalized throughout.

In Mission 1 (Search and Destroy), two of the actuators are required for success. The effectiveness of the second actuator depends on the effective application of energy to the first actuator, and success is measured by the successful application of energy to the second actuator. An example of such a mission might involve obtaining and maintaining an adequate track on a target while using energy to attack the target.

In Mission 2 (Contested Transit), two of the actuators are required for success. Success is measured by application of energy to the first actuator, but the use of the first actuator can be limited by situational conditions that can be remedied by the application of energy to the second actuator. An example of such a mission might involve moving along a path which may be occasionally obstructed by targets that can be removed by using energy to attack.

In Mission 3 (Fight or Flight), combinations of actuators may be employed to achieve success. An example of such a mission might involve a need to escape from a threat. Energy may be used to track and attack the threat, but energy can also be used to move, thus evading the threat.

In these missions, success requires different applications of energy to the system's actuators. The parameters for the notional problem are given in Table 5.1.

Table 5.1: Notional Problem Parameter Values

$\Delta t$	1 pu
$N$	60
$p_{track,max}$	1 pu
$p_{attack,max}$	1 pu
$p_{move,max}$	1 pu
$\beta_{track}$	0.489 pu
$\bar{\beta}_{track}$	1.96 pu
$\beta_{attack}$	9.49 pu
$k_{move}$	$\frac{35}{N \cdot 20^{\frac{3}{p_{move,max}}}}$ pu
$\bar{p}_{move,max}$	$(5/35)^3$ pu
$\alpha_{m1}$	$0.99^{\frac{1}{N}}$
$\alpha_{m2}$	$0.01^{\frac{1}{N}}$
$\alpha_{m3}$	$0.50^{\frac{1}{N}}$
$P_{obs}$	$\frac{3}{60}$
$p_{e,max}$	$\infty$
$p_{Y,e,max}$	$\infty$
$p_{Y,t,max}$	0.1

### 5.3.1 Mission 1 (Search and Destroy)

In this mission, a target must be tracked and neutralized. The mission state consists of a discrete state variable  $s$ , which indicates the mission progress. When  $s = 1$ , the target has not been adequately tracked, and this is the initial value of  $s$ . When  $s = 2$ , the target has been adequately tracked but not neutralized. When  $s = 3$ , the target has been neutralized. The mission action consists of two variables. The first,  $p_{track} \in [0, p_{track,max}]$ , is the power applied to tracking during the current period. The second,  $p_{attack} \in [0, p_{attack,max}]$ , is the power applied to attacking during the current period. The probability of being in the state where the target has not been tracked adequately in the next period is modeled as

$$P[s_{k+1} = 1] = \begin{cases} e^{-\frac{p_{track,k}}{\beta_{track}}} & \text{if } s_k = 1, \\ e^{-\frac{p_{attack,k}}{\beta_{attack}}} e^{-\frac{p_{track,k}}{\beta_{track}}} & \text{if } s_k = 2, \\ 0 & \text{if } s_k = 3, \end{cases} \quad (5.1)$$

where  $\bar{\beta}_{track} > 0$ ,  $\beta_{track} > 0$ , and  $\beta_{attack} > 0$  are parameters that represent the difficulty of obtaining a track on, maintaining a track on, and neutralizing a target. A greater value of these parameters indicates that these tasks require more power to achieve a high probability of success. Generally,  $\beta_{track} \leq \bar{\beta}_{track}$ . The probability of being in the state where the target has been tracked adequately but not neutralized

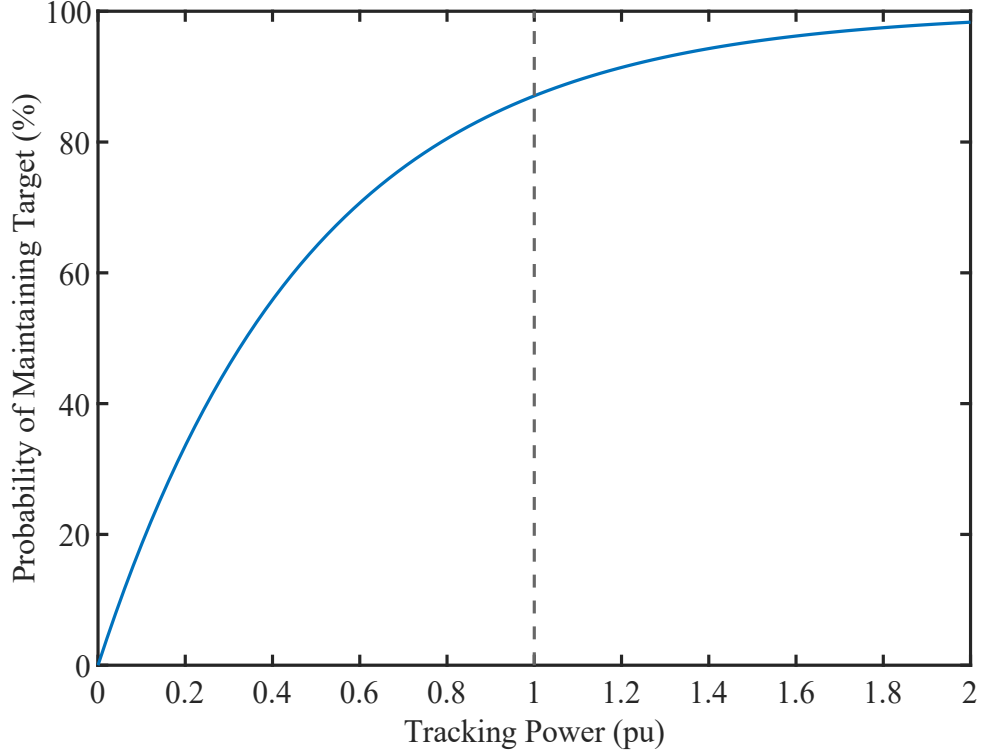


Figure 5.1: Probability of maintaining track on target versus tracking power. Power rating of tracking actuator is vertical line.

in the next period is modeled as

$$P[s_{k+1} = 2] = \begin{cases} 1 - e^{-\frac{p_{track,k}}{\beta_{track}}} & \text{if } s_k = 1, \\ e^{-\frac{p_{attack,k}}{\beta_{attack}}} \left( 1 - e^{-\frac{p_{track,k}}{\beta_{track}}} \right) & \text{if } s_k = 2, \\ 0 & \text{if } s_k = 3. \end{cases} \quad (5.2)$$

The probability of being in the state where the target has been neutralized in the next period is modeled as

$$P[s_{k+1} = 3] = \begin{cases} 0 & \text{if } s_k = 1, \\ 1 - e^{-\frac{p_{attack,k}}{\beta_{attack}}} & \text{if } s_k = 2, \\ 1 & \text{if } s_k = 3. \end{cases} \quad (5.3)$$

The probability functions described above have a similar characteristic. While not tied to the performance of any real actuator, these characteristics have the practical feature of increasing probability of success with higher power with diminishing incremental return. This is illustrated in Figure 5.1, where the probability of maintaining a track on a target is plotted with respect to the tracking power.

The possible mission state transitions are summarized in Figure 5.2.

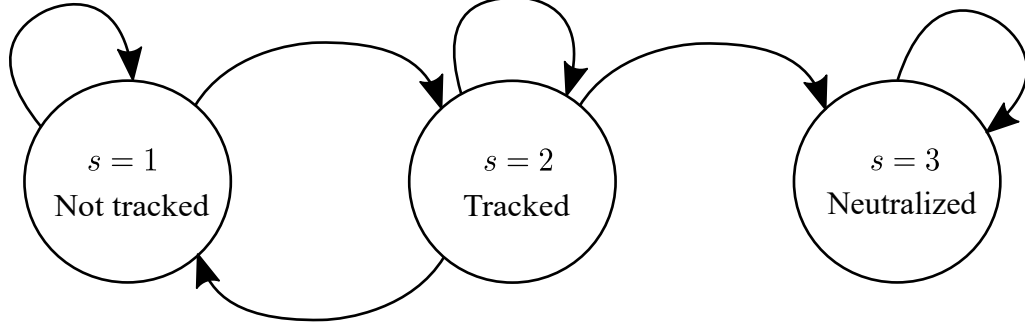


Figure 5.2: State transition diagram for Mission 1 (Search and Destroy).

The functional representing the performance of the system for Mission 1 (Search and Destroy) is given by

$$V = \frac{1}{\alpha} \sum_{k=0}^{\infty} \alpha^k i_{trans,k}, \quad (5.4)$$

where  $\alpha \in (0, 1]$  is a parameter that represents temporal discounting. A greater value of this parameter indicates that the future is given greater weight (i.e., is discounted less with respect to the present). The indicator variable  $i_{trans,k}$  is one on the transition from  $s_k = 2$  to  $s_{k+1} = 3$ , and is zero otherwise. The functional is normalized such that its maximum possible value is one, which occurs if the target is neutralized at  $s_k = 2$ .

### 5.3.2 Mission 2 (Contested Transit)

In this mission, movement along a path is required, but movement may occasionally be obstructed by a target that can be neutralized by attacking. The mission state involves one continuous and one discrete state variable. The continuous state variable  $l$  indicates the distance traveled along a path and is initially zero. The discrete state variable  $s$  is a logical variable that indicates whether the path is obstructed by a target, and is initially false. The mission action consists of two variables. The first,  $p_{move} \in [0, p_{move,max}]$ , is the power applied to moving during the current period. The second,  $p_{attack}$ , is the power applied to attacking during the current period. The distance traveled along a path in the next period is modeled as

$$l_{k+1} = l_k + v_{move}(p_{move,k})\Delta t, \quad (5.5)$$

where the function  $v_{move}(\cdot)$  mapping power applied to moving to distance traveled is given by

$$v_{move}(p_{move}) = k_{move} \sqrt[3]{p_{move}}, \quad (5.6)$$

and  $k_{move} > 0$  is a scaling parameter. The power applied to moving is limited such that  $l_{k+1} \leq 1$ :

$$p_{move,k} \leq -v_{move}^{-1}(1 - l_k). \quad (5.7)$$

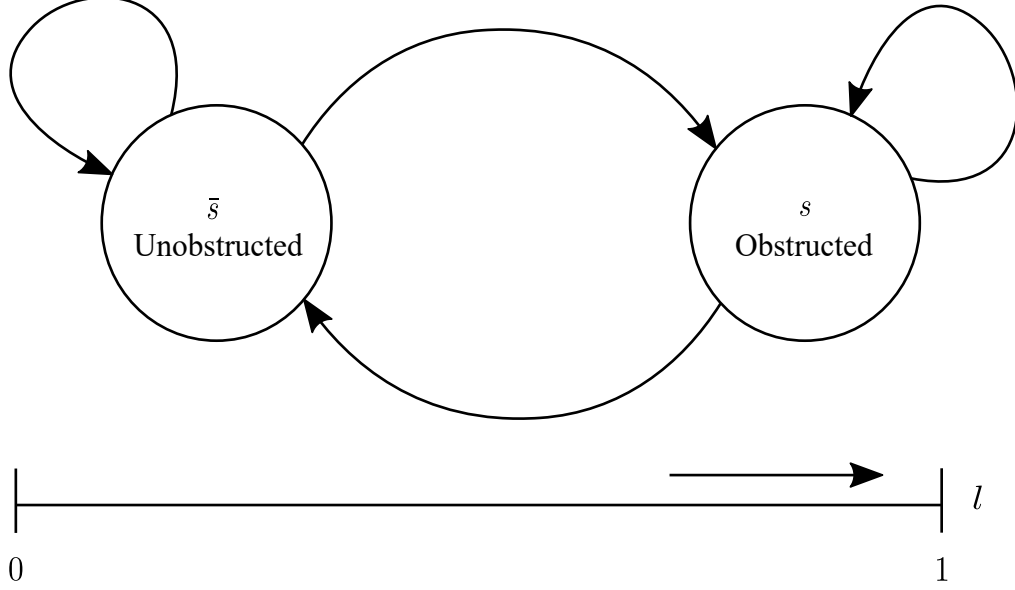


Figure 5.3: State transition diagram for Mission 2 (Contested Transit).

Moreover, if the path is obstructed ( $s$ ), the power applied to moving is limited such that  $p_{move} \leq \bar{p}_{move,max} \leq p_{move,max}$ , which represents the inability to traverse the path safely at higher speeds while it is obstructed. The probability of the path being obstructed in the next period is described by

$$P[s_{k+1}] = \begin{cases} P_{obs} & \bar{s}_k \\ e^{-\frac{p_{attack,k}}{\beta_{attack}}} & s_k, \end{cases} \quad (5.8)$$

where  $P_{obs} \in [0, 1]$  is the probability of the path becoming obstructed in a moment<sup>1</sup>. The mission states have been illustrated in Figure 5.3.

The functional representing the performance of the system for Mission 2 (Contested Transit) is given by

$$V = \frac{1}{V_{norm}} \sum_{k=0}^{\infty} \alpha^k (l_{k+1} - l_k). \quad (5.9)$$

The normalization constant is given by

$$V_{norm} = v_{max} \Delta t \left( \frac{1 - \alpha^{N_{norm}}}{1 - \alpha} \right) + \alpha^{N_{norm}} (1 - N_{norm} v_{max} \Delta t), \quad (5.10)$$

where  $v_{max} = v_{move}(p_{move,max})$ , and  $N_{norm} = \lfloor 1/(v_{max} \Delta t) \rfloor$ . This functional is normalized such that it is one if the path is transited at full speed without obstruction.

<sup>1</sup>Parameter values with the same symbol, e.g.  $\beta_{attack}$ , described in the different missions could have different values for each mission.

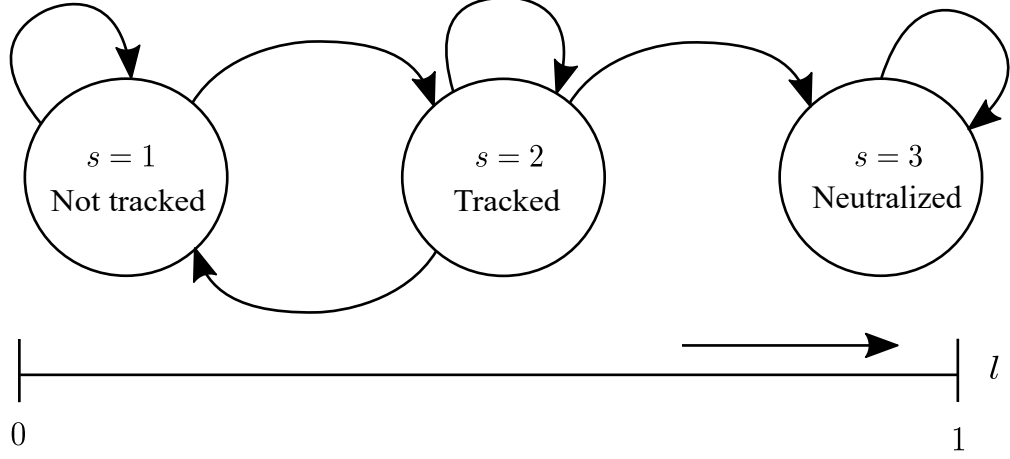


Figure 5.4: State transition diagram for Mission 3 (Fight or Flight).

### 5.3.3 Mission 3 (Fight or Flight)

In this mission, a target threat exists, and a given minimum distance from the target must be obtained through movement or through successfully tracking and neutralizing the target. The mission state involves one continuous and one discrete state variable. The continuous state variable  $l$  indicates the distance from the target and is initially zero. The discrete state variable  $s$  indicates the mission progress. When  $s = 1$ , the target has not been adequately tracked, and this is the initial value of  $s$ . When  $s = 2$ , the target has been adequately tracked but not neutralized. When  $s = 3$ , the threat has been neutralized. The mission action consists of three variables. The first,  $p_{track}$ , is the power applied to tracking during the current period. The second,  $p_{attack}$ , is the power applied to attacking during the current period. The third,  $p_{move}$ , is the power applied to moving during the current period. The distance from the target in the next period is modeled using (5.5) subject to the constraints in (5.6) and (5.7) without the limitation associated with obstruction in Mission 2 (Contested Transit).

The probability of being in the state where the target has not been tracked adequately in the next period is modeled using (5.1). The probability of the target being in the state where the target has been tracked adequately but not neutralized in the next period is modeled using (5.2). The probability of the target being in the state where the target has been neutralized in the next period is modeled using (5.3). The mission states are illustrated in Figure 5.4.

The functional representing the performance of a system for Mission 3 (Fight or Flight) is given by

$$V = \frac{1}{V_{norm}} \sum_{k=0}^{\infty} \alpha^k (\hat{l}_{k+1} - \hat{l}_k), \quad (5.11)$$

where

$$\hat{l}_k = \begin{cases} l_k & \text{if } s_k \neq 3, \\ 1 & \text{if } s_k = 3, \end{cases} \quad (5.12)$$



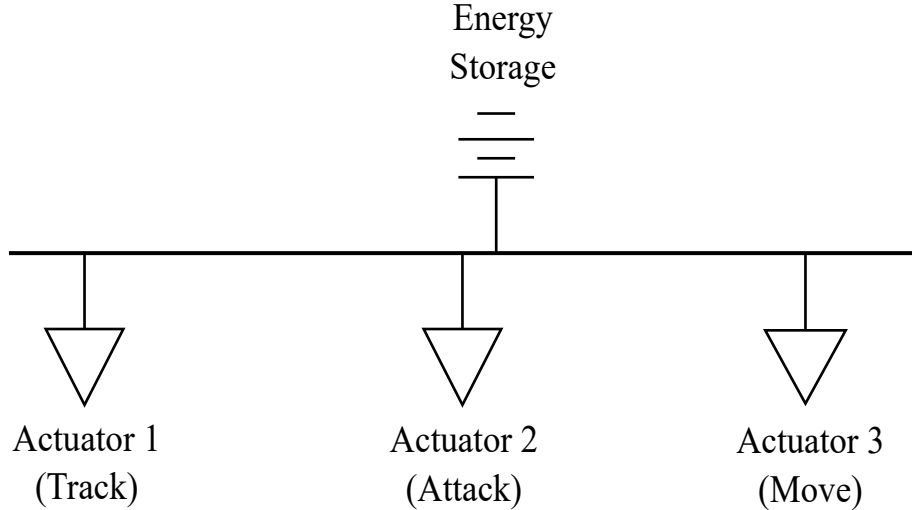


Figure 5.5: System 1 (Shared). This is an idealized system in which stored energy is freely available throughout system.

and

$$V_{norm} = v_{max} + \alpha(1 - v_{max}). \quad (5.13)$$

The functional is normalized such that its maximum possible value is one, which occurs if the target is neutralized at  $s_k = 2$  while moving at full speed.

## 5.4 System Implementations

Three potential system implementations are considered. Each system implementation has its own state variable(s), distinct from the state variables associated with individual missions described above. The system state variables are components of the problem state variable  $\mathbf{x}$  described earlier in Section 3.3. There are also constraints associated with each system implementation, again distinct from those associated with each mission, that are embedded in (3.3) as constraints on the action. The specific state variables and constraints for each system implementation are described below.

### 5.4.1 System 1 (Shared)

In System 1 (Shared), energy storage is shared between actuators as illustrated in Figure 5.5. This represents an idealized system in which stored energy is freely available for any purpose. In practical systems, it could be difficult for energy to be shared as freely depending on the system ratings and topology.

The system state is a scalar,  $e$ , that represents the normalized stored energy. The energy stored in the next period is described by

$$e_{k+1} = e_k - (p_{track,k} + p_{attack,k} + p_{move,k})\Delta t. \quad (5.14)$$

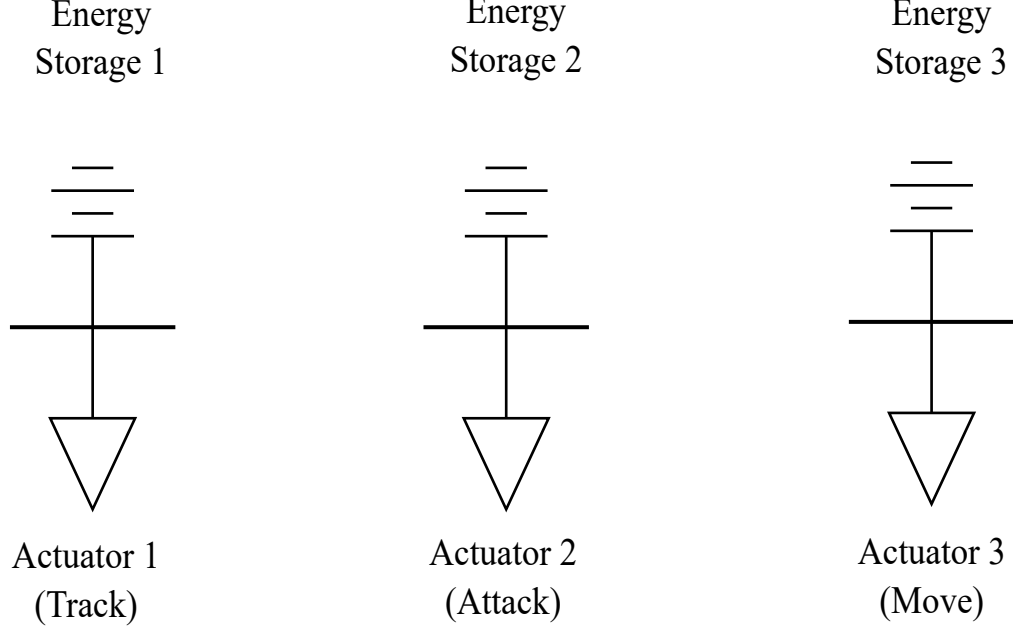


Figure 5.6: System 2 (Dedicated). Energy in system is allocated to a specific actuator and cannot be repurposed.

The total power flowing from the energy storage is constrained by the available energy and the power limit of the energy storage:

$$(p_{track,k} + p_{attack,k} + p_{move,k})\Delta t \leq e_k \quad (5.15)$$

$$p_{track,k} + p_{attack,k} + p_{move,k} \leq p_{e,max}, \quad (5.16)$$

where  $p_{e,max} \geq 0$  represents the power limit of the energy storage.

#### 5.4.2 System 2 (Dedicated)

In System 2 (Dedicated), stored energy is dedicated to each actuator, which is illustrated in Figure 5.6.

There are three state variables,  $e_{track}$ ,  $e_{attack}$ , and  $e_{move}$ , which represent the stored energy associated with each actuator. The energy stored in the next period is described by

$$e_{Y,k+1} = e_{Y,k} - p_{Y,k}\Delta t, \quad (5.17)$$

where  $Y \in \{track, attack, move\}$ .

The power flowing from each energy storage is constrained by the available energy and the power limit:

$$p_{Y,k}\Delta t \leq e_{Y,k} \quad (5.18)$$

$$p_{Y,k} \leq p_{Y,e,max}, \quad (5.19)$$

where  $Y \in \{track, attack, move\}$  and  $p_{Y,e,max} \geq 0$  represents the power limit of the energy storage associated with each actuator.

## Power Distribution

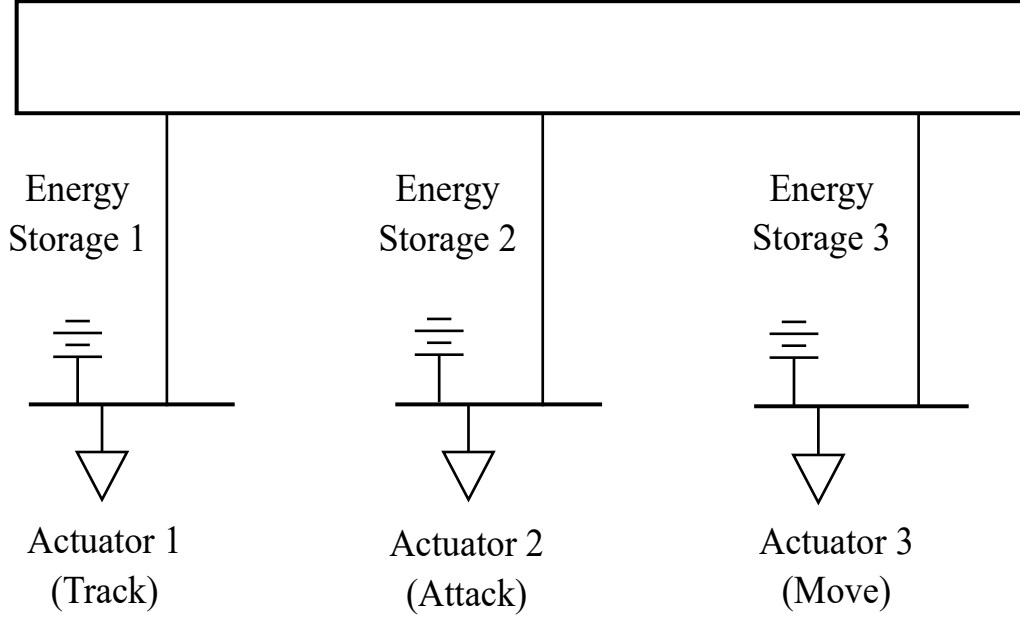


Figure 5.7: System 3 (Distributed). Energy allocated to specific actuators but can be moved with limited power through distribution system.

### 5.4.3 System 3 (Distributed)

A third implementation is considered, System 3 (Distributed), in which energy can be moved from one actuator to the other, perhaps necessitating more capability from the power distribution system, as illustrated in Figure 5.7. Hence, if there is insufficient energy available for an action, the power distribution system can be used to move energy among the actuators.

In System 3 (Distributed), three additional action variables,  $p_{track,t,k}$ ,  $p_{attack,t,k}$ , and  $p_{move,t,k}$  represent the flow of power from each actuator to the distribution system. The energy stored in the next period is described by

$$e_{Y,k+1} = e_{Y,k} - (p_{Y,k} + p_{Y,t,k})\Delta t, \quad (5.20)$$

where  $Y \in \{track, attack, move\}$ .

The actions are constrained such that:

$$e_{Y,k} - e_{Y,e,max} \leq (p_{Y,k} + p_{Y,t,k})\Delta t \leq e_{Y,k} \quad (5.21)$$

$$-p_{Y,e,max} \leq p_{Y,k} + p_{Y,t,k} \leq p_{Y,e,max} \quad (5.22)$$

$$-p_{Y,t,max} \leq p_{Y,t,k} \leq p_{Y,t,max}, \quad (5.23)$$

where  $Y \in \{track, attack, move\}$ ,  $p_{Y,t,max} \geq 0$  represents the power limits of the distribution system to accept power from each actuator, and  $e_{Y,e,max} \geq 0$  represents

the stored energy limits of the energy storage associated with each actuator. Power is conserved in the distribution system:

$$p_{track,t,k} + p_{attack,t,k} + p_{move,t,k} = 0. \quad (5.24)$$

## 5.5 Solution Algorithm

Each problem (i.e., mission and system implementation) is solved by solving the stochastic Bellman equation (3.3) numerically. Specifically, uniform grids over the continuous state space are established for each discrete value in the state space. For each grid point in the space,  $\mathbf{x}$ , an estimated value of  $\bar{V}(\mathbf{x})$  and of the optimal action  $\mathbf{u}^*(\mathbf{x})$  is stored. Both of these estimates are initialized at zero. The estimated values of  $\bar{V}$  are used with linear interpolation to approximate  $\bar{V}(\cdot)$  within the grid.

To solve the optimal control problem, value function iteration is employed. At each grid point  $\mathbf{x}$ , the stochastic Bellman equation is solved using MATLAB R2022a's `fmincon` function, with its default parameters, with a starting point of  $\mathbf{u}^*(\mathbf{x})$  using linear interpolation to approximate  $\bar{V}(\cdot)$  in (3.3). These optimization results are used to update the approximations of  $\bar{V}(\cdot)$  and  $\mathbf{u}^*(\cdot)$ , completing one iteration. This is performed for 100 iterations for each problem. The implementation of this algorithm is given in Algorithm 1 below.

---

### Algorithm 1 Value Function Iteration Implementation

---

```

 $X$  = set of grid points given in Table 5.2
 $N = 100$ 
for all  $\mathbf{x} \in X$  do
     $\bar{V}(\mathbf{x}) := 0$ 
     $\bar{\mathbf{u}}^*(\mathbf{x}) := \mathbf{0}$ 
end for
 $\bar{V}_{est} :=$  linear interpolant over  $(X, \bar{V})$ 
for  $n = 1, \dots, N$  do
    for all  $\mathbf{x} \in X$  do
        From initial guess of  $\bar{\mathbf{u}}^*(\mathbf{x})$  use fmincon to solve
        
$$\max_{\mathbf{u} \in \Omega(\mathbf{x})} E[R(\mathbf{x}, \mathbf{u}, \mathbf{x}_{next}) + \alpha \bar{V}_{est}(\mathbf{x}_{next})]$$

        for  $\bar{V}(\mathbf{x})$  and  $\bar{\mathbf{u}}^*(\mathbf{x})$ 
        subject to problem state dynamics and constraints
    end for
     $\bar{V}_{est} :=$  linear interpolant over  $(X, \bar{V})$ 
end for

```

---

The problems have different dimensions. For example, in Mission 1 (Search and Destroy) with System 1 (Shared), the mission state involves no continuous state variables and the system state has a single shared energy storage variable; this problem is one dimensional. The grid points for each problem are selected to control the scaling such that adding a dimension results in approximately five times more grid points

Table 5.2: Grids for Notional Problems

Mission	System Implementation	Grid points
Mission 1 (Search and Destroy)	System 1 (Shared)	$s \in \{1, 2\}$ $e \in [0, 120]$ 500 points
	System 2 (Dedicated)	$s \in \{1, 2\}$ $e_{track} \in [0, 60]$ 50 points $e_{attack} \in [0, 60]$ 50 points
	System 3 (Distributed)	$s \in \{1, 2\}$ $e_{track} \in [0, 60]$ 23 points $e_{attack} \in [0, 60]$ 23 points $e_{move} \in [0, 60]$ 23 points
Mission 2 (Contested Transit)	System 1 (Shared)	$s \in \{0, 1\}$ $l \in [0, 1]$ 50 points $e \in [0, 60]$ 50 points
	System 2 (Dedicated)	$s \in \{0, 1\}$ $l \in [0, 1]$ 23 points $e_{attack} \in [0, 60]$ 23 points $e_{move} \in [0, 60]$ 23 points
	System 3 (Distributed)	$s \in \{0, 1\}$ $l \in [0, 1]$ 16 points $e_{track} \in [0, 60]$ 16 points $e_{attack} \in [0, 60]$ 16 points $e_{move} \in [0, 60]$ 16 points
Mission 3 (Fight or Flight)	System 1 (Shared)	$s \in \{1, 2\}$ $l \in [0, 1]$ 50 points $e \in [0, 120]$ 50 points
	System 2 (Dedicated)	$s \in \{1, 2\}$ $l \in [0, 1]$ 16 points $e_{track} \in [0, 60]$ 16 points $e_{attack} \in [0, 60]$ 16 points $e_{move} \in [0, 60]$ 16 points
	System 3 (Distributed)	$s \in \{1, 2\}$ $l \in [0, 1]$ 16 points $e_{track} \in [0, 60]$ 16 points $e_{attack} \in [0, 60]$ 16 points $e_{move} \in [0, 60]$ 16 points

with the simplest one-dimensional problem using 500 grid points. Table 5.2 shows the grid structure for each of the problems considered herein.

## 5.6 Results and Discussion

The set of problems, i.e., the notional missions described in Section 5.3 and system implementations described in Section 5.4, are solved using the solution method

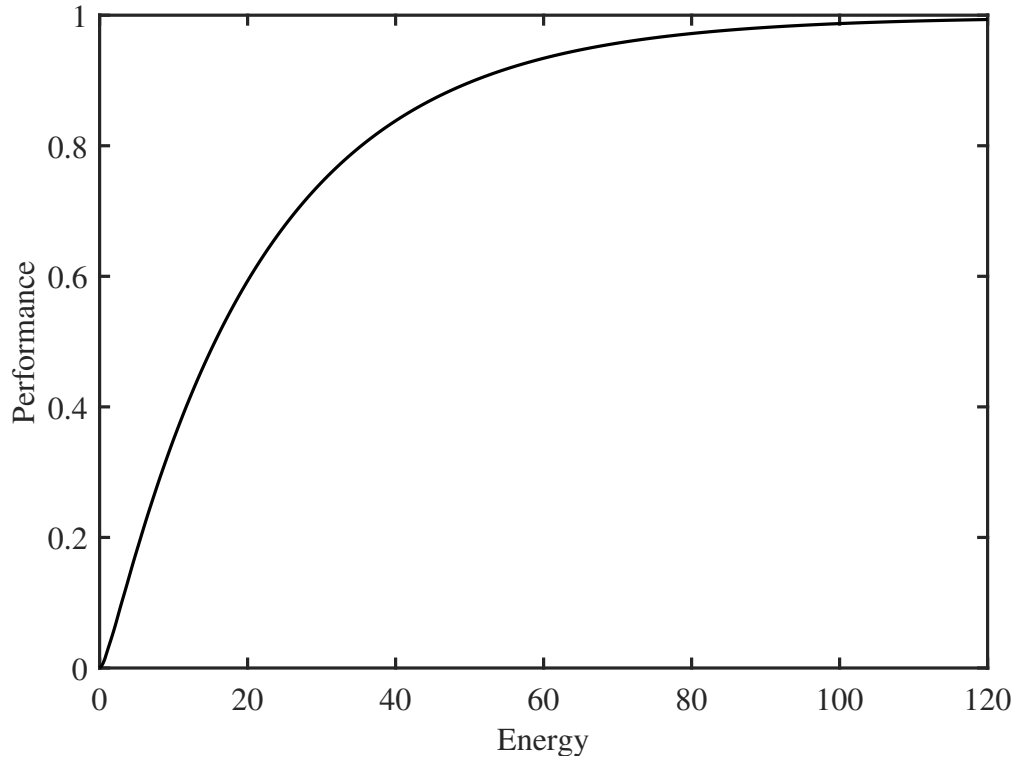


Figure 5.8: Expected performance for Mission 1 (Search and Destroy) with System 1 (Shared). Higher initial allocation of energy results in higher expected performance.

described in Section 5.5. The solutions and ways in which these solutions can be interpreted to understand overall system performance are described below.

### 5.6.1 Problem Solutions

For each mission with each system implementation, the stochastic Bellman equation is solved using the method described in the previous section. Each combination of mission and system implementation has a somewhat different structure as described in Table 5.2, resulting in nine different problems. For example, for System 1 (Shared), two different functions of one continuous variable are found in Mission 1 (Search and Destroy), and two different functions of two continuous variables are found in Mission 2 (Contested Transit). Given the initial condition for each mission, the expected performance of each problem is a function of the initial allocation of energy.

In a system implementation with one continuous energy variable, the expected performance is one dimensional. This occurs with System 1 (Shared) in all missions because energy is shared freely among actuators. An example of such a problem is Mission 1 (Search and Destroy) with System 1 (Shared). The expected performance of this problem is visualized in Figure 5.8. As expected, a higher initial allocation of energy results in higher expected performance.

In a system implementation with two continuous energy variables for a given mission, the expected performance is two dimensional. This occurs with System 2 (Ded-

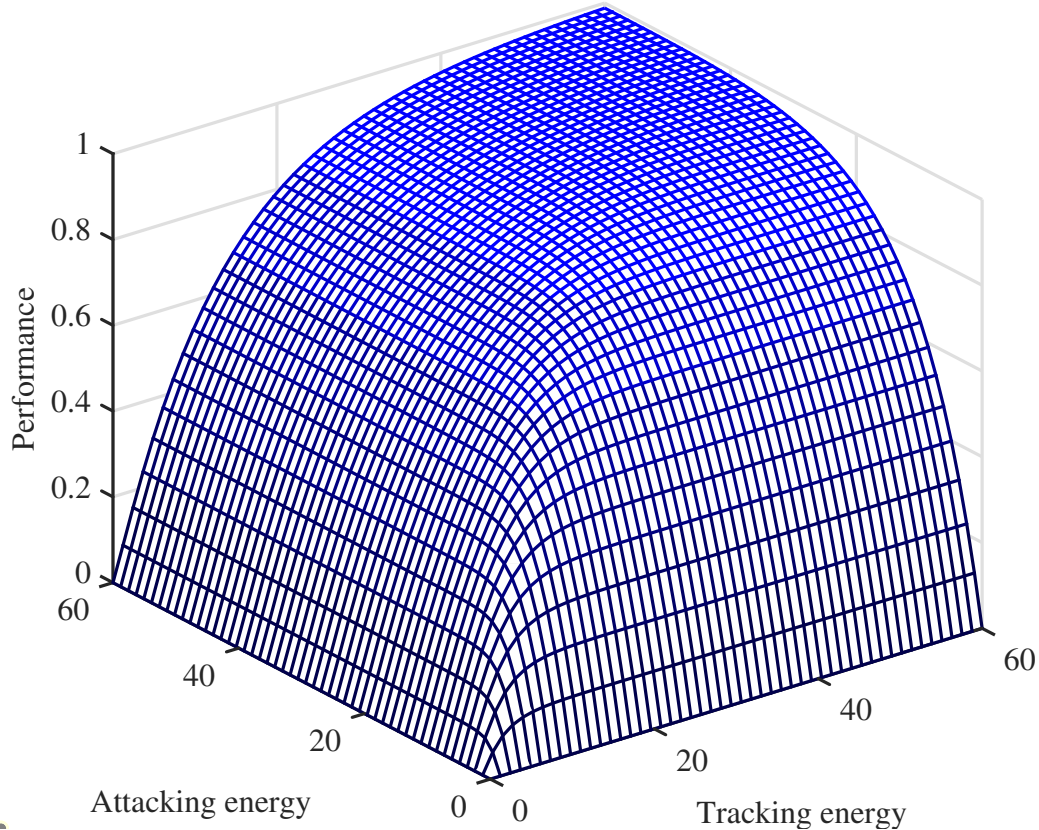


Figure 5.9: Expected performance for Mission 1 (Search and Destroy) with System 2 (Dedicated). Higher initial energy for either actuator results in higher expected performance. However, if very low energy is available for either actuator, the performance is low, even if the energy available for the other actuator is high.

icated) when only two actuators contribute to mission performance (i.e., the energy allocated to the other actuator does not affect expected performance). An example of such a problem is Mission 1 (Search and Destroy) with System 2 (Dedicated). The expected performance of this problem is visualized in Figure 5.9. Similar to System 1 (Shared), the expected performance is higher when higher energy is available for each actuator (tracking or attacking). However, if insufficient energy is available for either actuator (tracking or attacking), the expected performance will be low, even if energy available for the other actuator is high.

In a system implementation with three continuous energy variables for a given mission, the expected performance is three dimensional. This occurs with System 2 (Dedicated) when all actuators contribute to mission performance or with System 3 (Distributed) in all missions because energy can be moved through the distribution system. In the same way, in a system with three continuous variables, the problem is three-dimensional. An example of such a problem is Mission 1 (Search and Destroy) with System 3 (Distributed). The expected performance of this problem is more difficult to visualize because of the higher dimensionality, but it can be plotted against total initial energy as shown in Figure 5.10. Similar to the previous system

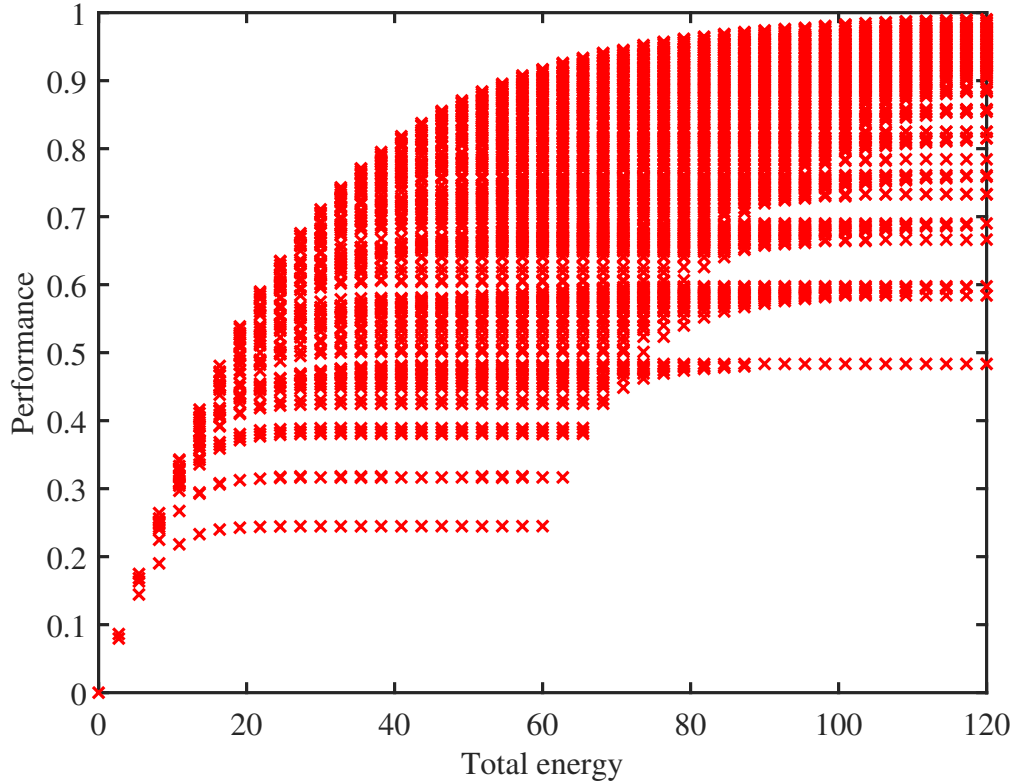


Figure 5.10: Expected performance for Mission 1 (Search and Destroy) with System 3 (Distributed). The performance is higher when higher energy is available for tracking, attacking, and moving. The vertical spread represents initial energy allocations that are not optimal with respect to this mission. Unlike System 2 (Dedicated), the performance is not zero unless no energy is available. If the initial energy allocation is not optimal, energy can be moved through the distribution system.

implementations, the performance is higher when higher energy is available. There is a vertical spread, representing initial energy allocations that are not optimal for this mission. If insufficient energy is available for either actuator (tracking or attacking), the system can move energy through the power distribution system to perform the given mission. However, this power transfer is limited by the capability of the distribution system, potentially resulting in lower performance.

For Missions 2 and 3 with System 3 (Distributed), similar figures can be obtained as illustrated in Figure 5.11 and Figure 5.12. The figures for the rest of the missions and system implementations are in Appendix A. Due to the increase in the dimension of the problem, the figures are two-dimensional.

### 5.6.2 Overall Performance

If the system is expected to perform missions from a distribution of missions, it is possible to determine the overall expected performance.



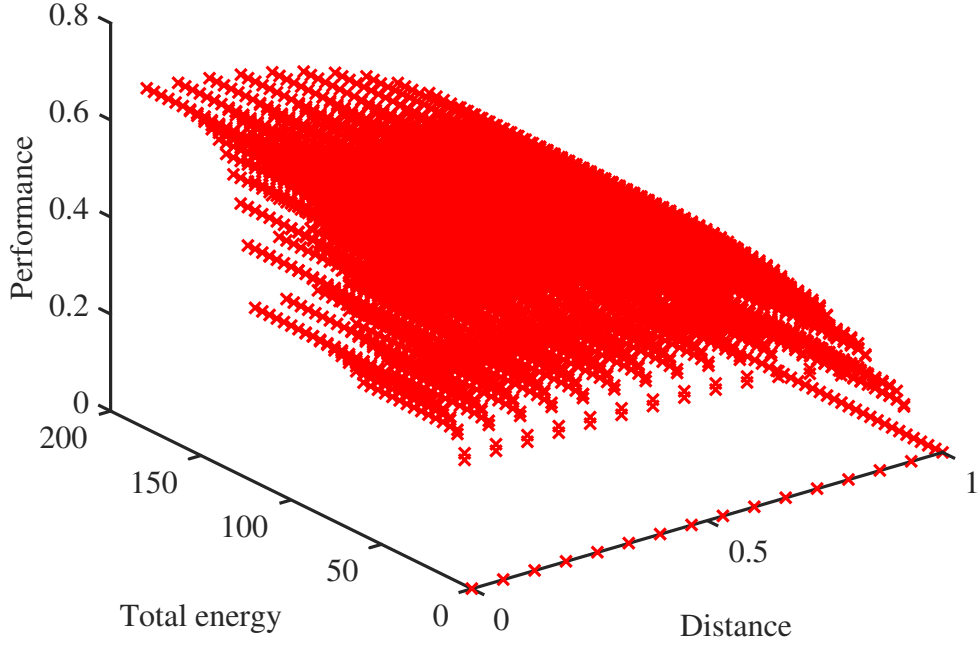


Figure 5.11: Expected performance for Mission 2 (Contested Transit) with System 3 (Distributed). The performance is higher when higher energy is available for tracking, attacking, and moving. The vertical spread represents initial energy allocations that are not optimal with respect to this mission.

For example, if the three missions considered herein are expected to occur with probabilities  $P_{m1}, P_{m2}, P_{m3} \geq 0$  with  $P_{m1} + P_{m2} + P_{m3} = 1$ , the overall expected performance is given by

$$\bar{V}_{overall} = P_{m1}\bar{V}_{m1} + P_{m2}\bar{V}_{m2} + P_{m3}\bar{V}_{m3}. \quad (5.25)$$

For each system, the performances are functions of the initial energy allocation (i.e.,  $e$  for System 1 (Shared), and  $e_Y$  for System 2 (Dedicated) and System 3 (Distributed)).

For System 2 (Dedicated) and System 3 (Distributed), it is possible to determine the optimal allocation of a specified amount of energy among the actuators.

Determining the optimal allocation of a fixed amount of energy is significant because the overall energy is strongly correlated with size, weight, and cost of the system. This problem for a given amount of energy  $e$  can be expressed as

$$\max_{\gamma_{track}, \gamma_{attack}, \gamma_{move} \geq 0} \bar{V}_{overall}(\gamma_{track}e, \gamma_{attack}e, \gamma_{move}e) \quad (5.26)$$

$$\text{subject to } \gamma_{track} + \gamma_{attack} + \gamma_{move} = 1. \quad (5.27)$$

Herein, the probabilities given in Table 5.3 are assumed.

By aggregating mission performance as indicated in (5.25), it is possible to understand the overall performance of the system implementations. For System 1 (Shared),

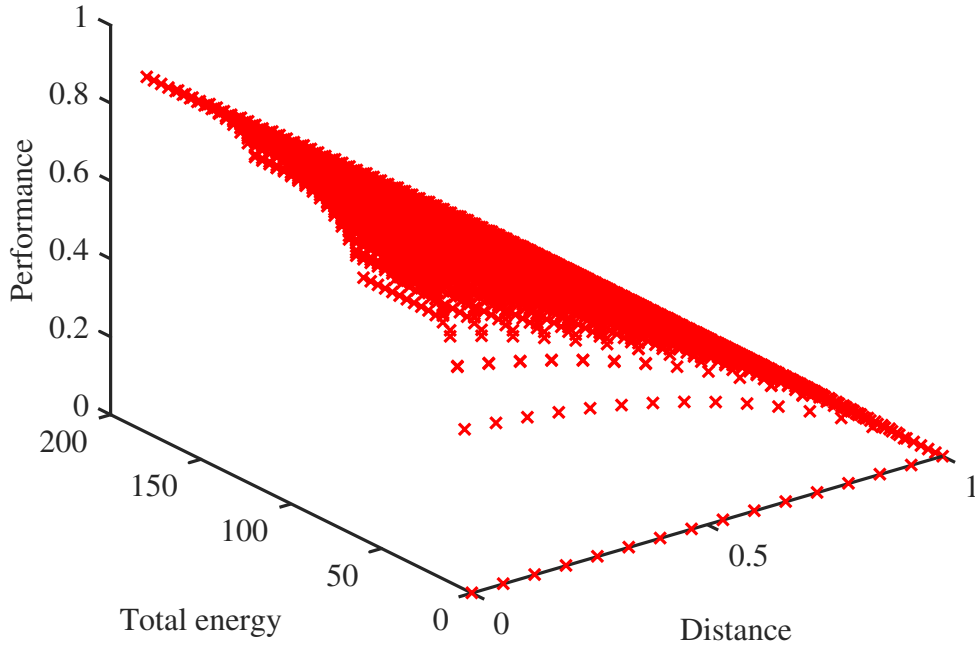


Figure 5.12: Expected performance for Mission 3 (Fight or Flight) with System 3 (Distributed). The performance is higher when higher energy is available for tracking, attacking, and moving.

Table 5.3: Notional Mission Probabilities

Probability of Mission 1 (Search and Destroy), $P_{m1}$	0.3
Probability of Mission 2 (Contested Transit), $P_{m2}$	0.3
Probability of Mission 3 (Fight or Flight), $P_{m3}$	0.4

the overall performance is shown in Figure 5.13. It has the expected characteristic that overall performance increases with greater available energy, which is similar to the expected performance of this system for individual missions (e.g., Figure 5.8). This system can be considered an idealized system as the energy is not allocated for any particular actuator, instead being freely available throughout the system. Therefore, the overall performance of this system represents an upper bound on the available performance based only on the available energy and the characteristics of the actuators and the missions themselves. The other two system implementations are compared against this upper bound in the following subsection.

Likewise, the overall mission performance of System 2 (Dedicated) with respect to total initial energy is shown in Figure 5.14. In this figure, different combinations of initial energy allocation are aggregated into one dimension. As for the individual missions (e.g., Figure 5.9), greater available energy generally results in higher performance. The wide vertical spread indicates that overall performance is very

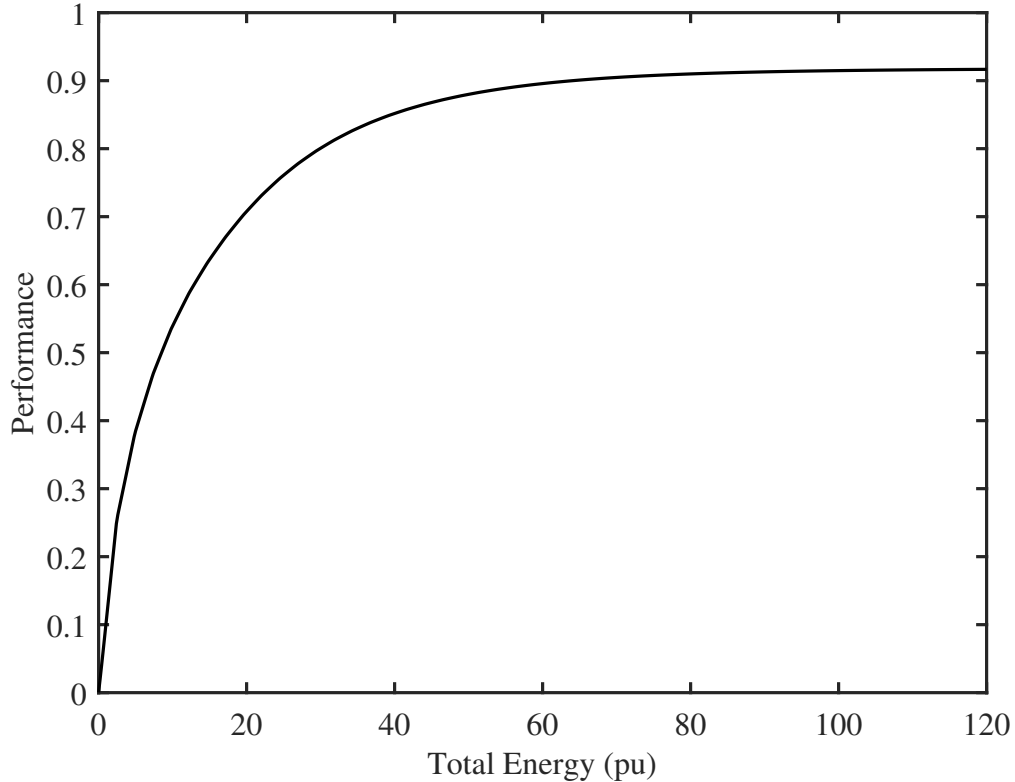


Figure 5.13: Overall mission performance for System 1 (Shared). Similar to individual mission performances for this system, higher allocation of energy results in higher expected performance.

sensitive to the initial allocation of energy, which is expected because energy cannot be repurposed for different uses in this dedicated system. By solving (5.26) for different amounts of total energy, it is possible to determine the optimal split of energy among the actuators that will result in optimal overall performance. The result of this optimization is shown in Figure 5.15. For lower amounts of energy, energy is only allocated to moving, meaning that the system is unable to perform Mission 1 (Search and Destroy) and can only apply energy to moving in Mission 2 (Contested Transit) and Mission 3 (Fight or Flight). As the total energy increases, the optimal ratio of the allocation of the total energy shifts, with the greatest amount allocated to tracking. The optimal overall performance for System 2 (Dedicated) is also shown in Figure 5.14.

For System 3 (Distributed), the overall mission performance with respect to total initial energy is shown in Figure 5.16. Like the previous system, different combinations of initial energy allocation are aggregated into one dimension. As expected, the overall performance increases with increase in initial allocation of energy. The vertical spread indicates the sensitivity of the overall performance to the initial allocation of energy. Unlike, System 2 (Dedicated), the vertical spread is relatively narrow, indicating that performance is considerably less sensitive to the initial allocation of energy. This observation, which is examined further below, is expected because this system

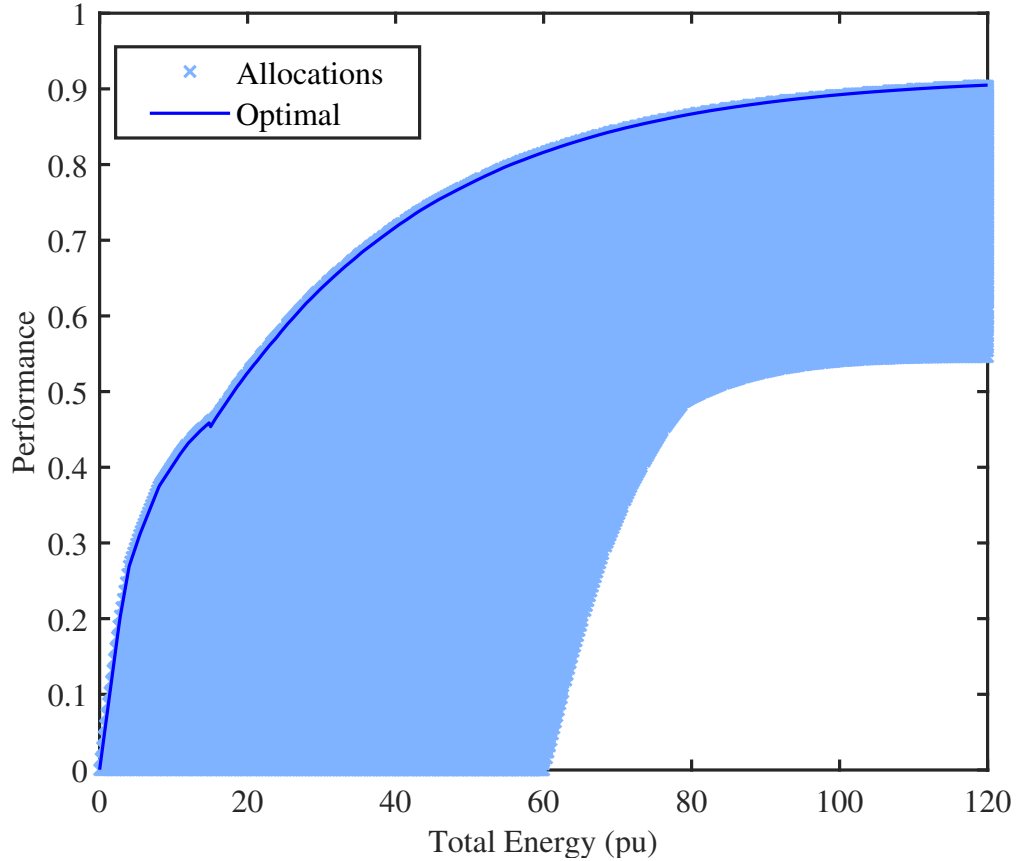


Figure 5.14: Overall mission performance for System 2 (Dedicated). Similar to individual mission performances for this system, higher allocation of energy results in higher expected performance. The wide vertical spread indicates high sensitivity to initial allocation of energy. The optimal curve indicates overall performance when energy is initially optimally allocated among actuators.

is able to move energy through the distribution system to the actuators that need it. By solving (5.26) for different amounts of total energy, it is possible to determine the optimal allocation of energy among the actuators that will result in optimal overall performance. The result of this optimization is shown in Figure 5.17. Compared with System 2 (Dedicated), energy is only allocated to a single actuator for a relatively smaller range of energy, and it is allocated to a different actuator (attack vs. move). This suggests that, for the distribution of missions considered and scarce available energy, there is more value in having energy allocated to move if it cannot be moved through the distribution system and there is more value in having energy allocated to attack if it can be repurposed dynamically through the distribution system. The optimal overall performance for System 3 (Distributed) is also shown in Figure 5.16.

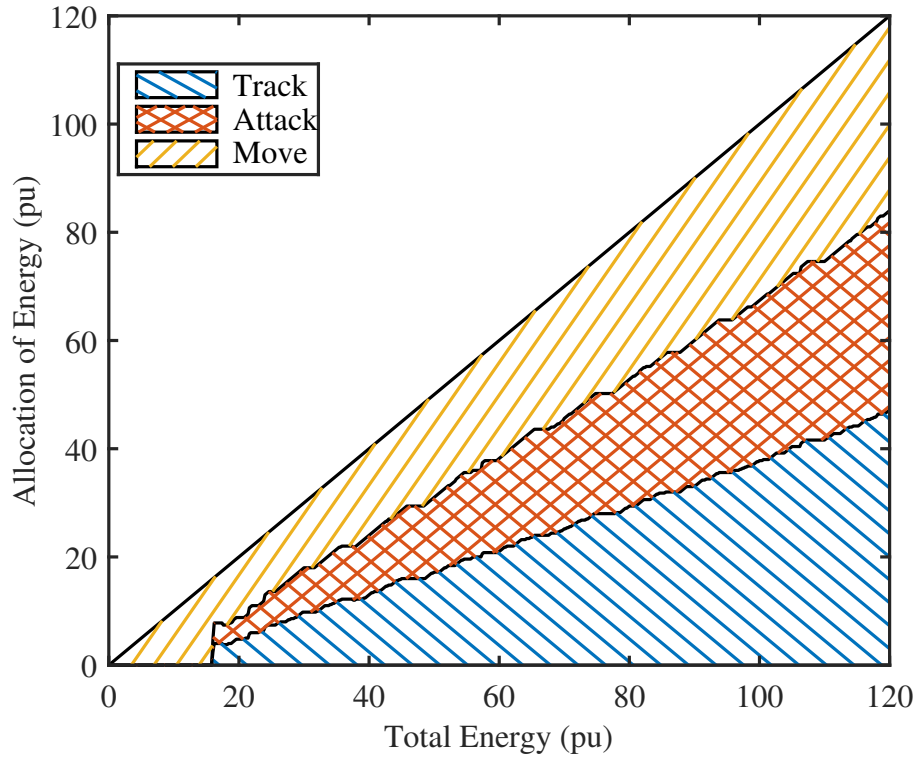


Figure 5.15: Optimal split of energy among three actuators for System 2 (Dedicated). For lower amounts of energy, energy is only allocated to moving, but ratio changes as total energy increases.

### 5.6.3 Comparison of Systems

When a given amount of energy is optimally allocated among the three actuators for each of the systems, it is possible to compare the systems on the basis of their overall performances. This comparison is shown in Figure 5.18. In this figure, System 1 (Shared) can be understood as the ideal performance. Because available energy is freely available, the performance of this system represents the maximum performance available based on the ratings and performance of the actuators and the nature of the missions. It can be seen that System 2 (Dedicated) performs worse at all amounts of energy than System 3 (Distributed). This result is expected because System 3 (Distributed) is able to move energy through the distribution system to the actuators that need it and System 2 (Dedicated) cannot reallocate energy to adjust to mission demands. This difference can be characterized in terms of the difference between the idealized System 1 (Shared) performance and the performance of System 2 (Dedicated) and System 3 (Distributed), which is indicated as the performance penalty. It can be seen that the greatest difference between the idealized and more practical systems occurs for approximately the same amount of energy. Moreover, the peak performance penalty for System 2 (Dedicated) is more than twice that of System 3 (Distributed). As a greater amount of energy is available, the performance penalty

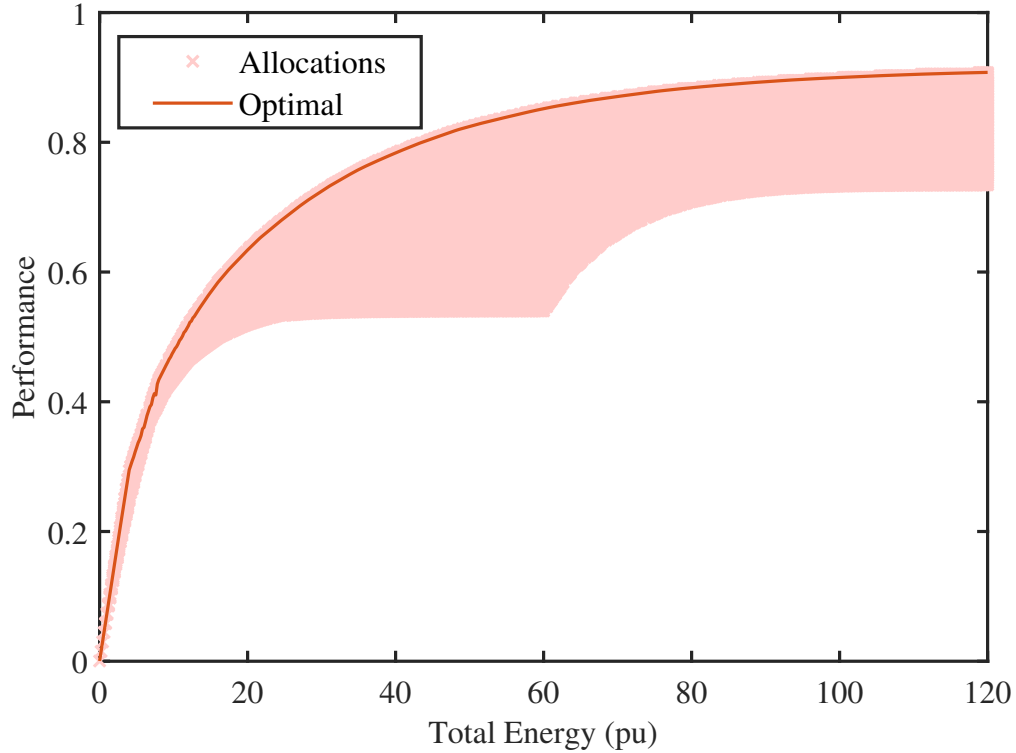


Figure 5.16: Overall mission performance for System 3 (Distributed). Similar to the individual mission performances for this system, higher allocation of energy results in higher expected performance. Narrow vertical spread indicates low sensitivity to initial allocation of energy. The optimal curve indicates overall performance when energy is initially optimally allocated among actuators.

of both practical systems diminishes and the overall performance of both approaches that of the idealized system. The vertical gap between System 2 (Dedicated) and System 3 (Distributed) represents the additional expected performance for System 3 (Distributed) compared with System 2 (Dedicated) for the same total energy. Likewise, the horizontal gap between System 3 (Distributed) and System 2 (Dedicated) represents the additional energy that must be available to System 2 (Dedicated) in order to have the same overall performance as System 3 (Distributed). While there are costs associated with a distributed system, it will generally be higher performing and require lower available energy than a dedicated system.

When an MDP is combined with a control policy, it results in a Markov reward model. In other words, a Markov chain is paired with reward that is accumulated. The performance values expressed above accumulate dynamically in time over sample trajectories of the Markov chain. It is possible to visualize the way in which reward is accumulated through Monte Carlo simulation of resultant Markov reward models. For example, Mission 2 (Contested Transit) involves reward accumulated through distance traveled. By sampling trajectories of the Markov reward model starting from a given state, it is possible to visualize the dynamic differences in performance that

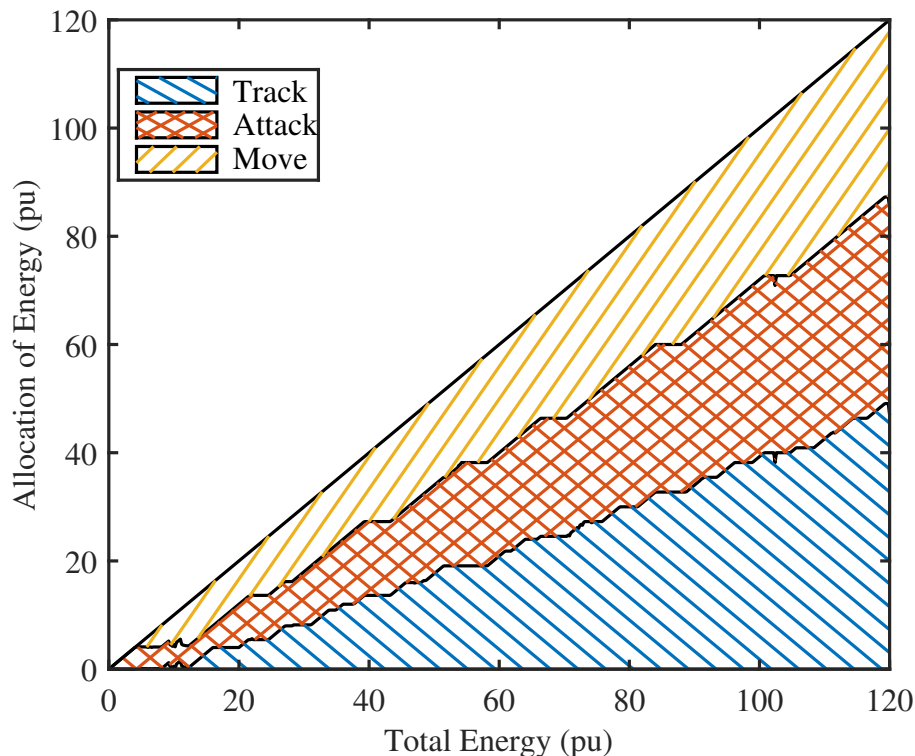


Figure 5.17: Optimal split of energy among three actuators for System 3 (Distributed). There is considerably smaller range of energy for which energy is only allocated to one actuator (attack).

result in the performance differences illustrated above. To see this, 30 pu of energy are distributed to both System 2 (Dedicated) and System 3 (Distributed) according to the optimal splits shown in Figure 5.15 and Figure 5.17, respectively. From this starting state, 500 trajectories of each were sampled simulating for 100 periods. This results in distributions of state values, actions, and performance for each system. Box plots showing the distributions of distance traveled at each time period for each system implementation are shown in Figure 5.19 and Figure 5.20, respectively. Specifically, the range (with outlier excluded based on interquartile range) and the lower and upper quartiles are shown. It can be seen that with the same amount of starting energy, System 3 (Distributed) is generally able to reach the target distance of 1 pu more often and more quickly than System 2 (Dedicated). This difference in time results in a difference in accumulated performance. The sample performances for the two systems are 0.67 and 0.74, respectively. These correspond with expected performance values from value function iteration of 0.63 and 0.71, respectively, with differences attributed to function approximation and truncation errors. This example illustrates how the value function solution approximates the dynamic performance of the system.

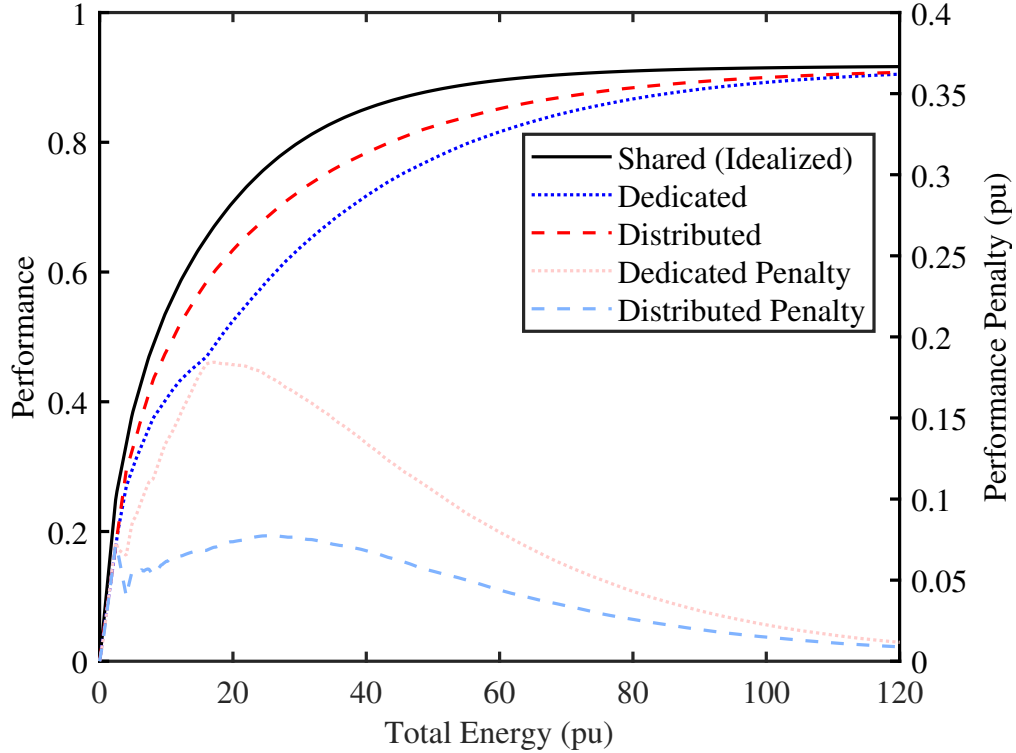


Figure 5.18: Performance comparison of systems. Energy for the System 2 (Dedicated) and System 3 (Distributed) is optimally allocated among three actuators. System 1 (Shared) is an idealized system and represents an upper bound on available performance. The performance penalty is computed by comparison of more practical systems with idealized System 1 (Shared). System 3 (Distributed) generally performs better for given amount of energy and requires lesser energy to achieve same performance as System 2 (Dedicated).

#### 5.6.4 Distribution System Unavailability

The previous subsection demonstrates that System 3 (Distributed) generally outperforms System 2 (Dedicated), but there are potential costs related to a distributed system. One such cost is the potential for the distribution system to be unavailable at the moment a mission is to be performed. Such unavailability could be caused by damage, maintenance, or other factors and would degrade the performance of System 3 (Distributed). Using the problem solutions above, it is possible to analyze the performance of System 3 (Distributed) while the distribution system is unavailable. Specifically, the optimal control of System 3 (Distributed) would follow the optimal control of System 2 (Dedicated), but the energy would not be optimally allocated. The performance of System 2 (Dedicated) is compared with the performance of System 3 (Distributed) with the distribution system both available and unavailable in Figure 5.21. It can be seen (as in Figure 5.18) that System 3 (Distributed) outperforms System 2 (Dedicated) when the distribution system is available and System 2 (Dedicated) outperforms System 3 (Distributed) when the distribution system is



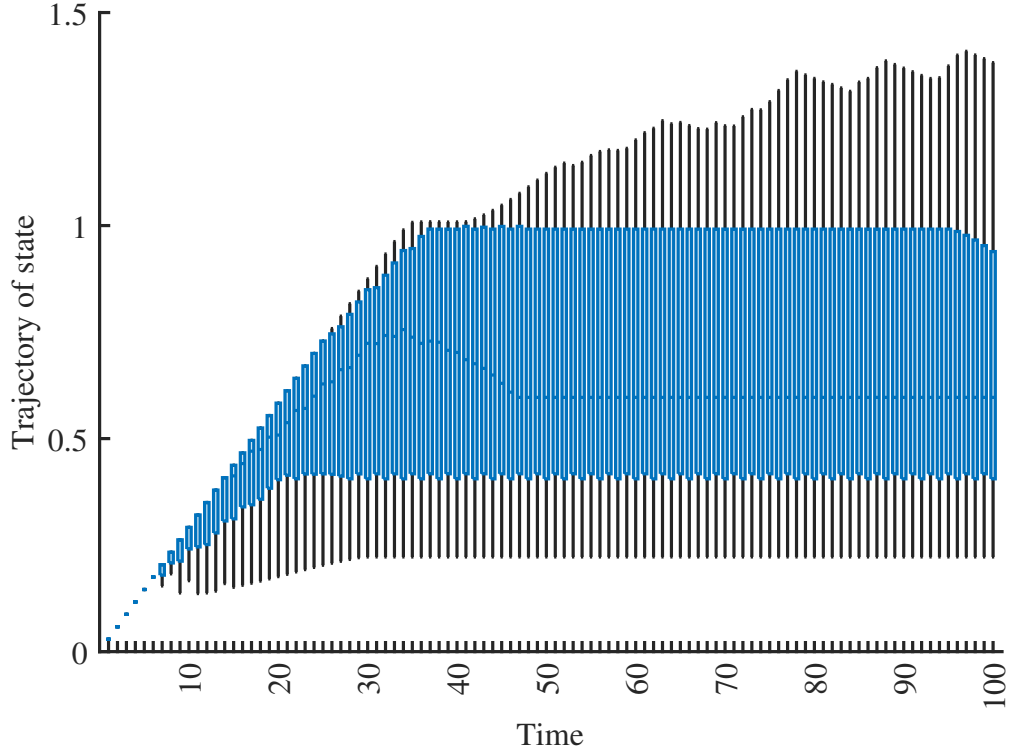


Figure 5.19: Distribution of distance traveled at each time period for Mission 2 (Contested Transit) with System 2 (Dedicated). Starting from optimally allocated 30 pu of energy, 500 sample trajectories are simulated for 100 periods. The range (with outliers excluded) and the lower and upper quartiles are shown.

unavailable. This makes conceptual sense because System 2 (Dedicated) and System 3 (Distributed) have the same topology when the distribution system is unavailable (i.e., Figure 5.6), but System 2 (Dedicated) is optimized for maximal performance in this configuration.

If the probability that the distribution system will be unavailable can be estimated, it is possible to evaluate the expected performance of System 3 (Distributed). It is assumed in the following discussion that this probability is 10%, which is likely very high for practical distribution systems. Figure 5.22 illustrates the expected performance of System 3 (Distributed), optimized for the distribution system being available but subject to unavailability. It can be seen that the expected performance is slightly lower than the performance when the distribution system is available, but it remains significantly greater than System 2 (Dedicated).

Given that there is an expected performance penalty for distribution system unavailability, it is possible to hedge against this unavailability. In particular, it is possible to solve for the optimal energy allocation (i.e., (5.26)) considering the assumed probability of unavailability, effectively hedging against the unavailability. This will result in a system with performance that is somewhat less dependent on the availability of the distribution system. The performance of such a system is shown in

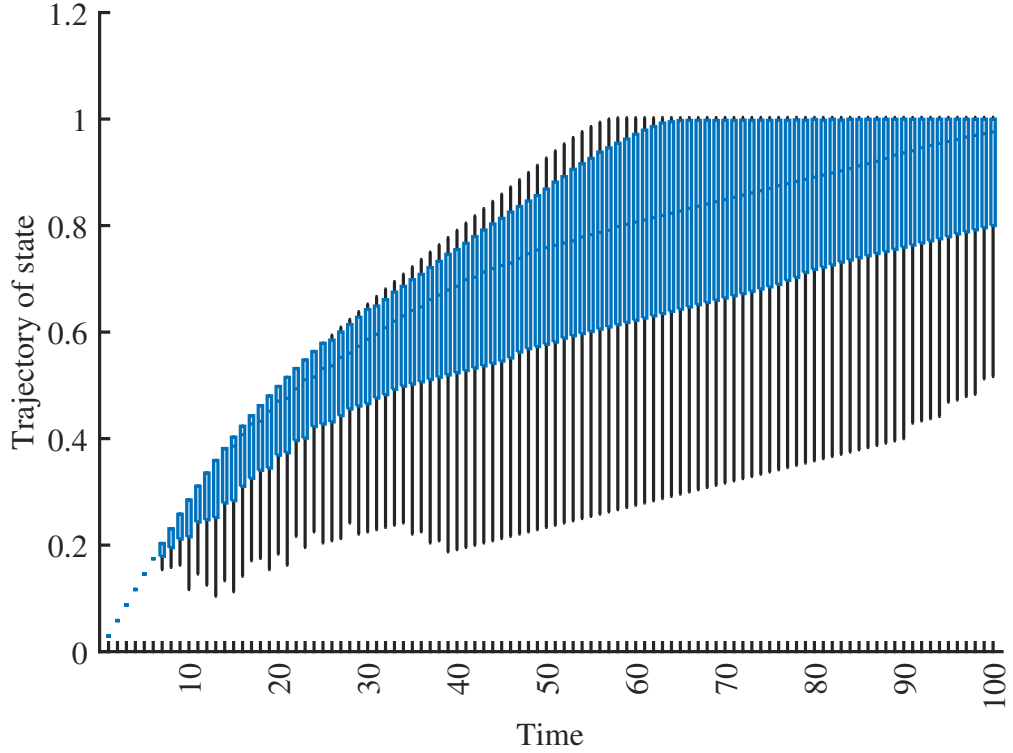


Figure 5.20: Distribution of distance traveled at each time period for Mission 2 (Contested Transit) with System 3 (Distributed). Starting from optimally allocated 30 pu of energy, 500 sample trajectories are simulated for 100 periods. The range (with outliers excluded) and the lower and upper quartiles are shown.

Figure 5.23 and compared with the performance of System 2 (Dedicated) with the distribution system being both available and unavailable. As without hedging, System 3 (Distributed) outperforms System 2 (Dedicated) when the distribution system is available and that System 2 (Dedicated) outperforms System 3 (Distributed) when the distribution system is unavailable. However, the range of energy for which System 2 (Dedicated) significantly outperforms System 3 (Distributed) is significantly smaller as a result of the hedging.

The expected performance of System 3 (Distributed) with and without hedging is compared with the performance of System 1 (Shared) and System 2 (Dedicated) in Figure 5.24. With or without hedging, System 3 (Distributed) has higher expected performance than System 2 (Dedicated). Hedging results in essentially identical expected performance as not hedging, but the performance when the distribution system is unavailable is significantly better as seen by comparing Figure 5.21 and Figure 5.23.

### 5.6.5 Mission Sensitivity

Mission-oriented power systems are often designed to have a very long service life (e.g., [22]). During this service life, the strategic environment in which these systems

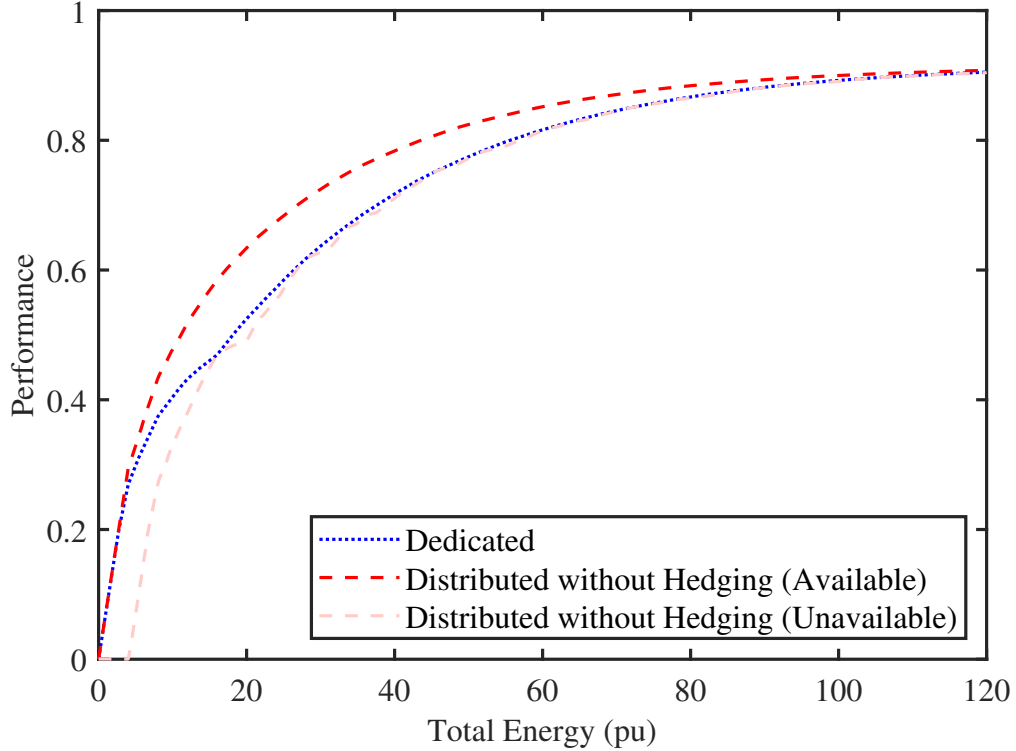


Figure 5.21: Performance comparison of systems with possibility of unavailable distribution system when there is no hedging against unavailability. System 3 (Distributed) outperforms System 2 (Dedicated) when distribution system is available, but System 2 (Dedicated) outperforms System 3 (Distributed) when it is unavailable.

Table 5.4: Assumed Mission Probabilities

Probability of Mission 1 (Search and Destroy), $P_{m1}$	0.5
Probability of Mission 2 (Contested Transit), $P_{m2}$	0.5
Probability of Mission 3 (Fight or Flight), $P_{m3}$	0.0

operate will change. Systems designed for certain missions will be tasked with new missions over their lifetimes.

The analyses performed in the previous subsections assume a particular distribution of missions (i.e., Table 5.3). In this subsection, the assumption that the specific distribution of missions is known at design time is relaxed. In particular, the energy allocations of System 2 (Dedicated) and System 3 (Distributed) are made with respect to the assumed mission distribution in Table 5.4 by solving (5.26), but the systems are evaluated with respect to the actual distribution in Table 5.3. The assumed distribution does not consider Mission 3 (Fight or Flight).

By comparing the real performance of the systems designed under the assumed distribution with those designed under the real distribution, it is possible to understand the sensitivity of performance to initial assumptions about mission distribution. This comparison is shown in Figure 5.25. In this figure, System 1 (Shared) does not

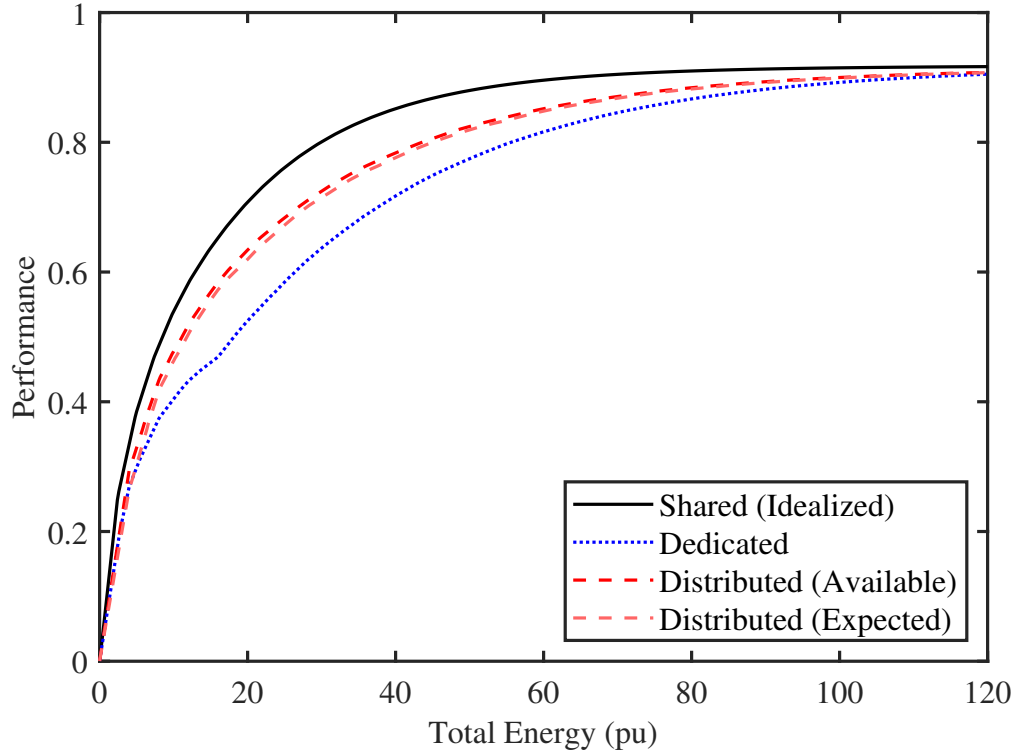


Figure 5.22: Performance comparison of systems with 10% probability of unavailable distribution system. Expected performance of System 3 (Distributed) is slightly lower than performance when distribution system is available. Expected performance remains significantly greater than System 2 (Dedicated).

change because there are no energy allocation decisions in this idealized system. However, the performance of System 2 (Dedicated) and System 3 (Distributed) will be somewhat worse when the energy allocation of these systems is performed with the assumed distribution instead of the real distribution of missions. Sensitivity is defined here as the difference between the real performance when the systems are designed with the real distribution and when the systems are designed with the assumed distribution and is an estimate of how sensitive the resulting performance is to the assumed mission distribution.

These results yield two observations. First, both systems are relatively insensitive to the assumed mission distribution. Without considering Mission 3 (Fight or Flight), the optimal energy allocations for both systems result in similar performance as if this mission is considered. This suggests that the analysis approaches proposed herein can yield meaningful results even when the specific mission environment in which such system will operate is unknown. Second, System 3 (Distributed) has considerably smaller sensitivity than System 2 (Dedicated), meaning its performance is less sensitive to the specific mission distribution that is considered when designing it. This seems reasonable because of the ability of this system to move energy through the distribution system, which can help compensate for suboptimal initial energy

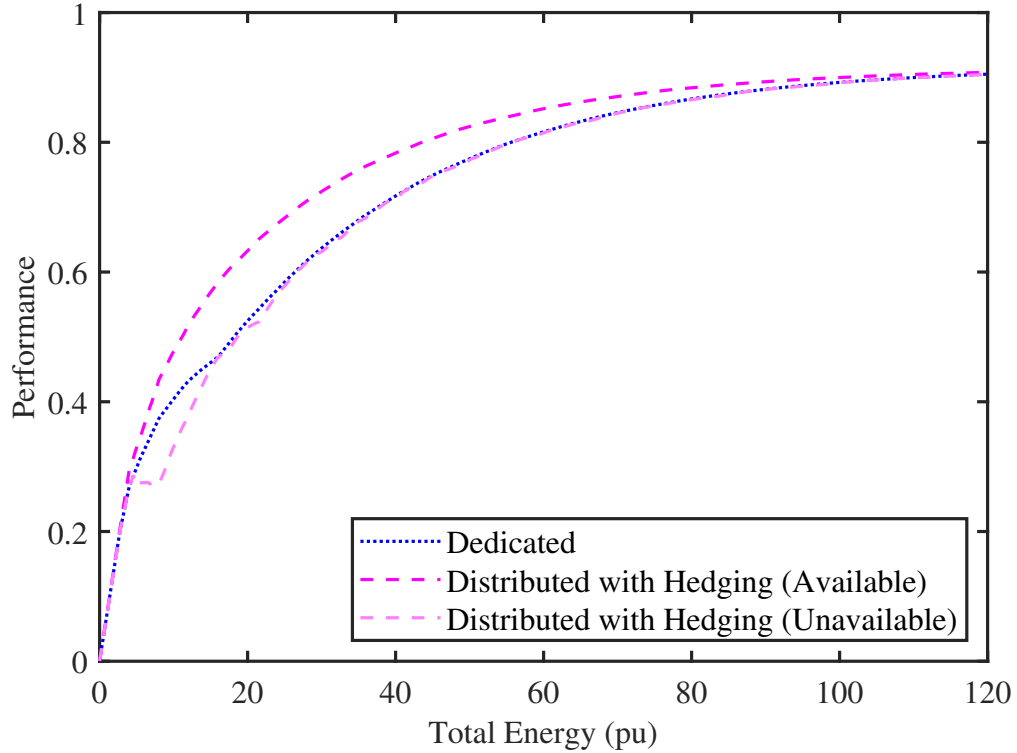


Figure 5.23: Performance comparison of systems with possibility of unavailable distribution system when there is hedging against unavailability. System 3 (Distributed) outperforms System 2 (Dedicated) when distribution system is available, but System 2 (Dedicated) outperforms System 3 (Distributed) when it is unavailable. However, range of energy for which System 2 (Dedicated) outperforms System 3 (Distributed) when distribution system is unavailable is significantly smaller than when no hedging is performed.

allocation due to the assumed mission distribution.

## 5.7 Conclusion

The evaluation of mission-oriented power system performance is advanced by formulating the evaluation as an optimal control problem. Specifically, the optimal control problem allows the dynamic interaction between the system and the mission to be considered directly. This approach is a natural evolution of existing simulation-based methods, where this interaction is modeled statically. The proposed approach is demonstrated using a notional, but representative, set of system implementations and missions. Furthermore, examples of the types of system trade offs that can be considered using this approach are presented and discussed. In the next chapter, market clearing-based algorithm is introduced as a method of solving optimization problems and its numerical challenges are explored.

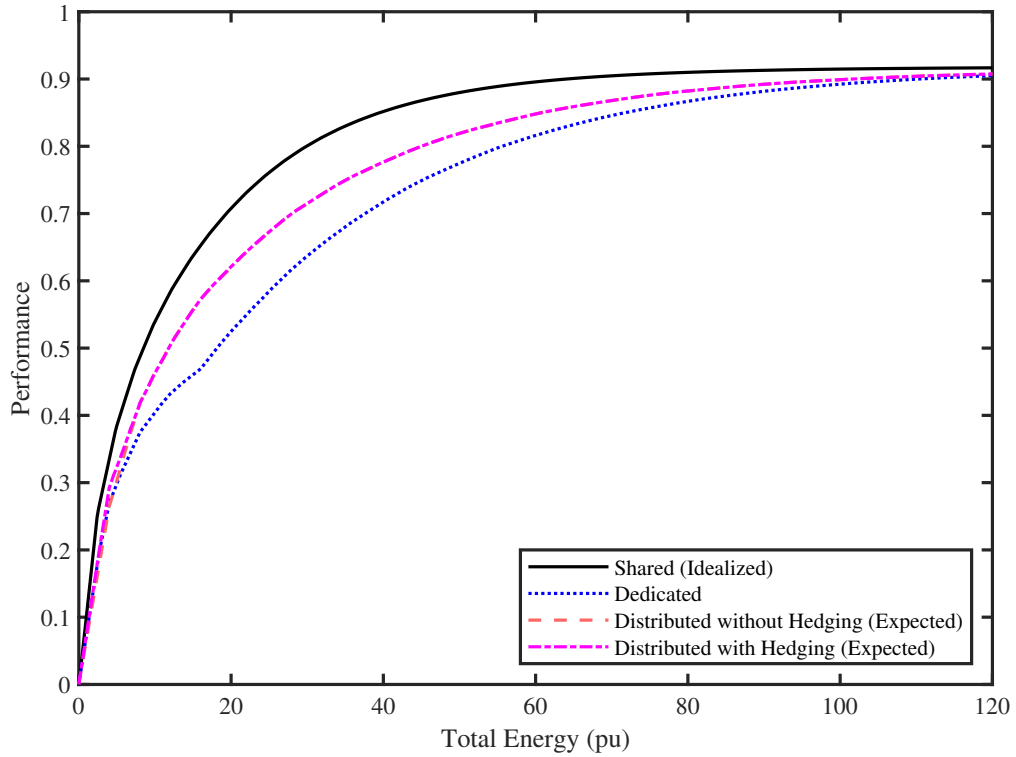


Figure 5.24: Performance comparison of systems considering the probability of distribution system unavailability. Expected performance of System 3 (Distributed) with hedging is essentially identical to expected performance without hedging and significantly better than System 2 (Dedicated), but hedging performance is generally better when distribution system is unavailable.

Copyright© Musharrat Sabah, 2024.

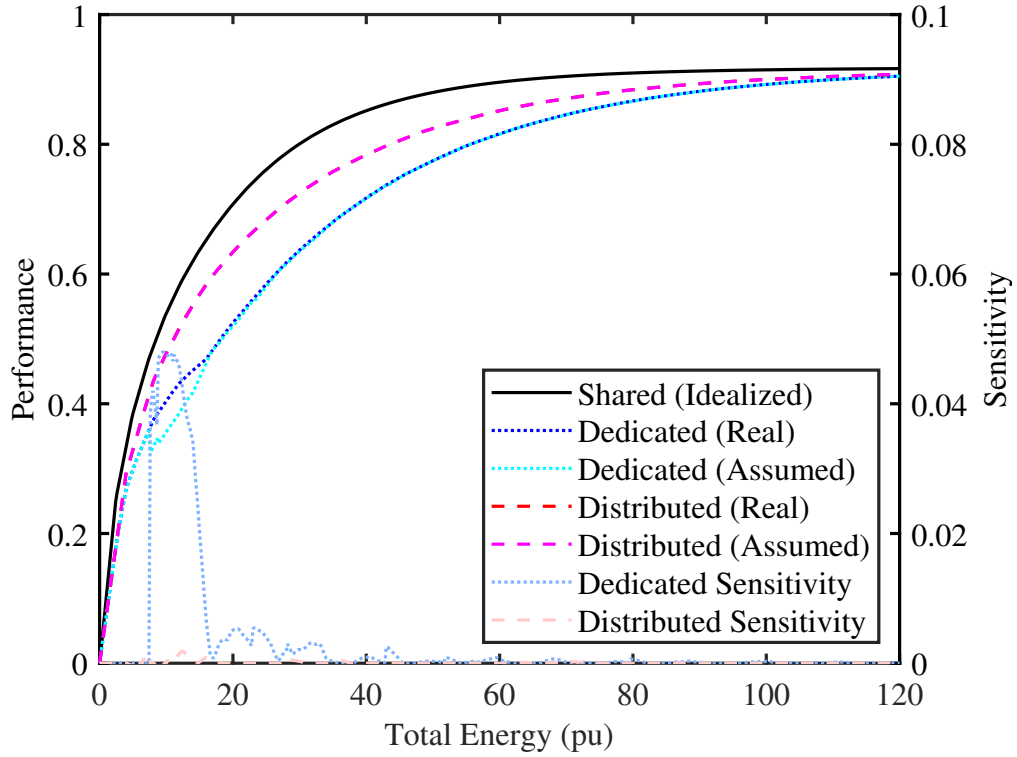


Figure 5.25: Performance comparison of systems under real mission distribution when designed considering real mission distribution or assumed mission distribution. There is small performance decrease associated with design using assumed distribution instead of real distribution. Difference is labeled sensitivity. System 2 (Dedicated) has higher sensitivity than System 3 (Distributed).

## Chapter 6 Market-Based Control in Power Electronics-Based Power Distribution Systems and its Challenges

### 6.1 Introduction

Market-based control is a widely used concept for controlling complex systems that are difficult to control and maintain. It has applications in a wide variety of power systems.

Power-electronics-based power distribution systems are arising in many different applications, ranging from the power systems of electric passenger vehicles [71] to microgrids [72, 73] to shipboard electric power systems [74]. A unique characteristic of these systems is their controllability [75, 76], which allows power to be directed more intentionally through the system to meet control objectives.

A conceptual framework for market-based control has been presented for the operation of emerging distribution systems in [77]. Optimal utilization of distributed resources and efficient strategy for system control can be obtained through market-based control. In [78], a multi-agent coordination system developed to provide coordination has been presented. In this system, there is an electronic market on which local control agents negotiate using strategies based on short-term microeconomics.

In [79], a bi-level optimization technique has been proposed to maximize profit and market clearing price. Mathematical programming with equilibrium constraints (MPEC) and Karush-Kuhn-Tucker (KKT) conditions have been used to find an optimal solution for the problem. Similarly, in [80], a bi-level optimization method has been proposed for these interactions between distributed system operator (DSO) and independent system operator, and the interactions among each of the DSOs. The proposed optimization model was converted into MPEC formulation. In [81], an integrated approach is applied to find the market clearing price of both electricity and heat.

Market clearing formulations have also taken power system security into account [82–84]. In [85], a market clearing procedure was used for the uncertainty of generating units in the form of system contingencies. This had been solved using a stochastic model consisting of two stages, using Monte-Carlo simulation for random scenario generation and as a series of deterministic optimization problems (scenarios) including non-contingent scenarios and different post-contingency states. The objective function consisted of the offered cost function, lost opportunity cost, and expected interruption cost. AC power flow and security constraints of the power system were considered to solve each optimization problem.

In [86], the market clearing method has been applied for the penetration of wind power into the grid. Due to the variable nature of wind power, it cannot be scheduled and dispatched in the traditional manner. It is difficult to forecast load demand using wind speed profile. Because of the difficulty to forecast wind speed, there needs to be a reserved amount of wind power to keep the power system stable and secure. Integrating wind power into the traditional grid impairs security. Multi-objective



market clearing method can be used to provide a balance between the total cost and risk level of the system. A metaheuristic technique and a multi-objective algorithm were adopted to derive a set of non-dominated solutions with sufficient diversity for decision-making support.

Market clearing prices can be predicted in daily power markets using historical prices, quantities, and other information [87]. A neural network method has been used for fitting and extrapolation of prices and quantities where the network is a three-layer back propagation network. In [88], a multi-objective market clearing method has been proposed for a wind-thermal power system that has uncertainties in wind power generation and load demand forecasts.

To enable market-based control of such systems, it is necessary that appropriate market-clearing algorithms exist that can locate the market-clearing prices that allow the system to operate at equilibrium. Finding the globally coordinating market-clearing prices is a root-finding problem. In this chapter, traditional root-finding algorithms have been used to attempt to solve the market clearing problem. The contributions of this chapter are

1. to examine the numerical challenges of solving the root-finding problem of finding the market-clearing prices using traditional root-finding algorithms by looking at three very simple systems (based on a notional shipboard power system) under three different operating conditions, and
2. to test the numerical algorithms on a more complex system: a notional MVDC system.

## 6.2 Problem Formulation

The problem being solved herein is equivalent to a distributed maximization problem where each component  $i$  (of  $I$ ) consumes power (or provides power if negative) to one or more buses:

$$\max_{\mathbf{P}_1, \mathbf{P}_2, \dots, \mathbf{P}_I} \sum_{i=1}^I U_i(\mathbf{P}_i) \quad (6.1)$$

$$\text{where } \sum_{i=1}^I \mathbf{P}_i = \mathbf{0}, \quad (6.2)$$

where  $\mathbf{P}_i$  is a vector describing the net power consumed by component  $i$  from each bus and  $U_i(\cdot)$  is a utility function that describes how much benefit is gained by that level of power consumption. The specific entries of  $\mathbf{P}_i$  that can be nonzero are based on the bus connectivity of the component, and the specific values of these entries are limited by the operating characteristics of the component (e.g., rating, efficiency). Each component can produce utility (i.e., value to the overall control objective, with arbitrary unit “util”).

If power at each bus is priced according to the vector  $\mathbf{\Pi}$  and utility is valued at an arbitrary price  $\Pi_u > 0$  (herein, 1 \$/util), the profit realized by component  $i$  can

be expressed as

$$\text{Profit}_i(\mathbf{P}_i) = \Pi_u U_i(\mathbf{P}_i) - \mathbf{\Pi}^T \mathbf{P}_i. \quad (6.3)$$

The decision function for that component represents its profit-maximizing operating point and is

$$\mathbf{F}_i(\mathbf{\Pi}) = \arg \max_{\mathbf{P}_i} \text{Profit}_i(\mathbf{P}_i). \quad (6.4)$$

These decision functions describe the profit-maximizing behavior of each component and allow the components to be described using a local model depending only on the interface conditions (i.e., prices).

If each component acts in this way, an artificial market economy is established. It can be shown that the optimization problem in (6.4) is equivalent under reasonable conditions to finding the market-clearing prices  $\mathbf{\Pi}$  such that

$$\mathbf{F}(\mathbf{\Pi}) = \sum_{i=1}^I \mathbf{F}_i(\mathbf{\Pi}) = \mathbf{0}, \quad (6.5)$$

where  $\mathbf{F}(\cdot)$  is the system decision function. The set of market-clearing prices are the prices at which power supplied and power demanded at each bus are equal. The equilibrium price  $\mathbf{\Pi}$  is determined by searching for the root of this function, i.e. where the total demand equals total supply.

The systems considered in this paper are comprised of four different fundamental types of components: generators, interconnects, converters, and loads. Each of these components is connected to one or more buses, and power at each bus is a commodity in the artificial market. All power values are normalized and expressed in per-unit (pu). The specific decision functions for each type of component are discussed in Section 6.3.

The system decision function practically has some structural characteristics. For example, it can be thought of as somewhat decreasing. It will not really be decreasing everywhere, but if the  $i$ th element of  $\mathbf{F}(\mathbf{\Pi}) > 0$  for  $\mathbf{\Pi}$  with  $i$ th element  $\Pi_i$ , there exists  $\Delta \Pi_i > 0$  such that,  $\mathbf{\Pi}$  with  $\Pi_i + \Delta \Pi_i$  makes the  $i$ th element of  $\mathbf{F}(\mathbf{\Pi}) \leq 0$  (and vice versa). In other words, if there is an imbalance in power consumption at a given bus, this imbalance can be forced to change signs by changing the price of power at that bus sufficiently.

The system decision function is largely flat over large ranges. This occurs because when components are operating at their rated limits or at zero, changes in prices will not cause the component to operate above its rating or below zero. Conversely, the decision function can have relatively large derivatives for operating points in the interior of the operating range of the various components.

Finally, because power electronic converters are modeled to have relatively constant efficiency, and the close electrical distances between buses, there is a stiffness associated with the system decision function. Components that can transfer power efficiently from one bus to another will shift their output dramatically in response to relatively small differences in price between these buses. Therefore, there is a relatively tight coupling among the prices throughout the system generally.

### 6.3 Decision Functions

The systems considered are comprised of four different fundamental types of components: generators, interconnects, converters, and loads. Each of these components is connected to one or more buses, and power at each bus is the commodity in the artificial market. In the example system considered herein, all power values are normalized. Each component can produce utility (i.e., value to the overall control objective), which is valued at an arbitrary price  $\Pi_u > 0$  (herein, one). The profit-maximizing decision functions of each type of component are presented in the following subsections.

#### 6.3.1 Generator

Generators have instantaneous operating limits based on the mechanical state of the variable (a detailed discussion is provided in [76]). The generator will not exceed its instantaneous maximum power  $P_{max}$ , but it may need to go below its instantaneous minimum power  $P_{min}$  if insufficient load exists in the system (e.g., due to a fault or load shedding).

Such deviations (represented by  $\Delta P$ ) are heavily penalized in the utility function via parameter  $w_{trip} > 0$  because they are associated with overspeed tripping of the generator. On the other hand, output power from the generator is lightly penalized in the utility function via parameter  $w > 0$ , which represents the cost of operating the generator. To balance the system operation, the utility function is also penalized using parameter  $\epsilon$  by the square of the output power. On the other hand, the generator receives revenue by selling power at its output bus at price  $\Pi_{bus}$ . The overall profit function of the generator is

$$\text{Profit} = \Pi_{bus}P_{out} - \Pi_u(w_g P_{out} + w_{trip}\Delta P + \frac{1}{2}\epsilon P_{out}^2) \quad (6.6)$$

subject to

$$0 \leq P_{out} \leq P_{max,inst} \quad (6.7)$$

$$P_{out} + \Delta P \geq P_{min,inst}. \quad (6.8)$$

The profit-maximizing output power is given by

$$P_{out} = \begin{cases} \frac{\Pi_{bus} - w\Pi_u}{\epsilon\Pi_u} & \Pi_{bus} \geq \epsilon\Pi_u P_{min,inst} + w\Pi_u \\ P_{min,inst} & \Pi_{bus} < \epsilon\Pi_u P_{min,inst} + w\Pi_u \\ & \text{and } \Pi_{bus} > \epsilon\Pi_u P_{min,inst} \\ & + (w - w_{trip})\Pi_u \\ \frac{\Pi_{bus} - (w - w_{trip})\Pi_u}{\epsilon\Pi_u} & \Pi_{bus} \leq \epsilon\Pi_u P_{min,inst} \\ & + (w - w_{trip})\Pi_u, \end{cases} \quad (6.9)$$

which must be limited to  $[0, P_{max,inst}]$ . The negative of the output power ( $-P_{out}$ ) appears in the element of the generator decision function corresponding to the generator's bus.

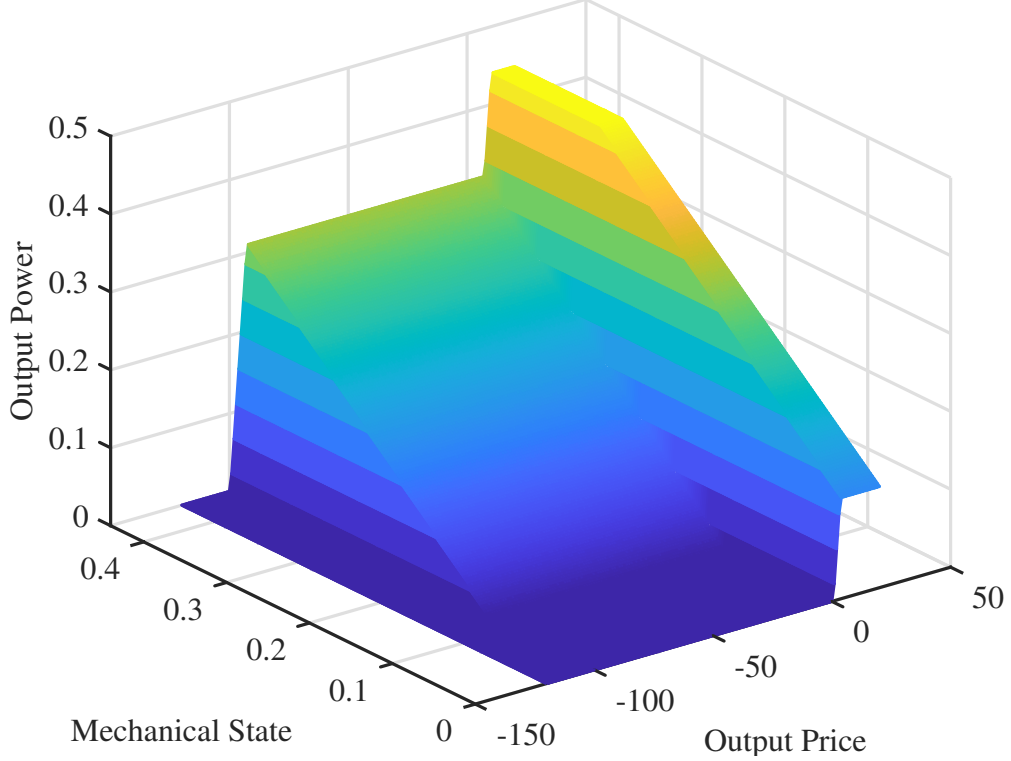


Figure 6.1: Generator output power as a function of bus price and mechanical state. The parameter  $\epsilon$  is artificially much larger than used herein to emphasize the high-slope regions.

In terms of generator ramp rate dynamics, the generator has a maximum step parameter  $P_{step}$  and a time constant  $\tau$  that represent its ramping capability. The generator can tolerate step changes to its output of  $P_{step}$  and ramping output at a rate  $P_{step}/\tau$ . An internal state variable  $P_m$  is a low-pass filtered version of the generator's output power:

$$\frac{dP_m}{dt} = \frac{P_{out} - P_m}{\tau}. \quad (6.10)$$

In discrete-time with time step  $\Delta t$ , this can be represented as

$$P_m(t + \Delta t) = P_m(t) + \frac{P_{out}(t) - P_m(t)}{\tau} \Delta t. \quad (6.11)$$

The instantaneous minimum and maximum operating limits are given by

$$P_{min,inst} = \max\{P_m - P_{step}, 0\} \quad (6.12)$$

$$P_{max,inst} = \min\{P_m + P_{step}, P_{rating}\}. \quad (6.13)$$

### 6.3.2 Converter

The converter can be thought to be controlled such that profit is maximized during power conversion operation. In essence, the converter operates such that its decision

function enables it to decide what the output power will be, given a set of market prices ( $\mathbf{\Pi}$ ), the converter's maximum power  $P_{max}$ , the converter's efficiency  $\eta$ , and the sharing parameter  $\epsilon$ . Mathematically, the profit can be represented as

$$\text{Profit} = \Pi_{out}P_{out} - \Pi_{in}\frac{P_{out}}{\eta} - \Pi_u\frac{1}{2}\epsilon P_{out}^2 \quad (6.14)$$

subject to  $0 \leq P_{out} \leq P_{max}$ . The profit-maximizing output power is

$$P_{out} = \frac{\Pi_{out} - \frac{\Pi_{in}}{\eta}}{\epsilon\Pi_u}, \quad (6.15)$$

which must be limited to  $[0, P_{max}]$ . The input power is  $P_{in} = P_{out}/\eta$ . The input power ( $P_{in}$ ) and the negative of the output power ( $-P_{out}$ ) appear in the elements of the converter decision function corresponding to the converter's input and output buses, respectively.

### 6.3.3 Interconnect

Interconnects are represented very similarly with converters. Their efficiency is unity and they are modeled as capable of bidirectional power flow. Practically, they would also have a smaller (by rating) value of the sharing parameter  $\epsilon$ . Their profit is

$$\text{Profit} = \Pi_{out}P_{out} - \Pi_{in}P_{out} - \Pi_u\frac{1}{2}\epsilon P_{out}^2 \quad (6.16)$$

subject to  $-P_{max} \leq P_{out} \leq P_{max}$ .

The profit-maximizing power flow through the interconnect (from "input" bus to "output" bus) is given by

$$P_{out} = \frac{\Pi_{out} - \Pi_{in}}{\epsilon\Pi_u}, \quad (6.17)$$

which must be limited to  $[-P_{max}, P_{max}]$ . The input power is  $P_{in} = P_{out}$ . The input power ( $P_{in}$ ) and the negative of the output power ( $-P_{out}$ ) appear in the elements of the interconnect decision function corresponding to the interconnect's input and output buses, respectively.

### 6.3.4 Load

Each load is assumed to have a weight  $w$  corresponding to its degree of importance, e.g. vital and nonvital loads that contributes to utility. The utility function is also penalized using the sharing parameter  $\epsilon$  by the square of the load power. The profit derived by a load is

$$\text{Profit} = \Pi_u w P_{in} - \Pi_{in} P_{in} - \Pi_u \frac{1}{2} \epsilon P_{in}^2 \quad (6.18)$$

subject to  $0 \leq P_{in} \leq P_{max}$ . The profit-maximizing power consumption of the load is given by

$$P_{in} = \frac{w\Pi_u - \Pi_{in}}{\epsilon\Pi_u}, \quad (6.19)$$

which must be limited to  $[0, P_{max}]$ . The input power ( $P_{in}$ ) appears in the element of the load decision function corresponding to the load's bus.

## 6.4 Numerical Algorithms for Market Clearing

Broyden’s method, a Newton-like method (e.g., [89, 90]), can be used to solve root-finding problems without knowledge of the Jacobian matrix of the function. The Jacobian matrix of a vector-valued function of several variables is the matrix of all its first-order partial derivatives. Computing the Jacobian matrix is a computationally expensive operation. Broyden’s method works by updating an estimated Jacobian of the function as the algorithm proceeds. Herein, Broyden’s method is studied with a starting Jacobian estimate of  $-\mathbf{I}$ , the negative of the identity matrix, based on the problem structure described above. As the systems considered herein are very small and it is reasonable to calculate the Jacobian matrix analytically based on the decision functions in Section 6.3, Newton-Raphson method is also considered, using the analytical Jacobian matrix directly. This represents an idealized algorithm, and its performance can be compared with Broyden’s method, which would be more practical in realistic situations in which the Jacobian was not available.

## 6.5 Example System and Scenarios

The three systems considered herein, are one-, two-, and three-bus representations of three similar systems. In each, there are two generators of different ratings and a load. In the first system, all components are connected to a single bus. In the second system, one of the generators is connected to a second bus through an interconnect. In the third system, the load is connected to a third bus through a power-electronic converter. The system configurations are shown in Figure 6.2, 6.3 and 6.4; and the parameters of the systems are shown in Table 6.1 in the appendix.

Table 6.1: System Parameters

Parameter	Value
Rated power of generator 1	0.44
Rated power of generator 2	0.06
Rated power of converter	0.35
Rated power of load	0.30
Efficiency of converter, $\eta$	0.99
Weighting of operating each generator, $w$	0.5
Weighting of tripping of each generator, $w_{trip}$	100
Weighting of load, $w$	26
Sharing parameter of generator 1, $\epsilon$	0.0227
Sharing parameter of generator 2, $\epsilon$	0.1667
Sharing parameter of interconnect, $\epsilon$	0.001
Sharing parameter of converter, $\epsilon$	0.0286
Sharing parameter of load, $\epsilon$	0.0333

Three scenarios are considered. The first, labeled Scarcity, corresponds to a situation in which insufficient generation is available to serve a load immediately. The

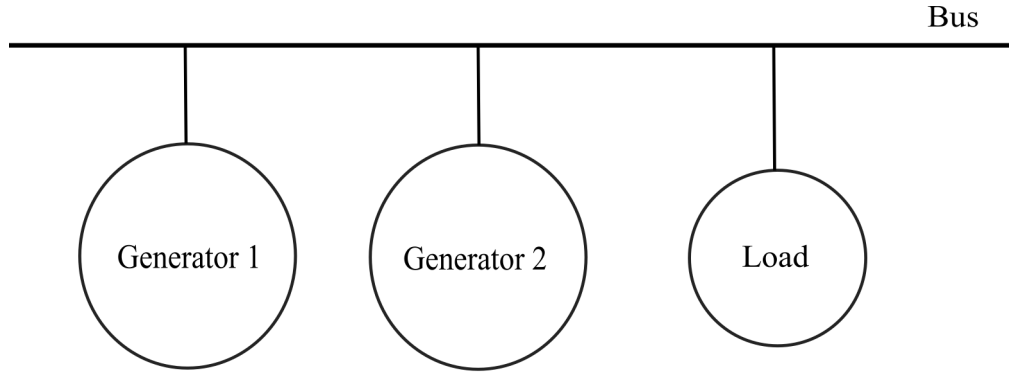


Figure 6.2: Representative System 1 with one bus, two generators, and a load.

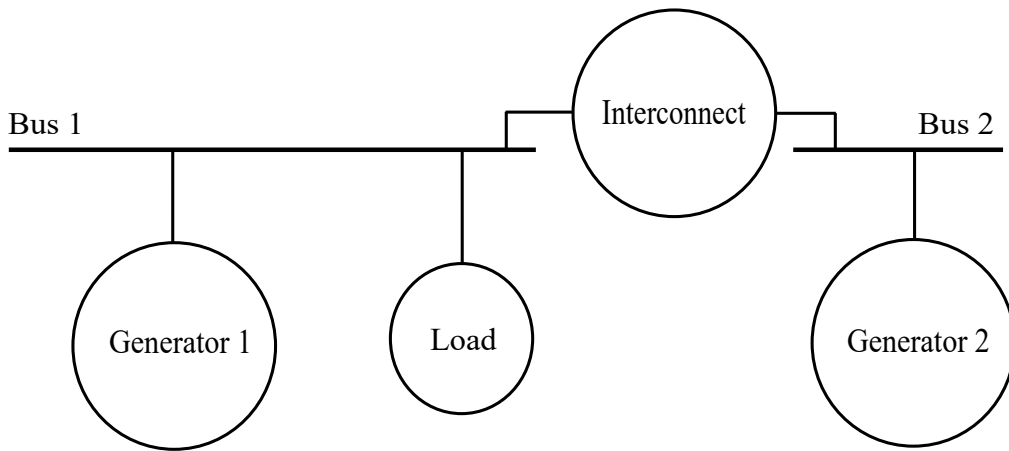


Figure 6.3: Representative System 2 with two buses, two generators, an interconnect, and a load.

second, labeled Abundance, corresponds to a situation in which sufficient generation is available. The third, labeled Overabundance, corresponds to a situation in which less load is connected to the system than the available generation can serve without going under its minimum instantaneous capacity. The parameters associated with these scenarios are shown in Table 6.2.

Table 6.2: Scenario Parameters

	Scarcity	Abundance	Overabundance
Generator 1 $P_{min}$	0.00	0.16	0.16
Generator 1 $P_{max}$	0.13	0.37	0.37
Generator 2 $P_{min}$	0.00	0.01	0.01
Generator 2 $P_{max}$	0.04	0.06	0.06
Load $P_{max}$	0.30	0.30	0.15

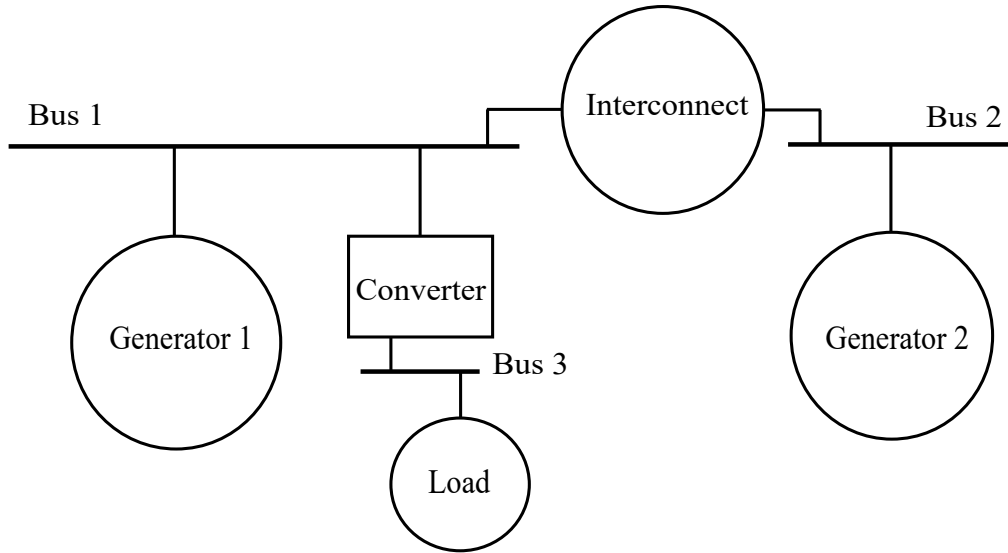


Figure 6.4: Representative System 3 with three buses, two generators, an interconnect, a converter, and a load.

## 6.6 Results

Monte Carlo analysis of both Broyden's method and Newton-Raphson method is performed for starting price guesses within various ranges of the equilibrium set of prices (i.e., uniformly distributed by up to the range in either direction independently in each direction). The equilibrium prices for each system and scenario are given in Table 6.3.

Table 6.3: Equilibrium Prices for Systems under Scenarios

System	Bus	Price		
		Scarcity	Abundance	Overabundance
1	1	25.9943	0.5060	-99.4968
	2	25.9942	0.5059	-99.4968
3	1	25.729	0.5060	-99.4968
	2	25.7296	0.5063	-99.4966
	3	25.9944	0.5199	-100.4974

High precision is required because of the stiffness of these problems as demonstrated herein.

The fraction of times each algorithm converges to the market-clearing set of prices is recorded. For example, the percentage of times the algorithms converge for System 1 in the Scarcity Scenario is shown in Figure 6.5. This is defined as the probability of convergence (%) in the figure. Similar figures emerge for other systems and scenarios. The figures are shown in the Appendix B.



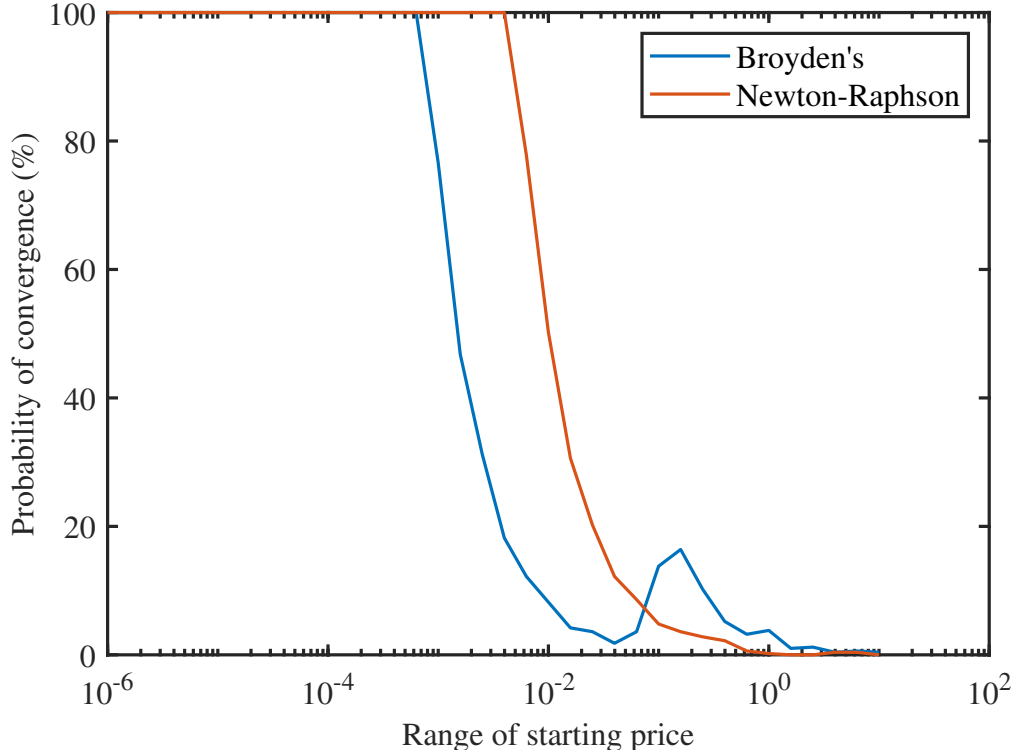


Figure 6.5: Price convergence probability for System 1 in Scenario 1 (Scarcity). Similar figures emerge for the other systems and scenarios.

Table 6.4: Maximum Range of Starting Prices

Scenario	System	Broyden's	Newton-Raphson
Scarcity	1	6.31e-4	3.98e-3
	2	2.51e-6	3.98e-4
	3	1.14e-6	4.25e-4
Abundance	1	2.51e-4	1.58e-3
	2	3.98e-6	3.98e-4
	3	6.31e-7	2.35e-4
Overabundance	1	6.31e-5	3.98e-3
	2	2.51e-6	3.98e-4
	3	6.31e-7	2.35e-4

From such figures, it is possible to compute the maximum range of starting prices for which the algorithm can solve the market-clearing problem. These ranges are shown in Table 6.4, and high values indicate that the algorithm is less sensitive to starting guesses.

As can be seen, using the analytic Jacobian matrix results in better convergence than estimating the Jacobian through Broyden's method. However, even Newton-Raphson suffers poor convergence. The reason for this is the structure of the decision functions described in Section 6.3. The large flat regions create large ranges in which

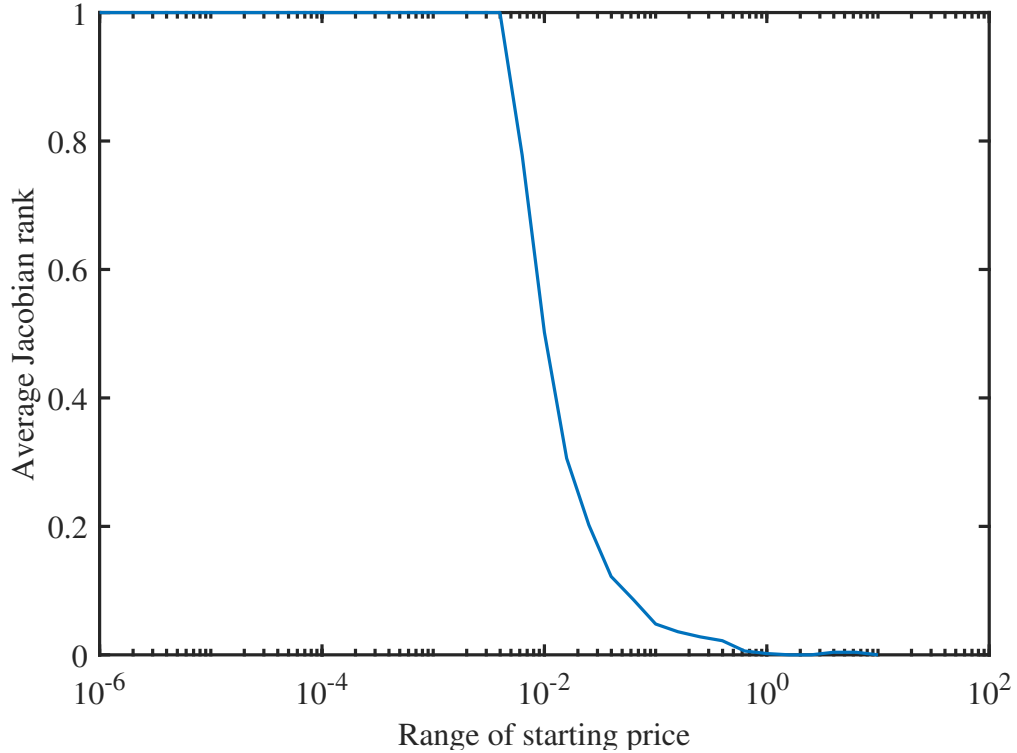


Figure 6.6: Average starting Jacobian rank for System 1 in Scenario 1 (Scarcity).

the Jacobian matrix will not have sufficient information (i.e., insufficient rank) to guide the algorithm toward a solution. This is illustrated by Figure 6.6, where it can be seen that the average starting Jacobian rank nearly identically mirrors the probability that the Newton-Raphson algorithm will converge.

## 6.7 Application in a Notional MVDC System

The challenges of solving the market clearing problem are demonstrated on a larger system, the notional medium-voltage DC (MVDC) system shown in Figure 6.7.

The system is based on a notional MVDC system developed by the Electric Ship Research and Development Consortium [1]. Parameters for the system are shown in Table 6.5.

The four-zone system consists of two main generators and two auxiliary generators. The two propulsion motor drives operate at power levels corresponding with the desired speed. The radar and the mission loads are used to engage in the mission. The zonal loads are fed through converter modules, and each zone contains some vital and some nonvital loads. The MVDC system has a variety of different component types: interconnects, generators, converters, energy storage, and loads. Each of these component types will act as firms in the artificial market-based economy and has a decision function that specifies its profit-maximizing operation for a given set of prices.

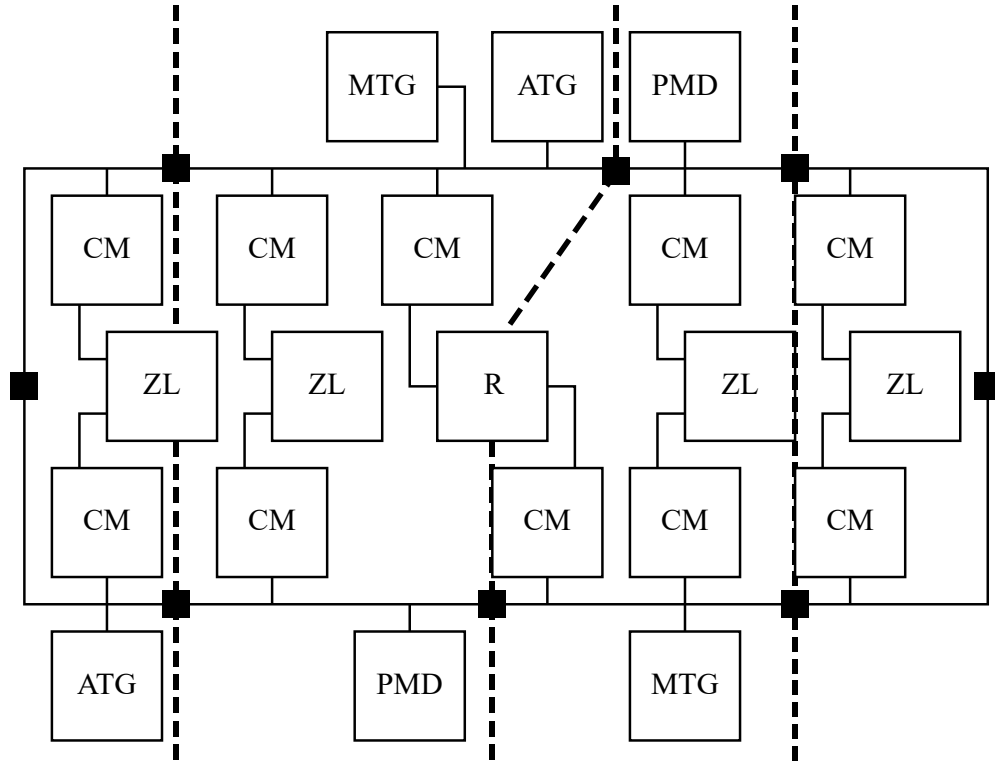


Figure 6.7: Notional MVDC system. MTG signifies main turbine generator, ATG signifies auxiliary turbine generator, PMD signifies propulsion motor drive, CM signifies converter module, R signifies radar, and ZL signifies zonal load [1]. The small black squares are used to separate the four zones in the horizontal direction, and the upper and lower zones in the vertical direction.

Table 6.5: Parameters of Notional MVDC System

Parameter	Value
Rating of main turbine generator (MTG)	36 MW
Rating of auxiliary turbine generator (ATG)	5 MW
Total rated propulsion load	60.4 MW
Radar load	3.8 MW
Vital load per zone	0.93 MW
Nonvital load per zone	0.84 MW
Zone 1 mission load	13 MW
Zone 2 mission load	5 MW
Zone 3 mission load	7 MW

For this system as well, Monte Carlo analysis of both Broyden's method and the Newton-Raphson method is performed as described in the earlier section. The percentage of times the algorithms converge for the MVDC system is shown in Figure 6.8.

As can be seen, using the analytic Jacobian matrix yields better convergence than estimating the Jacobian through Broyden's method. With Broyden's method,

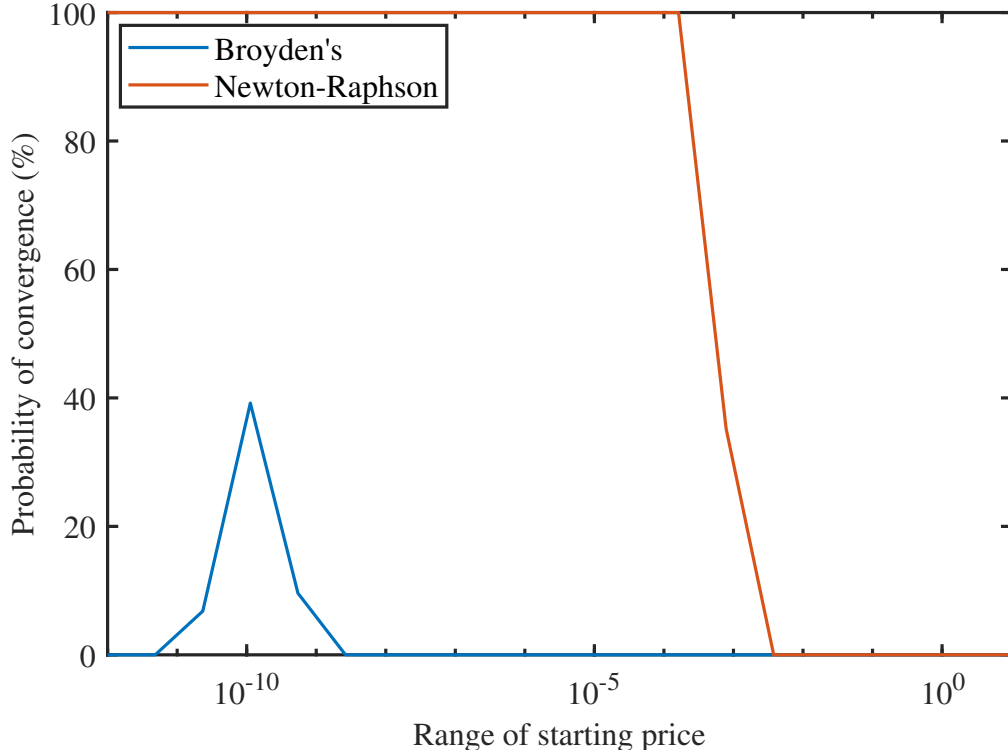


Figure 6.8: Price convergence probability for MVDC system

the solution converges in a very short range of the starting prices with very low probability. Generally, the Jacobian matrix will not have sufficient information (i.e., insufficient rank) to guide the algorithms toward a solution.

## 6.8 Conclusion

In this chapter, the advantages to using market-based control for power electronics-based electric power distribution systems are discussed. The practical application of such control techniques requires an algorithm that can find the market-clearing price. Because of the numerical structure of this problem, conventional algorithms for solving such root-finding problems struggle.

The computational difficulties of finding accurate market clearing price in different types of market conditions have been presented in this chapter. Three notional systems have been tested using Broyden's method and Newton-Raphson method, the conventional algorithms are used to solve such root-finding problems. Results have been illustrated for the systems under different conditions.

While these algorithms can solve the market-clearing problem, they only converge consistently when the starting guess is extremely close to the equilibrium value. This difficulty is caused by the numerical properties of the system decision function for these efficient and spatially compact power electronics-based power distribution systems and will need to be resolved to apply market-based control effectively to such

systems.

By exploiting the structure of the decision functions in Section 6.3, an algorithm is proposed in the next chapter that is able to solve the market-clearing problem to enable such control approaches to address the control of realistic systems.

## Chapter 7 Numerical Algorithm for Solving Market Clearing Problem in Power Electronics-Based Power Distribution Systems

### 7.1 Introduction

In the previous chapter, the numerical challenges of solving the root-finding problem of finding the market-clearing prices in power electronics-based power systems were examined by looking at a complex notional shipboard power system and three very simple systems (based on the notional shipboard power system). In this chapter, the work presented in the previous chapter and in [91] has been extended. A numerical algorithm has been proposed that solves the market clearing problem and determines the market clearing price of the systems under different operating conditions. A complex notional power system, similar to the one in [91] has been used. Three simpler systems have been based on the complex system. The systems have been tested under the three operating scenarios mentioned in [91]. Additionally, the proposed algorithm has been tested using dynamic simulation.

Dynamic simulation is a very important technique used in the analysis of power systems. System dynamics [92], control elements, disturbances [93], and load changes [94] can be accommodated in such an approach. In cases with load unbalance, three phase dynamic simulation can be used [95]. Fast and accurate dynamic simulation is very useful for power system operation companies for training operators, analyzing large sets of scenarios, assessing the dynamic security of the network in real-time or scheduling the day ahead operation [93]. Hence, dynamic simulation can serve a useful purpose in testing the robustness of an algorithm. In this paper, the robustness and accuracy of the proposed market clearing algorithm has been validated using dynamic simulation.

The specific contributions of this chapter are

1. to propose a market-based algorithm that solves the market clearing price under numerical challenges,
2. to compare the proposed algorithm with traditional root-finding algorithms like Broyden's method and Newton-Raphson method for different systems, and
3. to demonstrate that the proposed market-based control is efficient in clearing the market by using dynamic simulation.

### 7.2 Problem Formulation

The formulation of the problem has been discussed in Section 6.2.

### 7.3 Proposed Algorithm for Solving the Market Clearing Problem

The market-clearing problem is essentially a multi-variable root-finding problem, essentially finding the market-clearing set of prices  $\mathbf{\Pi}$  such that  $\mathbf{F}(\mathbf{\Pi}) = \mathbf{0}$ .

Many algorithms traditionally used for solving such problems use the Jacobian matrix of the function  $\mathbf{F}(\cdot)$ . For example, Broyden's method uses an estimate of the inverse of the Jacobian matrix  $\mathbf{J}_{est}^{-1}$ . Newton-Raphson method uses the Jacobian matrix directly to update the price vector. The Jacobian matrix of a vector-valued function of several variables is the matrix of all its first-order partial derivatives. While the Jacobian matrix may sometimes be available analytically (e.g., for the relatively simple component models in Section 6.3), it would more generally need to be estimated numerically, which can be computationally expensive.

Traditional algorithms for solving the problems considered herein struggle because of certain properties of system decision functions: The Jacobian function is generally singular because of large plateaus in the system decision function. There is high stiffness in these problems because of the high degree of coupling between prices at different buses.

The proposed algorithm exploits the problem structure. It maintains an estimate of the inverse of the Jacobian matrix  $\mathbf{J}_{est}^{-1}$  using Broyden's good method, but it makes relaxed updates to its estimate:

$$\mathbf{J}_{est}^{-1} := \mathbf{J}_{est}^{-1} + \epsilon \frac{(\Delta\mathbf{\Pi} - \mathbf{J}_{est}^{-1}\Delta\mathbf{P})}{(\Delta\mathbf{\Pi}^T \mathbf{J}_{est}^{-1} \Delta\mathbf{P})(\Delta\mathbf{\Pi}^T \mathbf{J}_{est}^{-1})}. \quad (7.1)$$

This update prevents the algorithm from overcorrecting the estimate, recognizing that the step over which the update is being calculated involves large flat regions of the system decision function. A visual depiction of this process is shown in Figure 7.1.

In this diagram, showing a one-dimensional version of the problem, the algorithm takes a step from a flat area of the decision function towards a point near the solution. If the derivative of this function were estimated on the basis of this step, it would significantly underestimate the magnitude of the derivative in the vicinity of the solution. This would cause the magnitude of the inverse of the derivative to be overestimated, which would make it appear that significantly larger steps were needed to reach the solution, causing poor convergence behavior. Using the relaxation parameter  $\epsilon$  (herein 0.05) helps the algorithm avoid overcorrection while maintaining useful direction information in  $\mathbf{J}_{est}^{-1}$ .

Exploiting the somewhat decreasing nature of the system decision functions, it is recognized that a zero crossing can be induced even when the decision function is flat by moving far enough in the appropriate direction. This is used in the proposed algorithm to take appropriate steps that create changes in the decision function even starting in regions where the function is flat. Line searches are used to approach the zero crossing more precisely with a tolerance of  $\gamma$  (herein  $10^{-12}$ ).

The high degree of coupling between the problem's dimensions makes it beneficial to pursue steps in directions aligned with this coupling rather than focusing on the

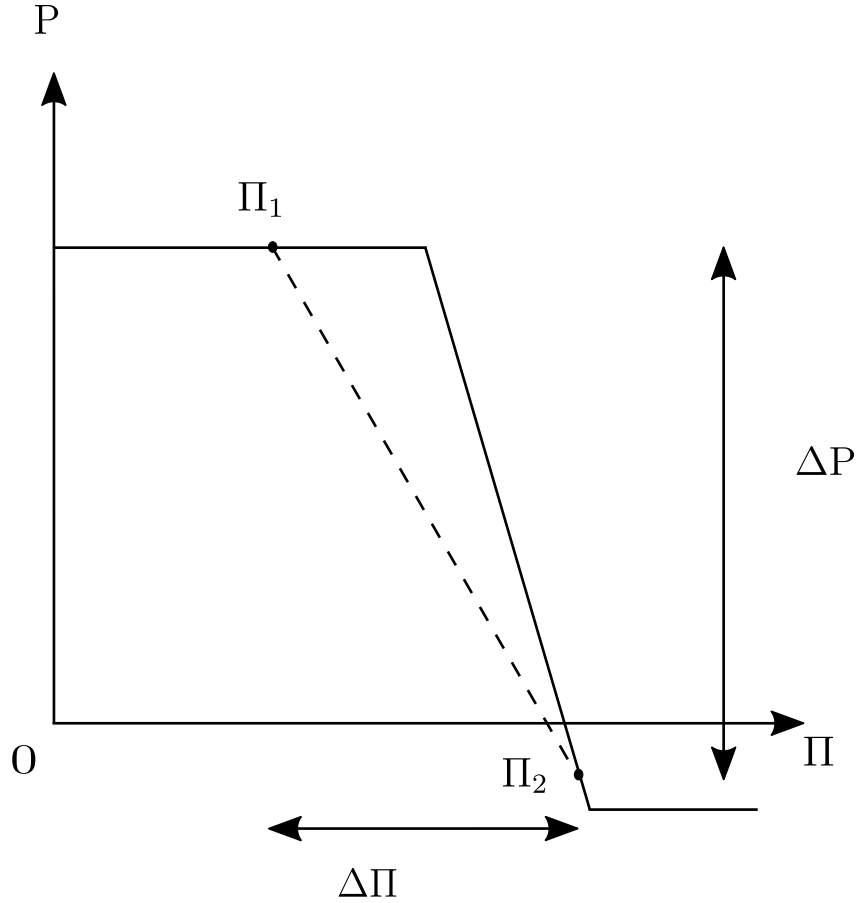


Figure 7.1: Root finding for a single dimensional problem

ordinary basis directions. Using the relaxed estimate  $\mathbf{J}_{est}^{-1}$ , it is possible to do principal component analysis using the singular value decomposition to explore the most important directions in terms of reducing error while reflecting the coupling between the dimensions.

Understanding the scope of the problem also provides some advantages. For example, it is known that the solutions are never very far from  $\mathbf{0}$ . If the initial guess has an error worse than starting from zero, the algorithm can start from zero instead. Likewise, if a candidate direction does not induce a zero crossing with a sufficiently small step  $M$  (herein  $10^6$  \$/s), the algorithm proceeds with the next most important direction.

The proposed algorithm is shown in Algorithm 2. Herein, the proposed numerical algorithm has a starting estimate  $\mathbf{J}_{est}^{-1} := -\mathbf{I}$ , the negative of the identity matrix, based on the somewhat decreasing nature of the system decision function described in Subsection 6.2 above. The algorithm proceeds until the error is reduced below  $\delta$  (herein  $10^{-6}$  pu) or it fails.

The proposed algorithm is compared with some reference algorithms as described in the next section. Monte Carlo analysis of the proposed algorithm and the reference algorithms are then performed for starting price guesses within various ranges of the



---

**Algorithm 2** Proposed Algorithm

---

```
 $\mathbf{J}_{est}^{-1} := -\mathbf{I}$   
 $\mathbf{P} := \mathbf{F}(\mathbf{\Pi})$   
if  $|\mathbf{F}(\mathbf{0})| < |\mathbf{P}|$  then ▷ reposition initial guess  
     $\mathbf{\Pi} := \mathbf{0}$   
     $\mathbf{P} := \mathbf{F}(\mathbf{\Pi})$   
end if  
while  $|\mathbf{P}| > \delta$  do  
     $\mathbf{USV}^T := \mathbf{J}_{est}^{-1}$  ▷ singular value decomposition  
     $\mathbf{U} = [\mathbf{u}_1 \ \mathbf{u}_2 \ \cdots \ \mathbf{u}_N]$   
     $\mathbf{S} = \begin{bmatrix} s_1 & & & & \\ & s_2 & & & \\ & & \ddots & & \\ & & & \ddots & \\ & & & & s_N \end{bmatrix}$   
     $\mathbf{V} = [\mathbf{v}_1 \ \mathbf{v}_2 \ \cdots \ \mathbf{v}_N]$   
     $I :=$  sort indices  $i$  in descending order of  $|s_i \mathbf{v}_i^T \mathbf{P}|$   
    for all  $i \in I$  do  
         $s := (\mathbf{v}_i^T \mathbf{P})$   
         $\mathbf{d} := -s \mathbf{u}_i$  ▷ bracket zero crossing  
        if  $(\mathbf{v}_i^T \mathbf{F}(\mathbf{\Pi} + \mathbf{d})) = s$  then  
             $lb := 1$   
             $ub := 2$   
            while  $(\mathbf{v}_i^T \mathbf{F}(\mathbf{\Pi} + ub \cdot \mathbf{d})) = s$  do  
                 $lb := ub$   
                 $ub := 2 \cdot ub$   
                if  $ub > M$  then ▷ bound step length  
                    skip to next direction in  $I$   
                    if no remaining directions, algorithm fails  
                end if  
            end if  
            end while  
        else  
             $lb := 0$   
             $ub := 1$   
        end if  
        while  $ub - lb \geq \gamma$  do ▷ locate zero crossing  
            if  $(\mathbf{v}_i^T \mathbf{F}(\mathbf{\Pi} + (ub + lb)/2 \cdot \mathbf{d})) = s$  then  
                 $lb := (ub + lb)/2$   
            else  
                 $ub := (ub + lb)/2$   
            end if  
        end while
```

---

---


$$\begin{aligned}
\Delta \boldsymbol{\Pi} &= ub \cdot \mathbf{d} \\
\boldsymbol{\Pi} &:= \boldsymbol{\Pi} + \Delta \boldsymbol{\Pi} \\
\Delta \mathbf{P} &:= \mathbf{F}(\boldsymbol{\Pi}) - \mathbf{P} \\
\mathbf{P} &:= \mathbf{P} + \Delta \mathbf{P} \\
\mathbf{J}_{est}^{-1} &:= \mathbf{J}_{est}^{-1} + \epsilon \frac{(\Delta \boldsymbol{\Pi} - \mathbf{J}_{est}^{-1} \Delta \mathbf{P})}{(\Delta \boldsymbol{\Pi}^T \mathbf{J}_{est}^{-1} \Delta \mathbf{P})(\Delta \boldsymbol{\Pi}^T \mathbf{J}_{est}^{-1})}
\end{aligned}$$

▷ relaxed Broyden update

**end for**  
**end while**

---

equilibrium set of prices (i.e., uniformly distributed by up to the range in either direction independently in each direction). With the method proposed herein, the numerical challenges faced in [91] can be minimized and the algorithm is able to guide the Jacobian towards a solution, that is, towards clearing the market with appropriate prices. The robustness of the algorithm is then tested using dynamic simulation.

## 7.4 Reference Algorithms

Three reference algorithms have been used for comparison with the proposed market-clearing algorithm.

### 7.4.1 Broyden's Method

The first reference algorithm is Broyden's method, a Newton-like method (e.g., [96, 97]) that can be used to solve root-finding problems without direct knowledge of the Jacobian matrix of the function. For practical systems in which the derivative information associated with component decision functions may not be known, the Jacobian matrix may not be available. Broyden's method works by maintaining an estimate of the inverse of the Jacobian matrix  $\mathbf{J}_{est}^{-1}$ .

The estimate of the inverse of the Jacobian matrix is initialized as  $\mathbf{J}_{est}^{-1} := -\mathbf{I}$ , which corresponds to the somewhat partially decreasing structure of the decision function described above. The price vector is updated as follows:

$$\boldsymbol{\Pi} := \boldsymbol{\Pi} - \mathbf{J}_{est}^{-1} \mathbf{P}. \quad (7.2)$$

This results in a change in the price vector of  $\Delta \boldsymbol{\Pi} = -\mathbf{J}_{est}^{-1} \mathbf{P}$  and a change in the power imbalance vector of  $\Delta \mathbf{P} = \mathbf{F}(\boldsymbol{\Pi} + \Delta \boldsymbol{\Pi}) - \mathbf{F}(\boldsymbol{\Pi})$ . Using Broyden's good method, the estimate of the inverse of the Jacobian matrix is updated as follows:

$$\mathbf{J}_{est}^{-1} := \mathbf{J}_{est}^{-1} + \frac{(\Delta \boldsymbol{\Pi} - \mathbf{J}_{est}^{-1} \Delta \mathbf{P})}{(\Delta \boldsymbol{\Pi}^T \mathbf{J}_{est}^{-1} \Delta \mathbf{P})(\Delta \boldsymbol{\Pi}^T \mathbf{J}_{est}^{-1})}. \quad (7.3)$$

The algorithm terminates successfully when  $|\mathbf{P}| \leq \delta$  or unsuccessfully when  $\Delta \mathbf{P}$  in denominator is zero,  $\Delta \mathbf{P} = 0$ .

### 7.4.2 Newton-Raphson Method

The second reference algorithm is the Newton-Raphson method, which uses the Jacobian matrix directly to update the price vector. For the relatively simple component models considered herein (Section 6.2), it is possible to evaluate the Jacobian matrix analytically, but this might not be as practical for more complex system models. Using the exact Jacobian matrix eliminates any error due to estimation, and the Newton-Raphson method might be expected to perform better than Broyden's method.

This method works by updating the price vector as follows:

$$\mathbf{\Pi} := \mathbf{\Pi} - \mathbf{J}^{-1}\mathbf{P}. \quad (7.4)$$

The algorithm terminates successfully when  $|\mathbf{P}| \leq \delta$  or unsuccessfully when  $\Delta\mathbf{P}$  in denominator is zero,  $\Delta\mathbf{P} = 0$ .

### 7.4.3 Fsolve Method

The third reference algorithm is MATLAB's fsolve function with its default parameters. This is a trust-region-dogleg algorithm and represents a more sophisticated implementation of numerical root finding than the first two reference algorithms. The algorithm is taken to be successful if it terminates with  $|\mathbf{P}| \leq \delta$ .

## 7.5 Example Systems

### 7.5.1 Representative System

The convergence of the proposed market-clearing algorithm is demonstrated on a suite of power-electronics based power systems of progressing complexity. The simpler systems (Systems 1–3) are based on a representative power system (System 4), which is shown in Figure 7.2. For survivability, this system is divided into four zones (Zones 1-4 from right to left) with two separate corridors providing connection between the zones (at the bottom and top of the diagram, respectively). There are interconnects between the zones in the corridors as well as connecting the corridors that can be disconnected to isolate sections of the system. The system is powered by two main generators (MG 1 and MG 2) in the inner zones and two auxiliary generators (AG 3 and AG 4) in the outer zones. These generators are connected primarily to one of the corridors but can also be connected to the opposite corridor. This system has a large peak propulsion load that is served by four propulsion motor drives situated throughout the system. Like the generators, the propulsion drives are primarily connected to one of the corridors but can also be connected to the opposite corridor. A series of mission loads situated in each zone is fed through pairs of converters from each corridor for redundancy. Each zone also contains service loads connected in each zone and in each corridor.

This system is labeled System 4, and its parameters are given in Table 7.1.

Table 7.1: Parameters of Representative System (System 4)

Parameter	Value
Main generator (MG) rating	0.44 pu
Auxiliary generator (AG) rating	0.06 pu
Interconnect (I) rating	1 pu
Propulsion load total (P) rating	0.75 pu
Mission load (M) rating	0.03 pu
Service load (L) rating	0.01 pu
Propulsion drive converter (P) rating	0.19 pu
Mission load converter (C) rating	0.03 pu
Generator operating weight $w$	0.5 util/s/pu
Generator tripping weight $w_{trip}$	20 util/s/pu
P weight	1 util/s/pu
M weight	4 util/s/pu
L weight	2 util/s/pu
MG sharing parameter	0.0229 util/s/pu <sup>2</sup>
AG sharing parameter	0.16 util/s/pu <sup>2</sup>
I sharing parameter	0.001 util/s/pu <sup>2</sup>
P sharing parameter	0.0133 util/s/pu <sup>2</sup>
C sharing parameter	0.4 util/s/pu <sup>2</sup>
M sharing parameter	0.4 util/s/pu <sup>2</sup>
L sharing parameter	0.8 util/s/pu <sup>2</sup>
P efficiency	100%
C efficiency	99%
MG load step parameter	0.1094 pu
AG load step parameter	0.0156 pu
MG time constant	2.50 s
AG time constant	2.50 s

### 7.5.2 Simplified Systems

Before considering the more complex system (System 4) described above, a sequence of simplified systems of increasing complexity is considered. The systems are based on the representative system and successively demonstrate its salient features.

In each of the simplified systems, there are two generators, a main generator (MG) and an auxiliary generator (AG). There is also a propulsion load (P), a mission load (M), and a service load (L).

In the first system (System 1), all of the components are connected to a single bus (B). In the second system (System 2), the main generator and the propulsion load are connected to one bus (B 1), and the auxiliary generator, mission load, and service load are connected to another bus (B 2). The buses are connected via an interconnect. The third system (System 3) resembles System 2, but the mission load

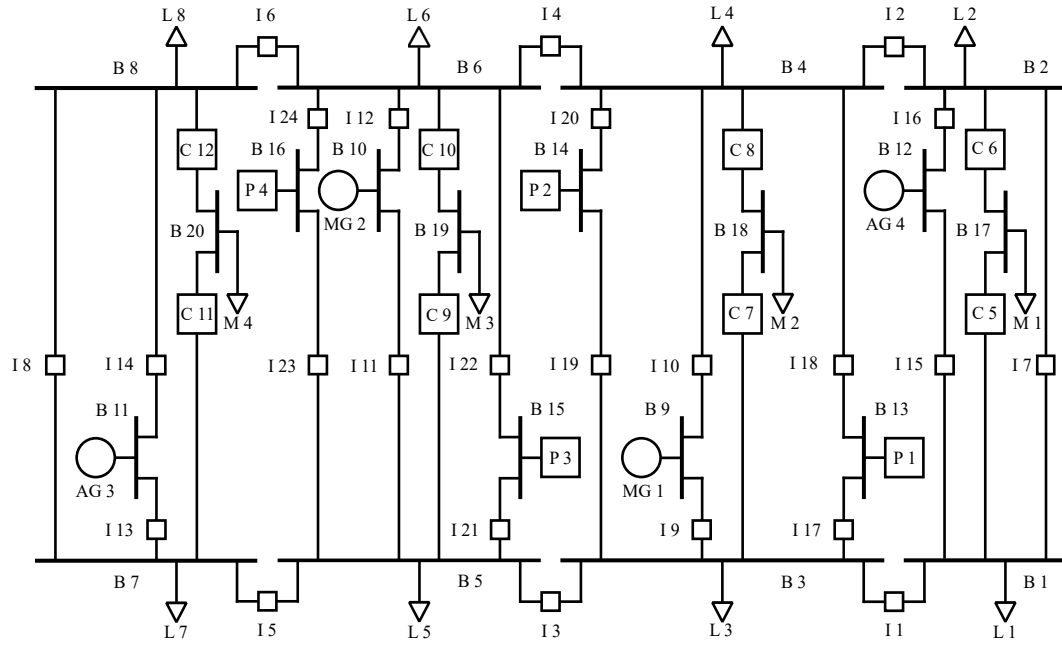


Figure 7.2: Diagram illustrating a complex, representative power system (System 4). It consists of two main generators on the inner zones (MG 1 and MG 2), two auxiliary generators on the outer zones (AG 3 and AG 4), four propulsion loads (P), mission loads (M) fed through converter module (C), service loads (L), and interconnects (I) to connect between buses (B).

is fed from a converter (C) connecting B 2 to a third bus (B 3) to which the mission load is connected.

The system configurations are shown in Figure 7.3–7.5, and the parameters of the systems are shown in Table 7.2.

B

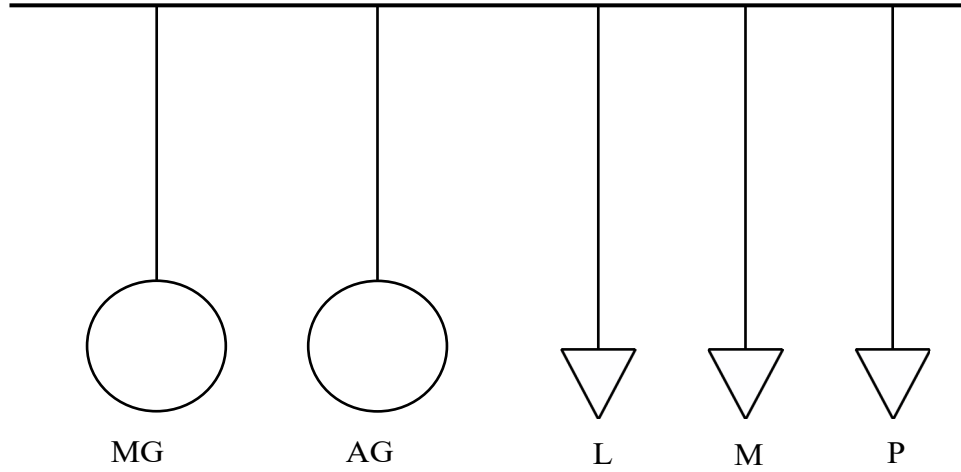


Figure 7.3: Diagram illustrating System 1. The main generator (MG), auxiliary generator (AG), service load (L), mission load (M), and propulsion load (P) are all connected to a single bus (B).

Table 7.2: Parameters of Simplified Systems (Systems 1–3)

Parameter	Value
Main generator (MG) rating	0.44 pu
Auxiliary Generator (AG) Rating	0.06 pu
Interconnect (I) rating	1 pu
Propulsion load total (P) rating	0.75 pu
Mission load (M) rating	0.1 pu
Service load (L) rating	0.1 pu
Efficiency of converter, $\eta$	99%
Generator operating weight, $w$	0.5 util /s/pu
Generator tripping weight, $w_{trip}$	20 util/s/pu
P weight	1 util/s/pu
M weight	4 util/s/pu
L weight	2 util/s/pu
MG sharing parameter	0.0229 util/s/pu <sup>2</sup>
AG sharing parameter	0.16 util/s/pu <sup>2</sup>
I sharing parameter	0.001 util/s/pu <sup>2</sup>
P sharing parameter	0.0133 util/s/pu <sup>2</sup>
M sharing parameter	0.1 util/s/pu <sup>2</sup>
L sharing parameter	0.1 util/s/pu <sup>2</sup>
Propulsion load converter sharing parameter	0.0133 util/s/pu <sup>2</sup>
Mission load converter sharing parameter	0.1 util/s/pu <sup>2</sup>
Service load converter sharing parameter	0.1 util/s/pu <sup>2</sup>

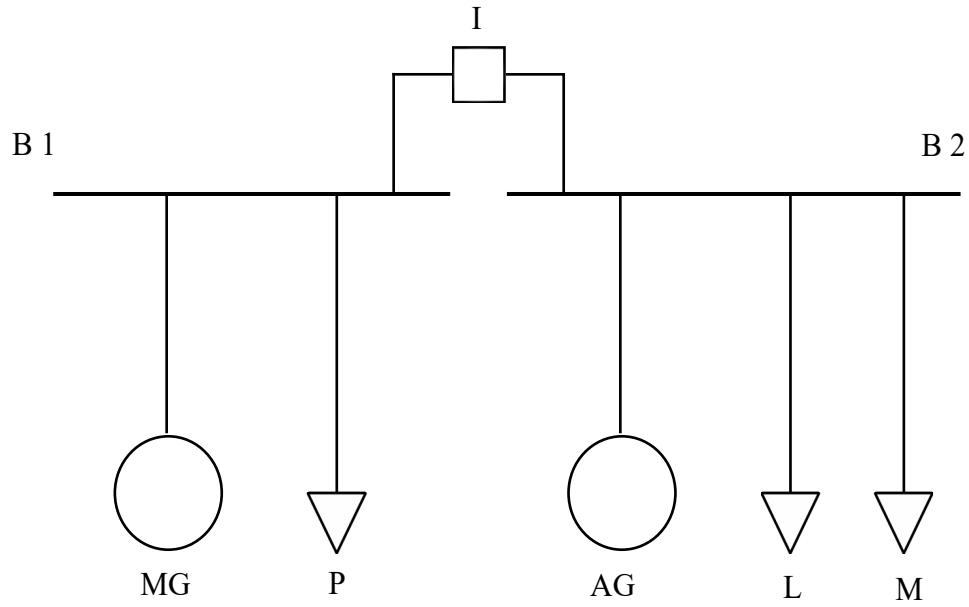


Figure 7.4: Diagram illustrating System 2. The main generator (MG) supplies power to the propulsion load (P) through one bus (B 1) since a higher rated load requires a higher rated generator. The mission load (M) and service load (L) are supplied power by the auxiliary generator (AG) through another bus (B 2). The two buses are connected via an interconnect (I).

### 7.5.3 Operating Scenarios

To test the proposed market-clearing algorithm, three different operating scenarios are considered for each system. Scenario 1 (Scarcity) corresponds to a situation in which insufficient generation is instantaneously available to serve load demand. Scenario 2 (Abundance) corresponds to a situation in which sufficient generation is available. Scenario 3 (Overabundance) corresponds to a situation in which less load is connected to the system than the available generation can serve without going under its minimum instantaneous capacity. This situation could lead to over-speed tripping of generators and may be associated with sudden load shed events (or faults, which could result in load being disconnected from generators). The parameters associated with these scenarios are shown in Table 7.3.

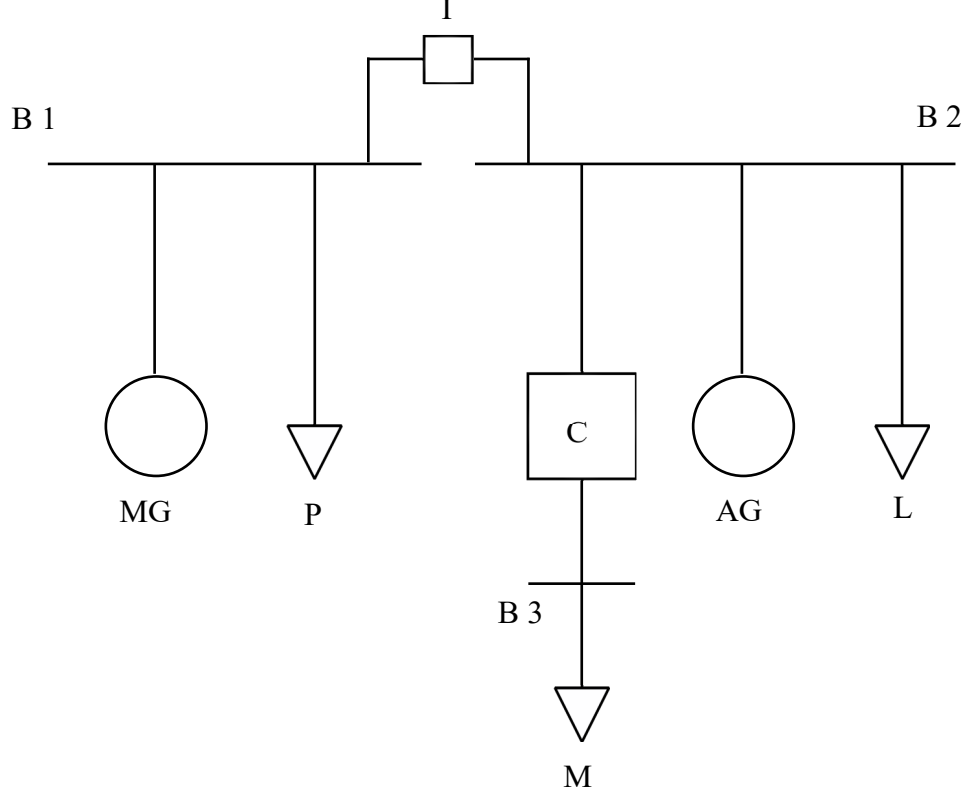


Figure 7.5: Diagram illustrating System 3. The main generator (MG) supplies power to the propulsion load (P) through one bus (B 1) since it has higher rating. The mission load (M) and service load (L) are supplied power by the auxiliary generator (AG) through another bus (B 2). The two buses are connected via an interconnect (I). The mission load (M) is connected to a converter module (C) via a separate bus (B 3).

Table 7.3: Scenario Parameters for All Systems (Systems 1–4)

	Scarcity	Abundance	Overabundance
MG $P_{min,inst}$	0.1422 pu	0.2844 pu	0.2844 pu
MG $P_{max,inst}$	0.3609 pu	0.4375 pu	0.4375 pu
AG $P_{min,inst}$	0.0203 pu	0.0406 pu	0.0406 pu
AG $P_{max,inst}$	0.0516 pu	0.0625 pu	0.0625 pu
Propulsion Load $P_{max}$	0.25 pu	0.25 pu	0.0625 pu
Mission Load $P_{max}$	Rated	Rated	Rated
Service Load $P_{max}$	Rated	Rated	Rated

## 7.6 Convergence of the Proposed Algorithm and Reference Algorithms

Monte Carlo analysis of the proposed algorithm and the reference algorithms is performed to understand the convergence properties of these algorithms. For a given



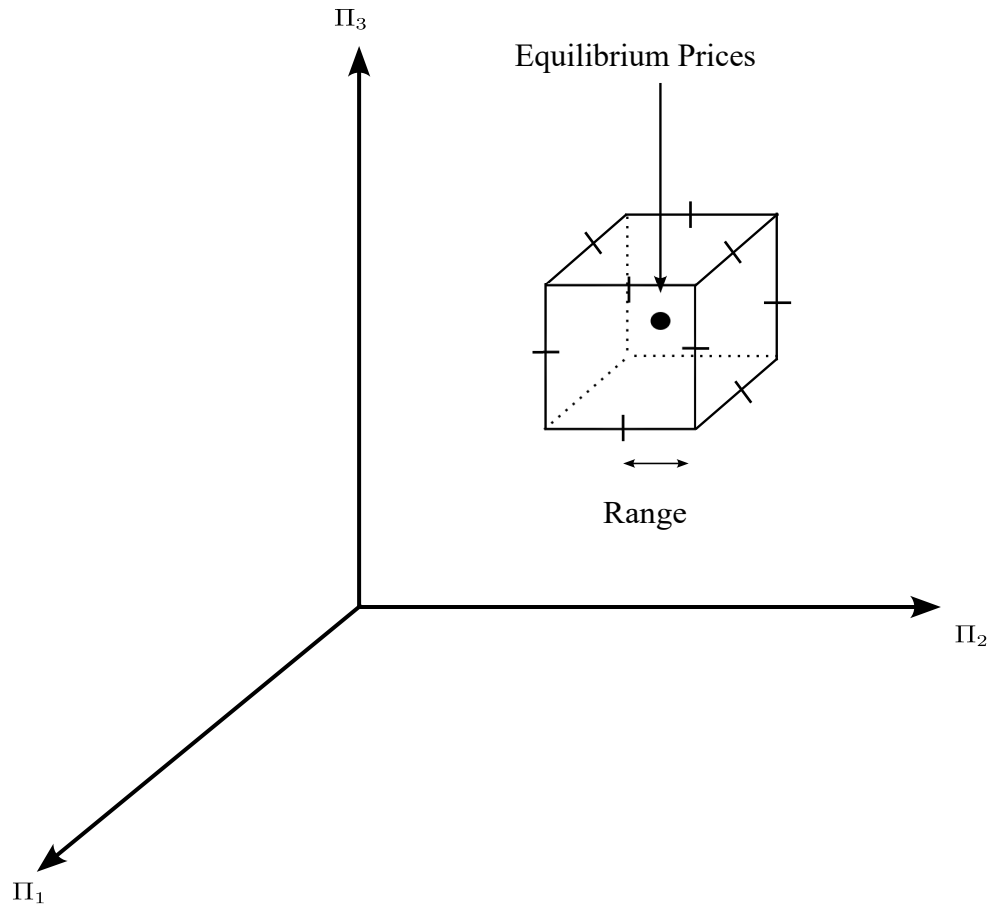


Figure 7.6: Monte Carlo sampling of starting prices.

range of starting prices, starting prices are uniformly distributed in cuboids about the equilibrium prices for that system and scenario. These cuboids extend independently in each dimension in both directions as shown in Figure 7.6.

For each range, 200 starting prices are considered, and each algorithm is executed until it converges or fails. By considering increasing range values, the performance of the algorithms with starting prices further from the equilibrium prices is considered. Herein, 41 ranges logarithmically distributed between  $10^{-8}$  and  $10^2$  are considered.

The equilibrium prices for each system and scenario are given in Table 7.4.

Table 7.4: Equilibrium Prices for Systems under Scenarios

System	Bus	Price (\$/s)		
		Scarcity	Abundance	Overabundance
1	1	0.9972	0.5090	-19.4948
2	1	0.9972	0.5090	-19.4948
	2	0.9973	0.5091	-19.4946
3	1	0.9972	0.5090	-19.4948
	2	0.9973	0.5091	-19.4946
	3	1.0124	0.5193	-19.6865
4	1	0.9943	0.5090	-19.4948
	2	0.9943	0.5092	-19.4946
	3	0.9943	0.5092	-19.4946
	4	0.9943	0.5092	-19.4946
	5	0.9944	0.5092	-19.4946
	6	0.9944	0.5093	-19.4946
	7	0.9944	0.5093	-19.4945
	8	0.9944	0.5093	-19.4945
	9	0.9941	0.5090	-19.4947
	10	0.9944	0.5093	-19.4946
	11	0.9944	0.5093	-19.4945
	12	0.9943	0.5092	-19.4946
	13	0.9943	0.5092	-19.4946
	14	0.9943	0.5092	-19.4946
	15	0.9944	0.5093	-19.4946
	16	0.9944	0.5093	-19.4946
	17	1.0093	0.5193	-19.6865
	18	1.0093	0.5193	-19.6865
	19	1.0094	0.5195	-19.6865
	20	1.0095	0.5195	-19.6865
	21	0.9972	0.5126	-19.4938

High precision is required because of the stiffness of these problems as demonstrated herein.

The fraction of times each algorithm converges for each range is recorded. For example, the percentage of times the algorithms converge for System 1 in Scenario 1 (Scarcity) is shown in Figure 7.7. Similar figures emerge for other systems and scenarios. The figures are shown in the Appendix C.

All of the algorithms converge when starting prices are close to the equilibrium prices. As the range increases, Broyden's method fails to converge first. The convergence behavior of the Newton-Raphson methods and the fsolve method are nearly identical. The proposed algorithm converges for every range considered.

Using such results, it is possible to compute the maximum range of starting prices for which the algorithms solved the problem consistently. These ranges are shown in Table 7.5. The low values for the reference algorithms indicate that they are very sen-

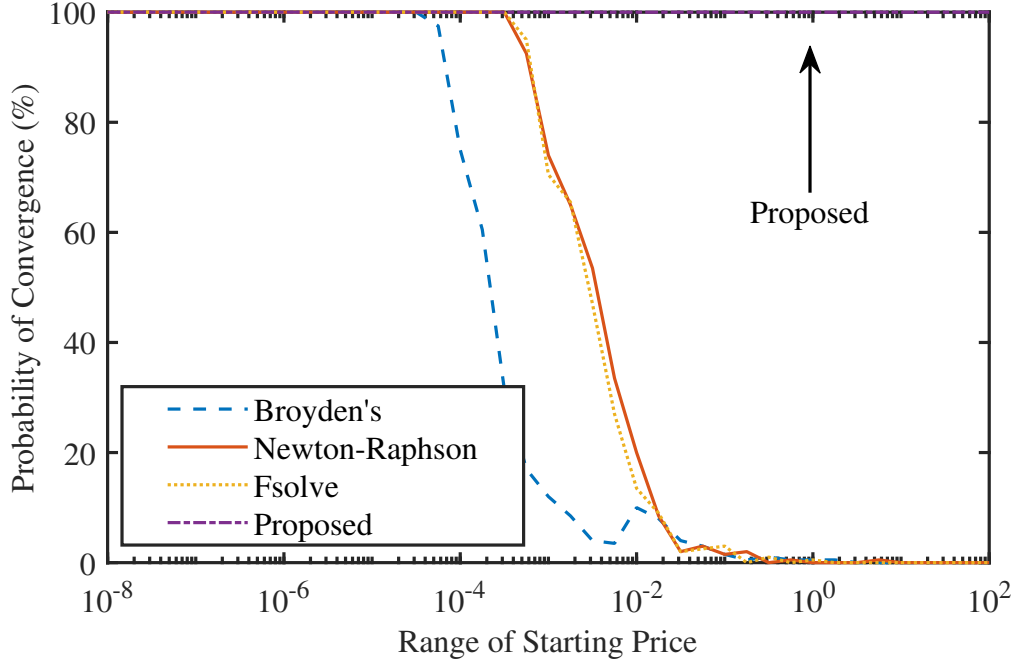


Figure 7.7: Price convergence probability for System 1 in Scenario 1 (Scarcity). Similar figures emerge for the other systems and scenarios. The arrow points to the plot for the proposed algorithm.

sitive to starting guesses. Among the three reference algorithms, Broyden’s method performs worst, which is evident from both Figure 7.7 and Table 7.5. Broyden’s method does not consistently converge for the representative system (System 4) even with the smallest range of starting prices. The traditional root finding algorithm, Newton-Raphson method exhibits the same performance as the commercially available algorithm fsolve, but fsolve does not require the analytical Jacobian matrix. The proposed algorithm converges over the full range, indicating that the algorithm is not sensitive to the starting guesses and successfully solves the market-clearing problem over a practically relevant range.

## 7.7 Dynamic Simulation of Representative System

In the previous section, it has been shown that the proposed algorithm does not suffer from the inability to converge to a market clearing price for large ranges of starting price unlike the reference algorithms. To further demonstrate the performance of the proposed algorithm, a dynamic simulation of the representative system (System 4) is performed. It is simulated for 60 s using a 0.1-s time step, and the market-clearing problem is solved in each time step using the proposed algorithm.

The scenario that is considered involves a dynamic situation in which the system enters different operating modes and different configurations.

The system starts with MG 1 and AG 4 online, and initialized to zero initial load- ing condition. Each service load initially demands 0.0125 pu, and the total propulsion

Table 7.5: Maximum Range of Starting Prices

Scenario	System	Broyden's	Newton-Raphson	Fsolve	Proposed
Scarcity	1	3.16e-5	3.16e-4	3.16e-4	$\geq 10^2$
	2	1.00e-6	5.62e-5	5.62e-5	$\geq 10^2$
	3	1.00e-6	5.62e-5	5.62e-5	$\geq 10^2$
	4	$< 10^{-8}$	1.78e-5	1.78e-5	$\geq 10^2$
Abundance	1	1.00e-4	1.00e-3	1.00e-3	$\geq 10^2$
	2	1.00e-4	1.00e-3	1.00e-3	$\geq 10^2$
	3	1.00e-6	3.16e-5	3.16e-5	$\geq 10^2$
	4	$< 10^{-8}$	1.78e-5	1.78e-5	$\geq 10^2$
Overabundance	1	1.78e-6	1.00e-4	1.00e-4	$\geq 10^2$
	2	1.78e-6	1.00e-4	1.00e-4	$\geq 10^2$
	3	1.00e-6	5.62e-5	5.62e-5	$\geq 10^2$
	4	$< 10^{-8}$	1.78e-5	1.78e-5	$\geq 10^2$

The identical values for Newton-Raphson and Fsolve are due to the sampling of ranges (4 per decade).

demand is 0.1875 pu. At 10 s, each mission load begins to demand 0.025 pu, and propulsion load increases to 0.25 pu. Starting at 20 s, the propulsion demand drops to 0.0625 pu. MG 2 is brought online (at zero initial loading condition). At 40 s, the system enters a split-plant configuration by opening I 7, 8, 10, 11, 14, 15, 18, 19, 22, and 23, effectively separating the two main corridors. At 50 s, the propulsion demand increases to 0.5 pu. The scenario concludes at 60 s.

Prices at different buses throughout the system tend to have similar values at different times (i.e., approximately equal to the product of  $\Pi_u$  and the weight of the least valuable load being served at that time). The prices at two representative buses are shown in In Figure 7.8. B 9 is the bus at which MG 1 is connected, and B 17 is the bus at which M 1 is connected.

Initially, B 9 has a price of approximately \$1/s/pu, representing a scarcity condition caused by the generators ramping up to serve the demand and incompletely meeting the propulsion demand. Once the generators ramp up, the price moves to approximately \$0.5/s/pu, representing an abundance condition because there is sufficient available generation to meet the connected load. During this time, B 17 has a price of \$0/s/pu. There is no mission load demand, so the price on these buses is \$0/s/pu and no power is transferred to these buses through the converter modules.

When mission load demand is added to the system at 10 s, the prices (including at B 17 at this point) again rise to approximately \$1/s/pu, indicating a temporary period of scarcity in which propulsion load is not completely met while the generators ramp up further. At 20 s, there is a sudden drop in propulsion load (faster than the generators would nominally ramp down), causing the system to enter an overabundance condition with large negative prices. After the generators ramp down, the abundance condition is restored.

When MG 2 is brought online at 30 s, there is not a strong shift in prices. Likewise, the plant realignment at 40 s does not cause significant changes in price. Finally, there

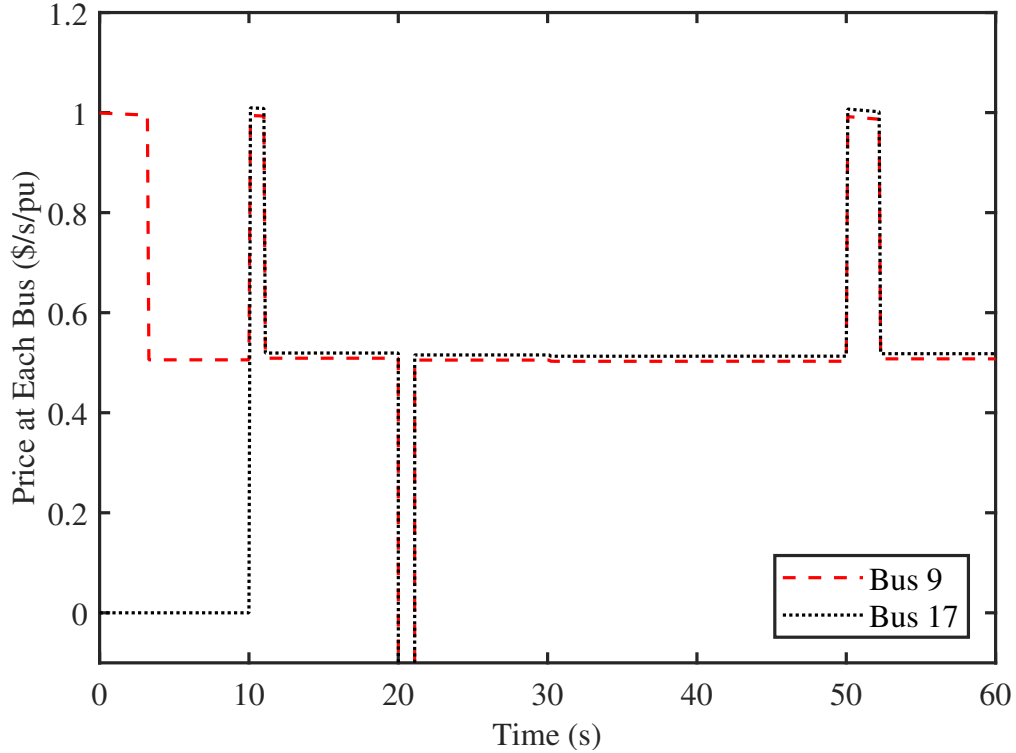


Figure 7.8: Bus prices for dynamic simulation. Bus 9 is the bus for main generator 1 and bus 17 is the bus for mission load 1. During the time interval between 20 s and 21.1 s, both prices decrease to approximately  $-\$20/\text{s}/\text{pu}$  (an overabundance condition).

is again a momentary price increase (scarcity condition) associated with the increased propulsion load at 50 s.

In Figure 7.9, the output power of the three generators is shown. Likewise, in Figure 7.10, the total load powers for the different load types are shown. Each mission load can be served through paralleled converter modules, and the total propulsion load is served through four propulsion drives. Output powers from one of the converters and one of the propulsion drives are shown in Figure 7.11. All of the power flows are governed by the market prices represented in Figure 7.8 and determined in each time step by the proposed algorithm.

At first, MG 1 and AG 3 are online. These two generators ramp up to meet the initial demand, consisting of service load and propulsion load.

After 10 s, the increase in mission and propulsion load power causes an increase in generator output power as indicated in the curve. The two generators ultimately share load in proportion to their ratings.

After 20 s, the propulsion load drops, causing drops in the output of the generators and the propulsion drives. At 30 s, an additional generator is brought online. The output powers of the generators shift so that all generators are sharing proportional to their ratings. This does not have an effect on the load powers, but it causes a very

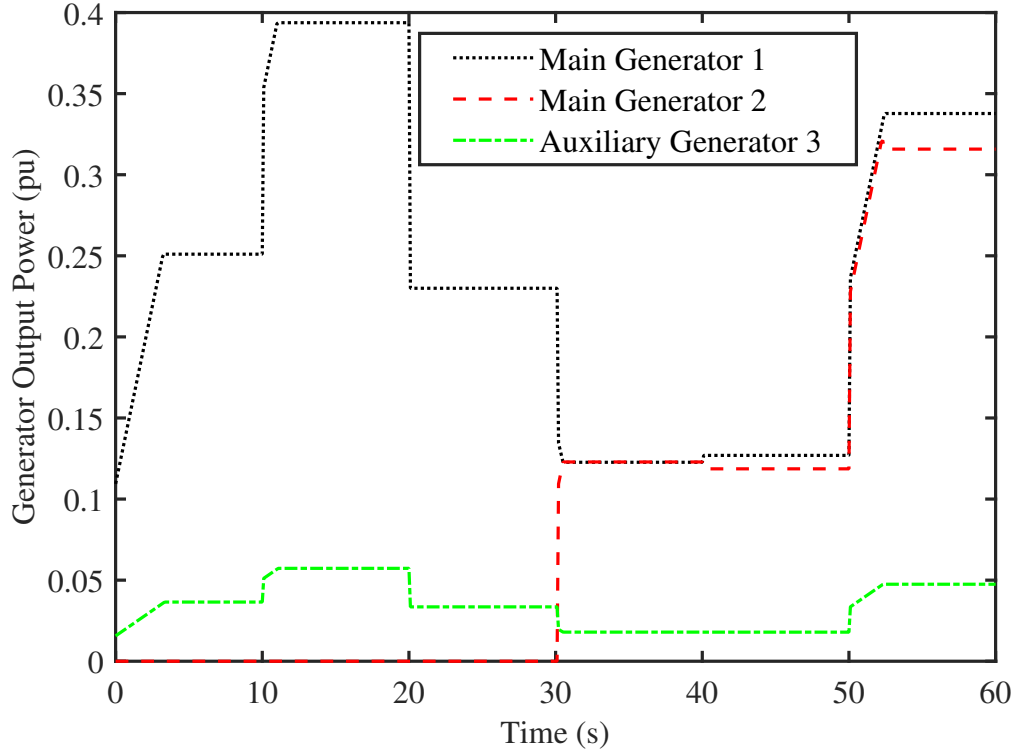


Figure 7.9: Generator output power for dynamic simulation.

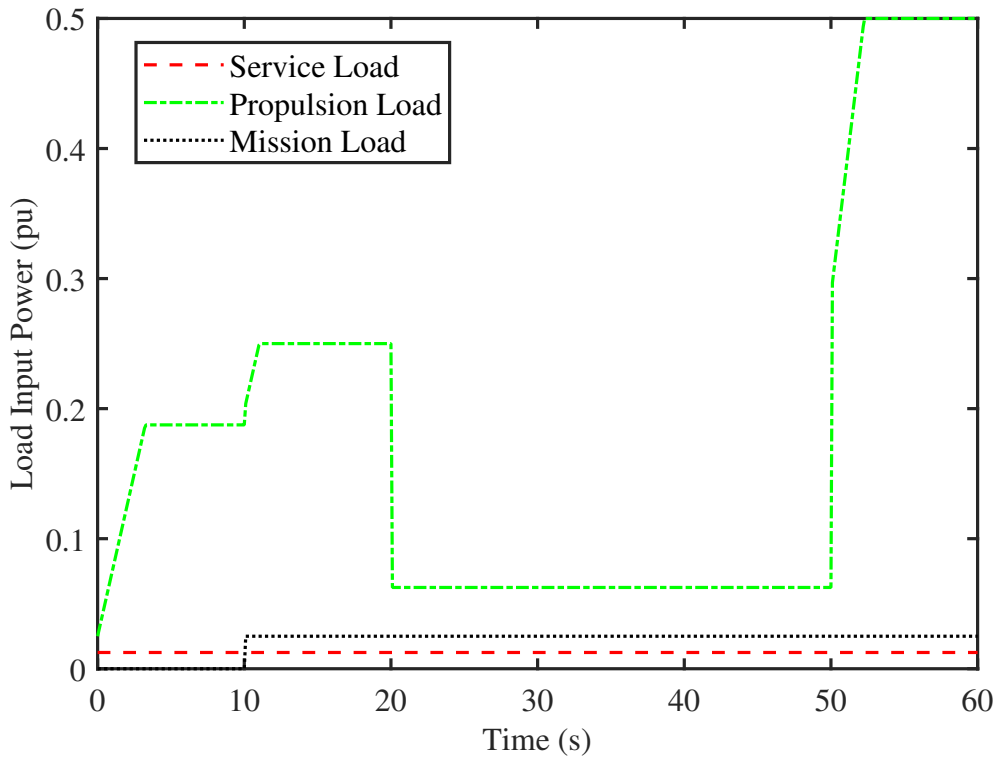


Figure 7.10: Load input power for dynamic simulation.

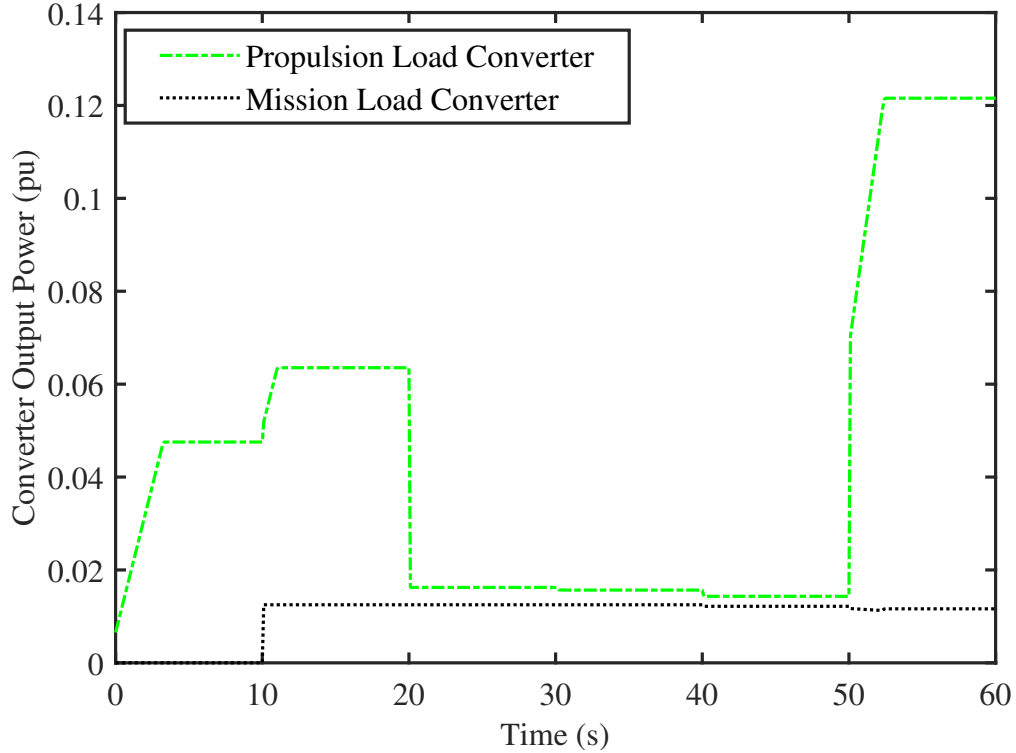


Figure 7.11: Converter output power for dynamic simulation.

slight shift in how propulsion load is shared among the propulsion drives because of the local availability of power.

At 40 s, the plant is realigned by separating the main corridors. Through use of the different propulsion drives and mission load converters, the overall load can still be more or less shared between the generators, but slight shifts are visible in the generator output powers as well as the converter powers.

After 50 s, the propulsion load power is increased again, hence the output power of each generator ramps up to meet the new demand.

This dynamic simulation shows how the market-clearing algorithm can be used to solve the market-clearing problem in a wide-range of dynamic scenarios for a representative system. The market-clearing solution at each time step (shown in Figure 7.8) drive the power-flow solutions shown in Figure 7.9–7.11. In this way, the market-based control approach can be implemented.

## 7.8 Conclusion

In this chapter, an algorithm has been proposed for solving the market-clearing problem. The market-clearing prices and the output power is obtained as a result of this evaluation. The proposed algorithm and existing reference root-finding algorithms are applied on a complex representative power system and three simplified power systems based on the representative system under different operational scenar-

ios, and the convergence of the algorithms is compared. Because of the numerical structure of the problem, conventional algorithms for solving root-finding problems struggle. All of the algorithms generally converge when starting prices are close to the equilibrium prices. However, as the range increases, Broyden's method fails to converge first, followed by Newton-Raphson method and the commercially available algorithm fsolve. The proposed algorithm converges for every range considered. This convergence behavior indicates that the reference algorithms are very sensitive to starting price guesses. The proposed algorithm converges over the full range, indicating that the algorithm is robust with respect to starting guesses and successfully solves the market-clearing problem over a practically relevant range. Dynamic simulation has been used additionally to demonstrate the efficacy of the proposed algorithm in clearing the market in a wide range of dynamic conditions.



## Chapter 8 Equivalence of Dynamic Programming Problem and Sequence of Static Optimizations

### 8.1 Introduction

In Chapter 6, market-based control has been introduced as an alternative to centralized control when the overall system structure and condition, including the statuses and internal characteristics of each component are not known globally. It reduces a global optimization problem into a series of smaller local optimization problems combined with finding the market clearing prices that result in market equilibrium. Hence, under sufficient conditions, the market clearing problem is equivalent to solving the global optimization problem (e.g., [17]). In other words, the market clearing problem is equivalent to a sequence of static optimization problems.

Static optimization means maximizing some objective function subject to a given set of constraints at each moment in time:

$$\max_{\mathbf{u}} U(\mathbf{u}). \quad (8.1)$$

The objective function in mathematical programming defines the criteria that the problem optimizes. Depending on how the problem is set up, the maximum or minimum value of the computation is usually desired [4]. Therein, a linear programming approach is presented to model this. However, linear programming does not always provide a unique solution. This lack of uniqueness arises when multiple optimal solutions exist. For example, if the objective function is parallel to a constraint boundary or if there are multiple intersections at the same optimal value, the linear programming problem will have several solutions that yield the same optimal value for the objective function. This characteristic can be particularly challenging in power systems optimization, where unique solutions might be necessary for consistent decision-making and operational stability.

In contrast, quadratic programming extends linear programming to include quadratic objective functions, which can model more complex relationships and nonlinearities present in real-world problems. The objective function in mathematical programming defines the criteria that the problem optimizes. For the quadratic programming problem, the objective is to find an  $n$ -dimensional vector  $\mathbf{u}$  in a single time step that will

$$\max_u -\frac{1}{2}\mathbf{u}^T\mathbf{H}\mathbf{u} + \mathbf{c}^T\mathbf{u} \quad (8.2)$$

subject to

$$\mathbf{A}\mathbf{u} \leq \mathbf{b}, \quad (8.3)$$

$$\mathbf{A}_{eq}\mathbf{u} = \mathbf{b}_{eq}. \quad (8.4)$$

where  $\mathbf{A}$  and  $\mathbf{A}_{eq}$  are matrices representing the inequality and equality constraints, respectively, and  $\mathbf{b}$  and  $\mathbf{b}_{eq}$  are vectors representing the right-hand side of the constraints. The notation  $\mathbf{A}\mathbf{u} \leq \mathbf{b}$  means that every entry of the vector  $\mathbf{A}\mathbf{u}$  is less than or equal to the corresponding entry of the vector  $\mathbf{b}$  (component-wise inequality) in a single time step.

Simulation proceeds via time steps in which the mathematical programming problem is solved in each moment. The elements of  $\mathbf{u}$  correspond to various power flows in a single time step. In discrete time simulation, the power flows in the system are the solutions to the quadratic programming problem. State variables of the problem are updated discretely based on the power flows of the current state.

On the other hand, in market-based control, the behavior of each of the individual components can be aggregated into an overall system consumption function  $\mathbf{F}(\mathbf{\Pi})$ , which maps the vector of bus prices  $\mathbf{\Pi}$  to the net consumption of power at each bus. The market clearing problem tries to find a set of equilibrium prices such that:

$$\mathbf{F}(\mathbf{\Pi}) = \sum_{i=1}^I \mathbf{F}_i(\mathbf{\Pi}) = \mathbf{0}, \quad (8.5)$$

and the profit is maximized

$$\text{Profit}_i(\mathbf{P}_i) = \Pi_u U_i(\mathbf{P}_i) - \mathbf{\Pi}^T \mathbf{P}_i, \quad (8.6)$$

$$\mathbf{F}_i(\mathbf{\Pi}) = \arg \max_{\mathbf{P}_i} \text{Profit}_i(\mathbf{P}_i). \quad (8.7)$$

Solving for the set of prices  $\mathbf{\Pi}$  results in same power flow as solving (8.2).

In Chapter 2, the metric operability was introduced as a way to measure the degree to which the performance of the power system contributes to mission effectiveness in a particular scenario. Operability was initially represented as an integral of weighted power flows to loads. In discrete-time form, it can be defined as

$$O = \frac{\sum_{k=k_1}^{k_{end}} \sum_{i=1}^I w_i P_i(k)}{\sum_{k=k_1}^{k_{end}} \sum_{i=1}^I w_i P_{max,i}(k)}, \quad (8.8)$$

where  $I$  is the number of loads in the system,  $P_i(k)$  is the power consumption of load  $i$ ,  $P_{max,i}(k)$  is the maximum (or demanded) power of load  $i$ , and  $w_i$  is a mission-specific weighting function indicating the relative importance of load  $i$ .  $k$  indicates the period (of time) as an integer from  $k_0$  to  $k_{end}$ . Hence, operability can be represented as the performance obtained from simulation of a sequence of static optimizations:

$$O = \sum U(\mathbf{u}). \quad (8.9)$$

In Chapters 3, 4, 5, dynamic optimal control has been used to represent the performance of notional systems and missions. In the context of power systems, the evolution of dynamic optimal control has been driven by the need to manage the complexities of modern energy systems. Early applications focused on integrating

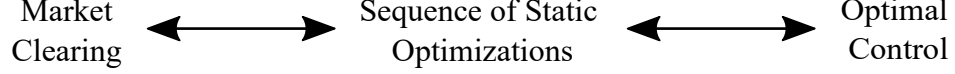


Figure 8.1: Relationship between optimization concepts.

instantaneous reward functions in continuous or discrete time to evaluate system performance. However, these methods did not adequately capture the dynamic interdependencies and uncertainties inherent in power systems. Recent advancements have leveraged techniques such as multiperiod optimal power flow, where the optimization problem is solved over multiple time periods, considering both current and future states. This approach effectively transforms the dynamic problem into a sequence of static optimizations, where each step's solution informs the next, ensuring that the overall control strategy is optimized over the entire planning horizon. Thus, the dynamic problem can also be represented as a sequence of static optimization problems, which will be explored in this chapter. That is, all of these ideas are equivalent, as shown in Figure 9.1.

## 8.2 Problem Equivalence

In Chapter 2, it was mentioned that the previous approaches to operability have been based on integrating a discounted instantaneous reward function in continuous time. Hence, the continuous-time operability or performance can be mathematically represented as

$$V = \int_0^{\infty} e^{-rt} R(t) dt. \quad (8.10)$$

if  $R(t) \in [0, R_{max}]$ . Here,  $r$  is the discounting rate.

In discrete-time with step  $\Delta t$ , the performance  $V$  can be represented as

$$V = \sum_{k=0}^{\infty} \frac{e^{-rk\Delta t}(1 - e^{-r\Delta t})}{r} \mathbf{R}_k = M \sum_{k=0}^{\infty} \alpha^k \mathbf{R}_k = M \sum_{k=0}^{\infty} \alpha^k R(\mathbf{x}_k, \mathbf{u}_k, \mathbf{x}_{k+1}), \quad (8.11)$$

where,  $M = \frac{1 - e^{-r\Delta t}}{r}$  and  $\alpha = e^{-r\Delta t}$ , which is useful for proper normalization when the same problem is considered with different time steps.

The optimal control problem can be represented as

$$\max_{(u_0, u_1, \dots)} E[V(x_0, x_1, \dots, u_0, u_1, \dots)]. \quad (8.12)$$

The stochastic Bellman equation can be solved for

$$\arg \max_{\mathbf{u}_k \in \Omega(\mathbf{x}_k)} E[R(\mathbf{x}_k, \mathbf{u}_k, \mathbf{x}_{k+1}) + \alpha \bar{V}(\mathbf{x}_{k+1})]. \quad (8.13)$$

Solving the Bellman equation yields the optimal action at each time step with respect to the performance measure in (8.12).

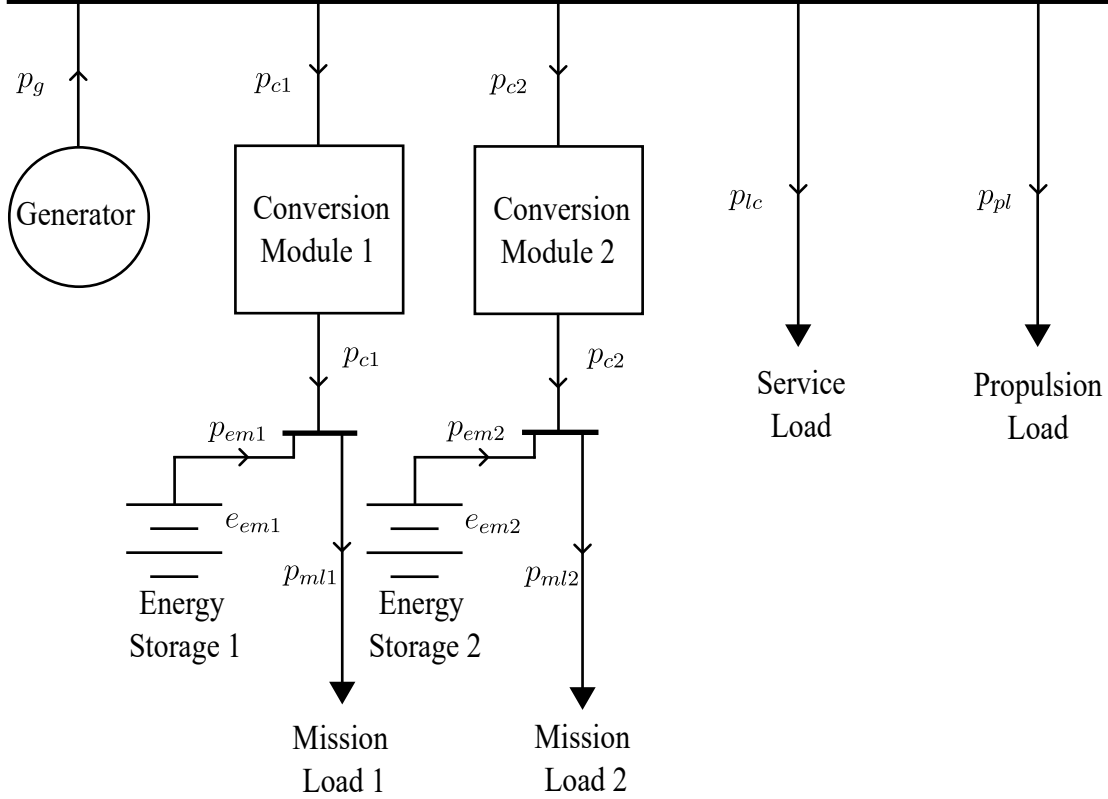


Figure 8.2: Diagram of representation of the notional system showing the power flows.

Alternatively, with mathematical programming, the optimal action can be found using quadratic programming where objective function to be maximized is quadratic. This can be formulated as:

$$\max_{\mathbf{u}_k \in \Omega(\mathbf{x}_k)} -\frac{1}{2} \mathbf{u}^T \mathbf{H} \mathbf{u} + \mathbf{c}^T \mathbf{u}, \quad (8.14)$$

where  $\mathbf{H}$  is a symmetric positive definite matrix representing the quadratic terms and  $\mathbf{c}$  is a vector representing the linear terms. Depending on the nature of the instantaneous reward, state transitions, etc., it is possible to equate the optimal control to mathematical programming. For example, by choosing  $\mathbf{H}$  and  $\mathbf{c}$ , it is possible to equate these two as shown in subsequent sections.

### 8.3 Demonstration Problem

In the previous section, the quadratic programming problem was introduced as the initial step to solving a sequence of static optimizations. In this section, details on how quadratic programming can solve the optimization problem will be discussed.

The system being considered is shown in Figure 8.2. The power flows of each of the components are shown to indicate which component is supplying power to the buses and which component is getting power from the buses. The parameters of the system are shown in Table 8.1.

Table 8.1: System Parameters

Total generator rating, $p_{g,max}$	9
Total outer zone converter rating, $p_{c,max1}$	8
Total inner zone converter rating, $p_{c,max2}$	4
Total outer zone mission load demand, $p_{ml,max1}$	3.2
Total inner zone mission load, $p_{ml,max2}$	1.6
Total service load demand, $p_{lc,max}$	6.4
Total propulsion load demand, $p_{pl,max}$	1.25
Weight of mission load, $w_{ml}$	2
Weight of service load, $w_{lc}$	1
Weight of propulsion load, $w_{pl}$	0.75
Weight of discharging energy, $w_d$	0.8

Table 8.2: Discretization Parameters

Time step, $\Delta t$	10
Total time, $t_{expected}$	120
Time scaling, $t_{scale}$	$t_{expected}$
$\gamma_{scale}$	0.1
$r$	$\log(\gamma_{scale}) / -t_{scale}$

There are two discrete states- the first state represents the period of time in which the system operates with insufficient available generation, and the second state represents the time when the system has sufficient generation. When the system reaches state 2, the reward  $R_k = R_{max}$ . The transition from state 1 to state 2 can be modeled stochastically in one step with a given probability. The parameters required for discretization of the problem considered in the system are shown in Table 8.2. The probability of transition from one state to another is  $p$ :

$$p = \frac{\Delta t}{t_{expected}}. \quad (8.15)$$

The diagram of the state transition is shown in Figure 8.3.

For the system,  $\mathbf{A}_{eq}$ ,  $\mathbf{b}_{eq}$ ,  $\mathbf{A}$ ,  $\mathbf{b}$ , upper bound, and lower bound are based on the action constraints. The action  $\mathbf{u}$  is defined by:

$$\mathbf{u} = [p_g \ p_{c1} \ p_{c2} \ p_{em1} \ p_{em2} \ p_{ml1} \ p_{ml2} \ p_{lc} \ p_{pl}]^T, \quad (8.16)$$

where  $p_g$  is generator power,  $p_{c1}$  is outer zone converter power,  $p_{c2}$  is inner zone converter power,  $p_{em1}$  is outer zone energy magazine power,  $p_{em2}$  is inner zone energy magazine power,  $p_{ml1}$  is outer zone mission load power,  $p_{ml2}$  is inner zone mission load power,  $p_{lc}$  is service load power, and  $p_{pl}$  is propulsion load power.

The actions are constrained such that the total power flowing each energy storage is limited by the available energy, and the total power flow from the generation is

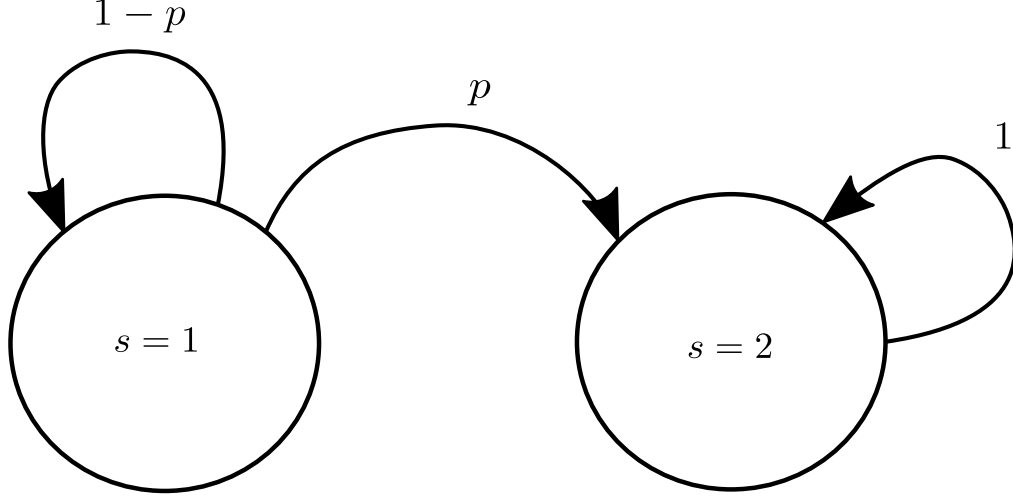


Figure 8.3: State transition diagram.

limited by the available power:

$$-p_g + p_{c1} + p_{c2} + p_{lc} + p_{pl} = 0 \quad (8.17)$$

$$-p_{c1} - p_{em1} + p_{ml1} = 0, \quad (8.18)$$

$$-p_{c2} - p_{em2} + p_{ml2} = 0, \quad (8.19)$$

$$0 \leq p_g \leq p_{g,max}, \quad (8.20)$$

$$0 \leq p_{c1} \leq p_{c,max1}, \quad (8.21)$$

$$0 \leq p_{c2} \leq p_{c,max2}, \quad (8.22)$$

$$p_{em1} \Delta t \leq e_{em1}, \quad (8.23)$$

$$p_{em2} \Delta t \leq e_{em2}, \quad (8.24)$$

$$0 \leq p_{ml1} \leq p_{ml,max1}, \quad (8.25)$$

$$0 \leq p_{ml2} \leq p_{ml,max2}, \quad (8.26)$$

$$0 \leq p_{lc} \leq p_{lc,max}, \quad (8.27)$$

$$0 \leq p_{pl} \leq p_{pl,max}, \quad (8.28)$$

$$p_{em1} \geq 0, \quad (8.29)$$

$$p_{em2} \geq 0, \quad (8.30)$$

where  $e_{em1}$  is the energy of the outer zone energy magazine and  $e_{em2}$  is the energy of

Table 8.3:  $\mathbf{H}$  matrix parameters and values

$\epsilon_{ml,max1}$	$0.001/p_{ml,max1}$
$\epsilon_{ml,max2}$	$0.001/p_{ml,max2}$
$\epsilon_{lc,max}$	$0.001/p_{lc,max}$
$\epsilon_{pl,max}$	$0.001/p_{pl,max}$

the inner zone energy magazine. Matrices  $\mathbf{c}$  and  $\mathbf{H}$  can be defined as:

$$\mathbf{c} = \begin{bmatrix} 0 \\ 0 \\ 0 \\ 0 \\ 0 \\ w_{ml} \\ w_{ml} \\ w_{lc} \\ w_{pl} \end{bmatrix}, \quad (8.31)$$

$$\mathbf{H} = \begin{bmatrix} 0 & 0 & 0 & 0 & 0 & 0 & 0 & 0 & 0 \\ 0 & 0 & 0 & 0 & 0 & 0 & 0 & 0 & 0 \\ 0 & 0 & 0 & 0 & 0 & 0 & 0 & 0 & 0 \\ 0 & 0 & 0 & 0 & 0 & 0 & 0 & 0 & 0 \\ 0 & 0 & 0 & 0 & 0 & 0 & 0 & 0 & 0 \\ 0 & 0 & 0 & 0 & 0 & \epsilon_{ml,max1} & 0 & 0 & 0 \\ 0 & 0 & 0 & 0 & 0 & 0 & \epsilon_{ml,max2} & 0 & 0 \\ 0 & 0 & 0 & 0 & 0 & 0 & 0 & \epsilon_{lc,max} & 0 \\ 0 & 0 & 0 & 0 & 0 & 0 & 0 & 0 & \epsilon_{lc,max} \end{bmatrix}. \quad (8.32)$$

The actual values of the parameters in the  $\mathbf{H}$  matrix are given in Table 8.3 The power flows can be used to determine the reward  $R_k$ , which accounts for the nonlinearities in the system:

$$R_k = w_{ml}(p_{ml1} + p_{ml2}) + w_{lc}p_{lc} + w_{pl}p_{pl} - \frac{1}{2}\epsilon_{ml1}p_{ml1}^2 - \frac{1}{2}\epsilon_{ml2}p_{ml2}^2 - \frac{1}{2}\epsilon_{lc}p_{lc}^2 - \frac{1}{2}\epsilon_{pl}p_{pl}^2. \quad (8.33)$$

From this, the maximum reward can be determined to be:

$$R_{max} = w_{ml}(p_{ml,max1} + p_{ml,max2}) + w_{lc}p_{lc,max} + w_{pl}p_{pl,max} - \frac{1}{2}\epsilon_{ml1}p_{ml,max1}^2 - \frac{1}{2}\epsilon_{ml2}p_{ml,max2}^2 - \frac{1}{2}\epsilon_{lc}p_{lc,max}^2 - \frac{1}{2}\epsilon_{pl}p_{pl,max}^2. \quad (8.34)$$

In (8.11), the performance  $V$  was defined. Using (8.33), the performance  $V_{samples}$  over a total period of  $N_{time}$  can be defined as:

$$V_{samples} = M \sum_{k=0}^{N_{time}} \alpha^k R_k. \quad (8.35)$$

Table 8.4: Monte Carlo Simulation Parameter Values

Stopping time, $t_{stop}$	$10t_{scale}$
Total time steps, $N_{time}$	$\text{floor}[t_{stop}/\Delta t]$
Total samples, $N_{samples}$	300
Switching time, $t_{switch}$	$\text{exprnd}(\text{repmat}(t_{expected}, 1, N_{samples}))$

Monte Carlo simulation can be employed to obtain the overall performance  $V_{overall}$  by averaging the performance across multiple sample paths. The parameters for Monte Carlo simulation are given in Table 8.4.

This process involves the following steps:

1. **Generate Sample Paths:** Multiple sample paths are generated, each representing a possible sequence of states and actions over the time horizon. Each path simulates the system behavior under different random events and uncertainties.
2. **Compute Performance for Each Path:** For each sample path, compute the performance  $V_{samples}$  using the equation above.
3. **Average Performance:** Calculate the average performance  $V_{overall}$  across all sample paths to estimate the expected overall performance of the system.

The overall performance  $V_{overall}$  can be expressed as:

$$V_{overall} = \frac{1}{N_{samples}} \sum_{i=1}^{N_{samples}} V_{samples,i}, \tag{8.36}$$

where  $N_{samples}$  is the number of sample paths.

Hence, obtaining the overall performance  $V_{overall}$  from Monte Carlo simulation of  $V_{samples}$  validates the equivalence of solving the Bellman equation for the maximum performance in (8.13). In other words, Monte Carlo simulation validates the estimate of the expected performance of a control policy. Thus, this establishes the connection between dynamic optimal control and sequence of static optimizations.

#### 8.4 Demonstration Problem with Fixed Weights for Discharging

In the previous section, the matrix  $\mathbf{c}$  had been defined for the values of weights of each of the components. In a practical system, some penalty has to be assigned for discharging power from the energy magazine. This penalty is the weight for discharging  $w_d$ . The value of  $w_d$  is provided in Table 8.1. If weights are used for



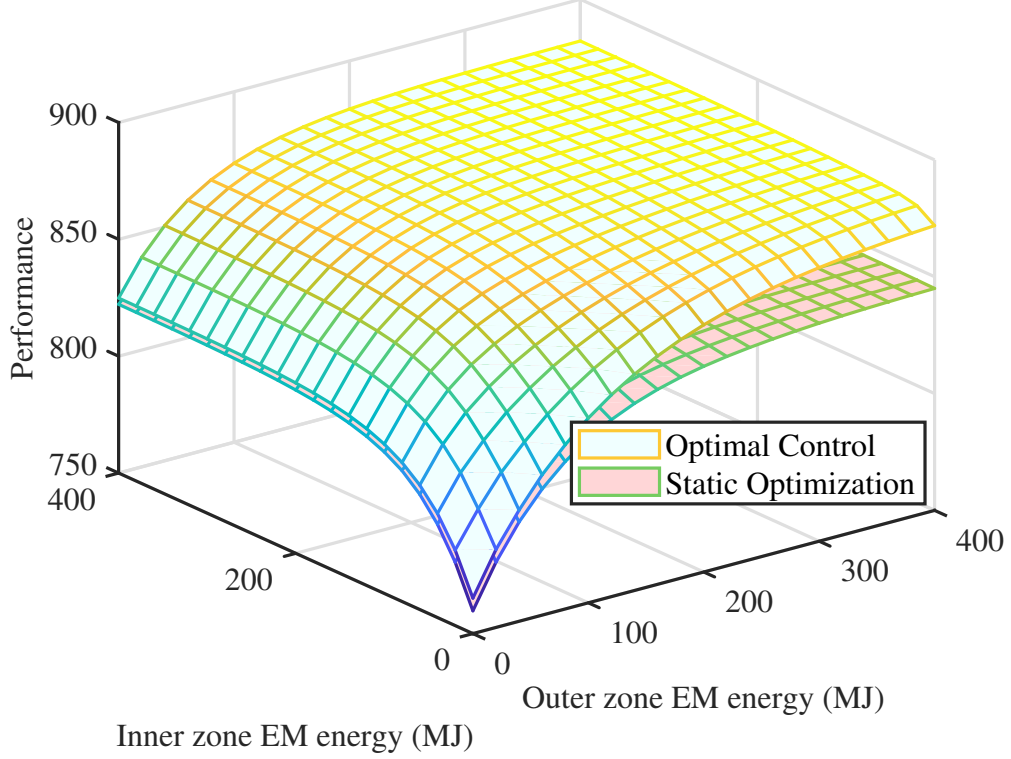


Figure 8.4: Performance comparison between MDP-based optimal control and sequence of static optimization for fixed discharging weights. The plot on the bottom indicates that slightly lower performance is obtained with sequence of static optimizations.

discharging energy from the energy storage, the matrix  $\mathbf{c}$  can be updated to  $\mathbf{c}_{new}$ :

$$\mathbf{c}_{new} = \begin{bmatrix} 0 \\ 0 \\ 0 \\ -w_d \\ -w_d \\ w_{ml} \\ w_{ml} \\ w_{lc} \\ w_{pl} \end{bmatrix}. \quad (8.37)$$

This is an attempt to maximize expected reward  $R_k$  time step by time step with a little penalty on energy.

The plot for fixed discharging weights is shown in Figure 8.4. As expected, higher initial energy in the energy magazine results in higher performance. The performance is more highly dependent on the energy stored in the outer zone energy magazines because the outer zone mission loads require more power. The shapes of the two curves are identical and mostly overlapping which indicates that the performance of dynamic optimal control is very similar to sequence of static optimizations. There

is however a slight decrease in performance with static optimizations as indicated by its plot which lies below the dynamic optimal control plot.

## 8.5 Demonstration Problem with Varying Weights for Discharging

In the previous section, fixed weights had been used for discharging energy from the energy storage in matrix  $\mathbf{c}_{new}$  in (8.37). In a practical mission-oriented system, the discharge of energy is not expected to occur at a constant rate. Hence, the weights for discharging would vary in every time step. The discharging weights would be functions of the performance  $V$  with respect to the initial allocation of energy  $E$ , i.e.,  $\partial V/\partial E$ :

$$V[x_{k+1}] \approx V[x_k] + \frac{\partial V}{\partial E} * E, \quad (8.38)$$

With varying discharging weights, the problem is trying to maximize  $\mathbf{c}_{new}^T \mathbf{u}$ . In other words, it is trying to maximize the expected sum of reward  $R_k$  and the penalty,  $E[R(\mathbf{x}_k, \mathbf{u}_k, \mathbf{x}_{k+1}) + \alpha \bar{V}(\mathbf{x}_{k+1})]$ . Here,

$$E[V(x_{k+1})] = \sum pV[x_{k+1}] \quad (8.39)$$

$$= (1 - p)(V_1(e_{k+1})) + pV_{max} \quad (8.40)$$

$$= (1 - p) \left( V_1(e_k) + \frac{\partial V_1}{\partial e} \Delta e \right) + pV_{max}. \quad (8.41)$$

The  $M$ ,  $p$ , and  $\alpha$  values are chosen to equate the mathematical programming problem to the dynamic optimal control problem. The discharging weights are as follows:

$$w_{em1} = (1 - p) \frac{1}{M} \left( \alpha \Delta t \frac{\partial V}{\partial E_1} \right) \quad (8.42)$$

$$w_{em2} = (1 - p) \frac{1}{M} \left( \alpha \Delta t \frac{\partial V}{\partial E_2} \right) \quad (8.43)$$

The expected performance from the value function iteration in (8.13) are used to determine the value of the discharging weight for each energy magazine at each time step. The variation of discharging weight is shown in Figure 8.5. As seen, the discharging weight decreases with progression of the mission in each time step.

The matrix  $\mathbf{c}_{new}$  is updated at each time step to account for the varying weights for discharging energy. Monte Carlo simulation is then performed as described in the previous section with the updated  $\mathbf{c}_{new}$  at each time step.

The performance for dynamic optimal control is compared with that for sequence of static optimizations for varying discharging weights. Similar to the plot for fixed discharging weight in Figure 8.4, a plot can be generated for variable discharging weights as shown in Figure 8.6. In this case, the two plots are almost overlapping with only slight differences between them. This indicates that static optimizations with varying discharging weights at every time step more closely resembles dynamic

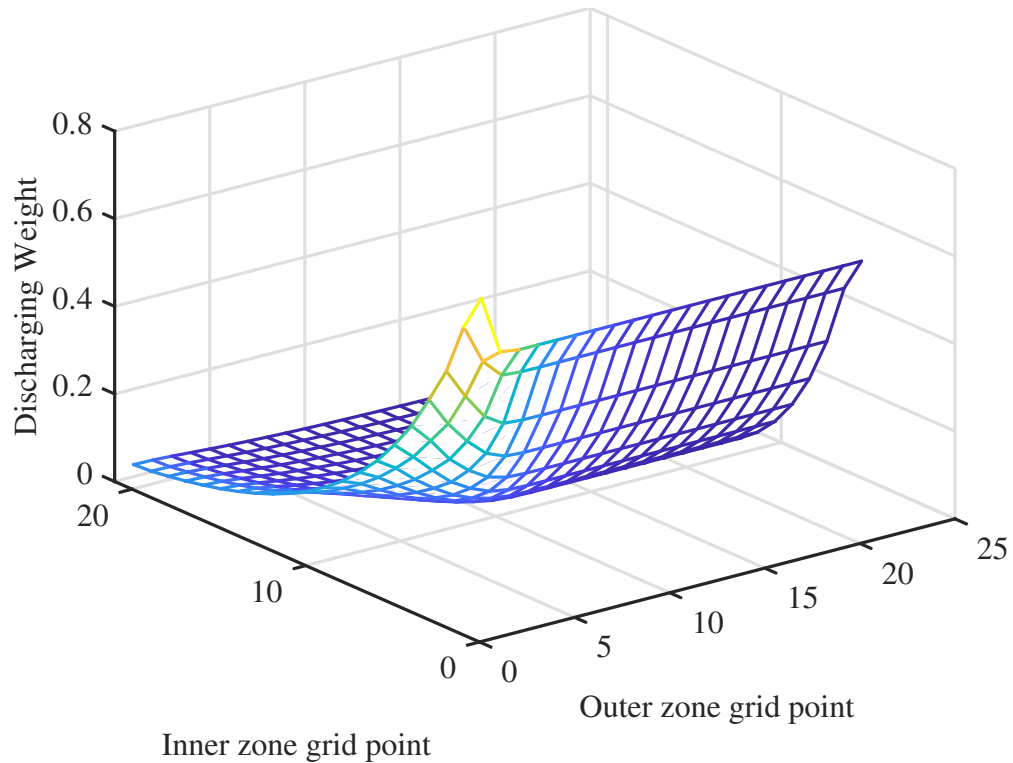


Figure 8.5: Variation of discharging weight.

optimal control. This further validates the equivalence of the two optimization approaches. In a practical system, it is more likely for the discharging weights to vary at each time step.

## 8.6 Conclusion

In this chapter, the connection between market-based control and sequence of static optimizations has been discussed, showing the equivalence of the two optimization approaches. The equivalence of dynamic optimal control and sequence of static optimization has been explored and validated with results. Moreover, the results for static optimization with fixed and varying discharging weights have been compared with dynamic optimal control to illustrate the dynamics of a practical system.

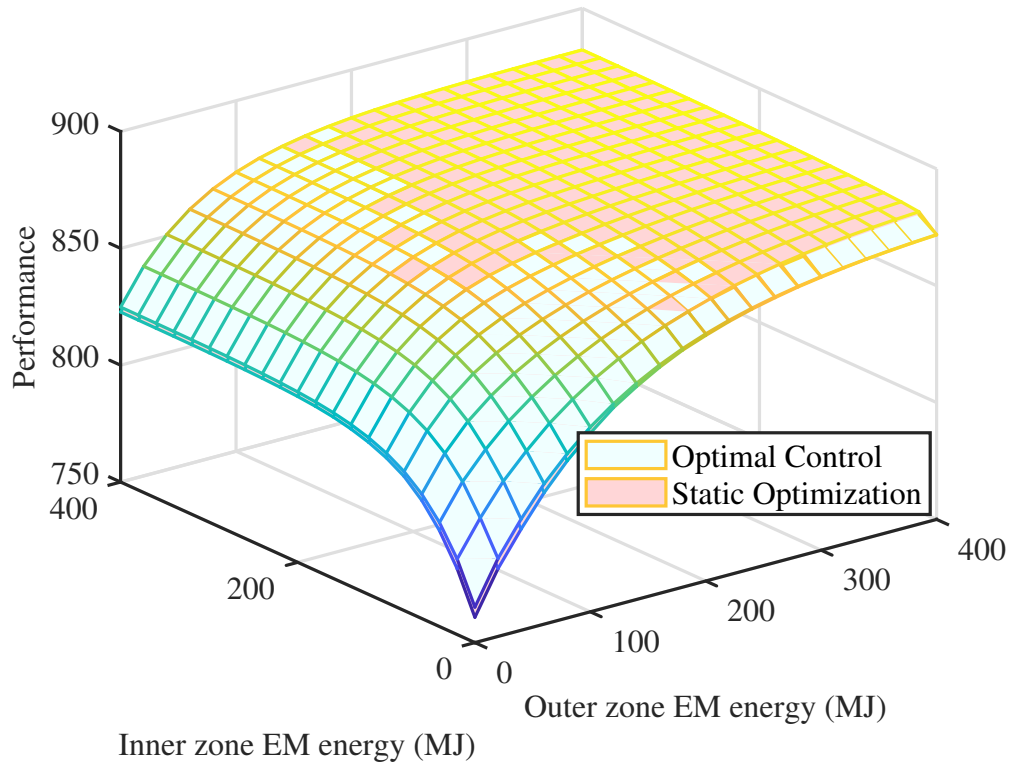


Figure 8.6: Performance comparison between MDP-based optimal control and sequence of static optimization for variable discharging weights. The two plots are comparable indicating the equivalence of the two optimization approaches. The slight differences are due to sampling errors.

## Chapter 9 Summary and Opportunities for Future Developments

### 9.1 Introduction

In current research, the evaluation of the performance of mission-oriented systems is advanced by formulating it as an optimal control problem. This formulation allows the dynamic interaction between the system and the mission to be considered directly. The approach of modeling the combined system and mission as a hybrid discrete/continuous, stochastic/deterministic dynamic system and combining with mission-specific rewards to be optimized is naturally represented as a Markov decision process (MDP). This has been demonstrated using a notional, but representative, set of system implementations and missions. Examples of the types of system trade-offs using this approach have been considered.

In case of power electronics-based power systems, generally, the control objective involves directing power to specific loads as required under the current conditions, which can typically be formulated as a mathematical optimization problem. If the overall system structure and condition, including the statuses and internal characteristics of each component, are not known globally and there are changes in system configuration and design, market-based control can be used instead of a centralized control approach.

The dynamic problem can also be represented as a sequence of static optimization problems. Quadratic programming can be used to represent the linearities and nonlinearities of the system. The elements of  $\mathbf{u}$  correspond to various power flows in a single time step. In discrete time simulation, the power flows in the system are the solutions to the quadratic programming problem. This gives the reward which can be used to determine the performance at a single time step. Monte Carlo simulation of the performance can be used to obtain the overall performance by averaging the performance across multiple sample paths over a total period. This gives the overall performance across sample paths which is equivalent to solving the dynamic optimal control for maximum performance.

Additionally, it has also been shown that the sequence of static optimizations is equivalent to solving the market clearing problem which tries to find a set of equilibrium prices such that the resultant system is in equilibrium. In other words:

$$\mathbf{F}(\mathbf{\Pi}) = \sum_{i=1}^I \mathbf{F}_i(\mathbf{\Pi}) = \mathbf{0}, \quad (9.1)$$

Whereas, the static optimization problem tries to maximum some objective function subject to a given set of constraints at each moment in time:

$$\max_{\mathbf{u}} U(\mathbf{u}). \quad (9.2)$$

Thus, in this work, performance evaluation has been explored using dynamic optimal control, market-based control, and sequence of static optimizations. In addition

the connection between market-based control with sequence of static optimizations, and the connection between sequence of static optimizations with dynamic optimal control has been explored.

## 9.2 Future Developments

In Chapter 2, operability metric was introduced as an ability for a system to perform during a single scenario (or vignette). It is possible to calculate operability for all points in time at once rather than period by period. Mathematical programming can be used to solve for power flow in each time step where the optimal power flow can be mathematically concatenated to obtain the maximum operability. The continuity conditions between each time step can be represented as linear equations where the physical behavior of the system can be expressed in terms of linear equality and inequality constraints, and the desired behavior at each time step as a quadratic objective function. The system configuration can be set up to match the scenario that is being considered. For example, there can be a case where the energy magazine is lost. In such a scenario, the energy magazine would need to be turned off in the problem configuration. If the capacity of the energy storage is reduced, this would similarly be reflected in the problem setup. The load demands and weights need to have the same time step as the multiperiod solution. While it is possible to calculate maximum operability over an entire interval of time, the system configurations are updated manually for each case in a spreadsheet. In future developments of this work, this process of matching the system configuration for each scenario can be automated. Moreover, the work can be expanded to include the system dynamic behavior.

In Chapter 5, various system trade-offs have been considered to optimally evaluate the performance of different missions for different system configurations. However, there might be brief pauses (e.g. 30s) in a mission. How the systems react for such pauses has not been explored. In Mission 3 (Fight or Flight), a target threat exists, and a given minimum distance from the target must be obtained through movement or through successfully tracking and neutralizing the target. In a real scenario, there might be multiple threats. In this case, moving away from the target or neutralizing multiple targets at once may become tricky. Hence, it is necessary to consider how the system would react and how the performance would vary in such a case.

In addition, expanding the problem to include more types of missions and combinations of the system configurations already discussed is necessary for more accurate representation of the system.

In Section 5.6, some results are demonstrated using two-dimensional figures even though the nature of the problem is three-dimensional or higher. The ability to visualize higher dimensional problems using higher dimensional figures would help understand the relationship among the variables considered. Hence, it is necessary to find a solution that appropriately visualizes the problems based on their nature. One possible way might be to use pseudo axes for some dependent variables.

In Chapter 6 and 7, a centralized method has been described for finding the market clearing price by taking advantage of the system decision functions. In future, it might be helpful if a decentralized method of finding price is found.

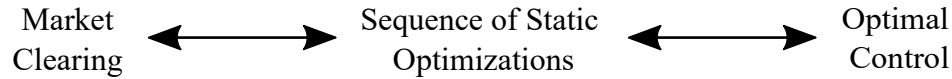


Figure 9.1: Relationship between optimization concepts.

The connection shown in Figure 9.1 has been explored in this work. However, how market-based control relates to dynamic optimal control has not been directly explored in this work. Exploration of this connection is important in the understanding of optimal control-based evaluation. In other words, the application of market-based control in the notional systems in Chapters 3, 4, and 5 need to be explored. Market-based control allows a controller with local information to provide global outcomes. If the market-based control is combined with the weights for energy storage in 8.5, a decision about global optimal control could be made in a completely decentralized way.

Other than these developments, there are some general developments that could be incorporated in future:

1. Implementation of the complex, representative power system (System 4) shown in Figure 7.2 in a real time digital simulator (RTDS),
2. Reducing the run times of the simulations, especially problems with higher dimensions. Exploiting the use of cluster computing could be a possible way,
3. Exploring other optimization techniques that can be used to evaluate and optimally control mission-oriented power system.

Overall, many progresses has been made in terms of representing systems and modeling system-mission interactions. This research has bridged conceptual gaps between systems that have existed for a long time. This creates a scope for continued growth in this area.

## Appendices

### Appendix A: Figures for Chapter 5

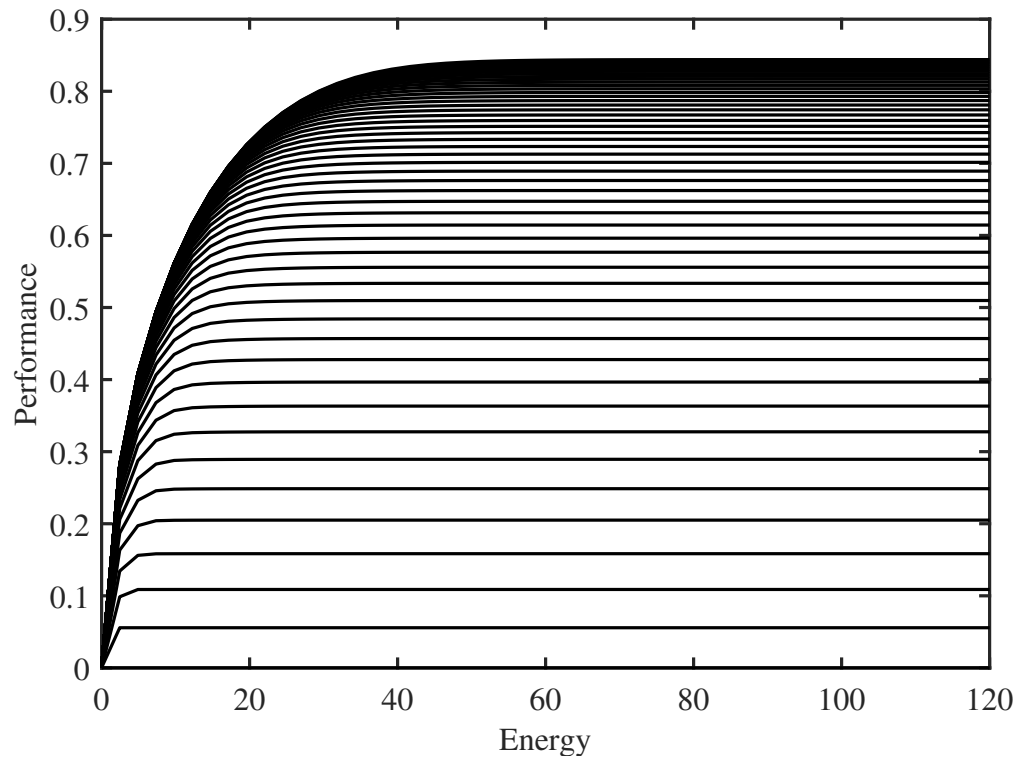


Figure 1: Expected performance for Mission 2 (Contested Transit) with System 1 (Shared).



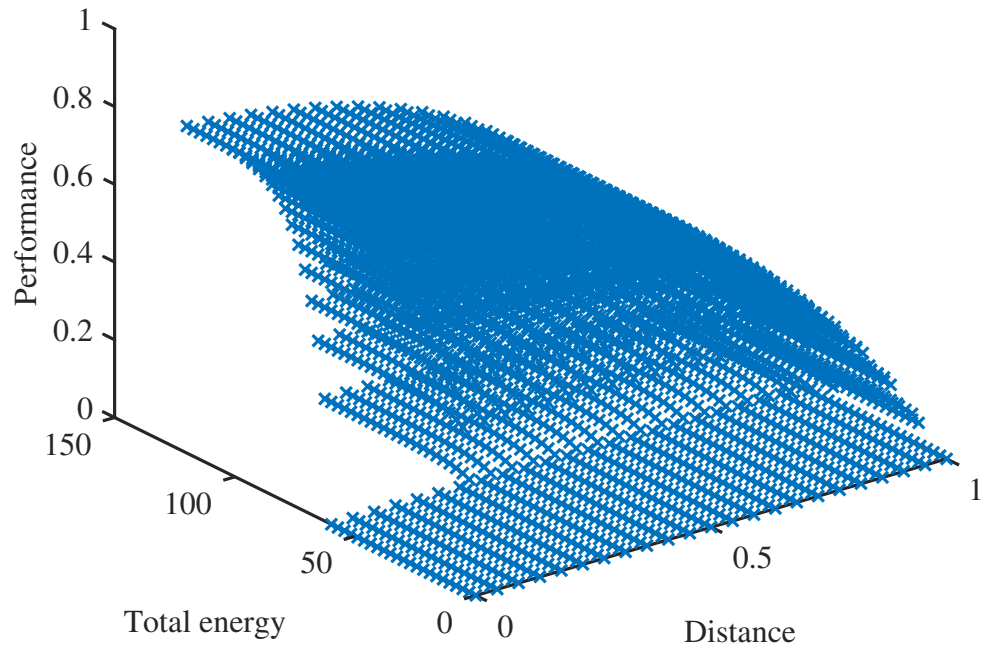


Figure 2: Expected performance for Mission 2 (Contested Transit) with System 2 (Dedicated).

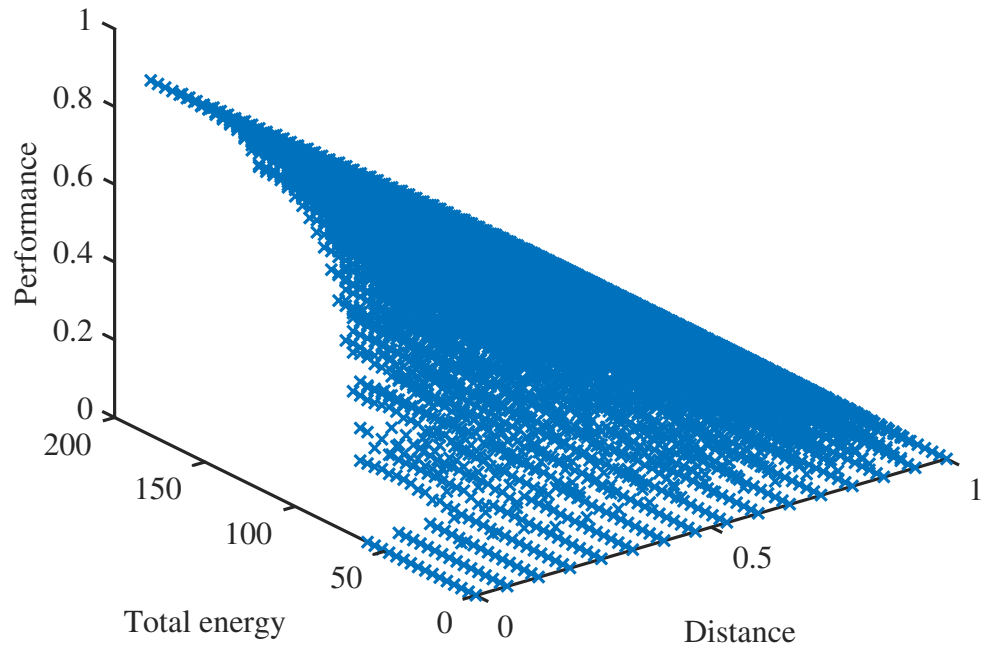


Figure 3: Expected performance for Mission 3 (Fight or Flight) with System 2 (Dedicated).

## Appendix B: Figures for Chapter 6

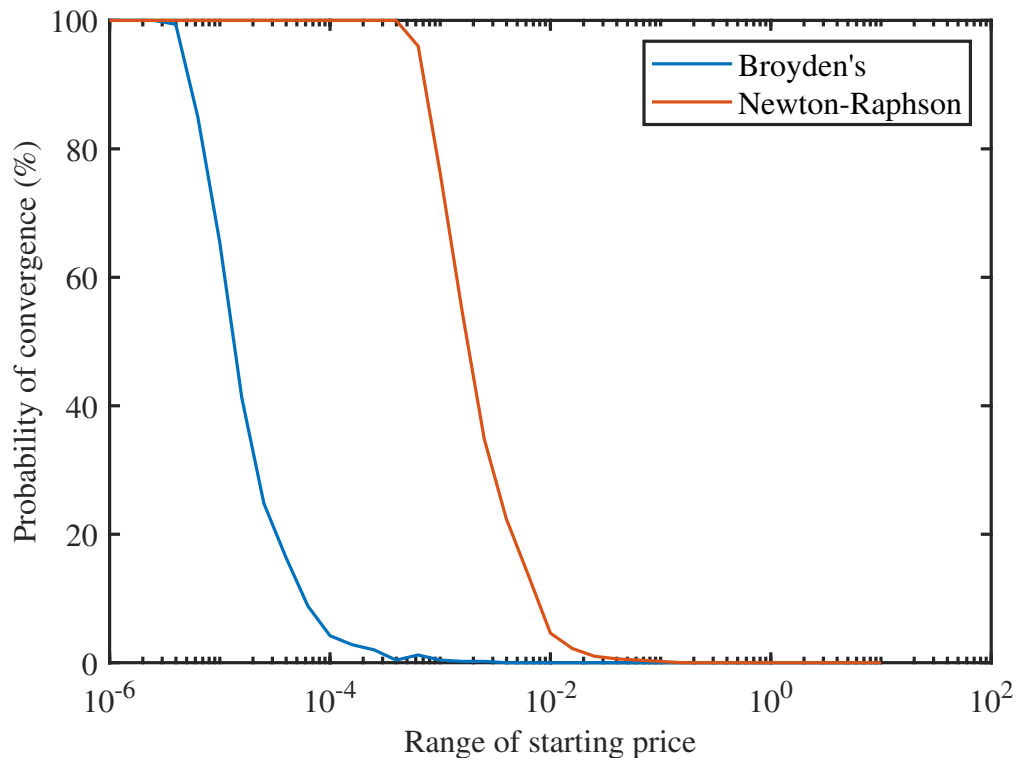
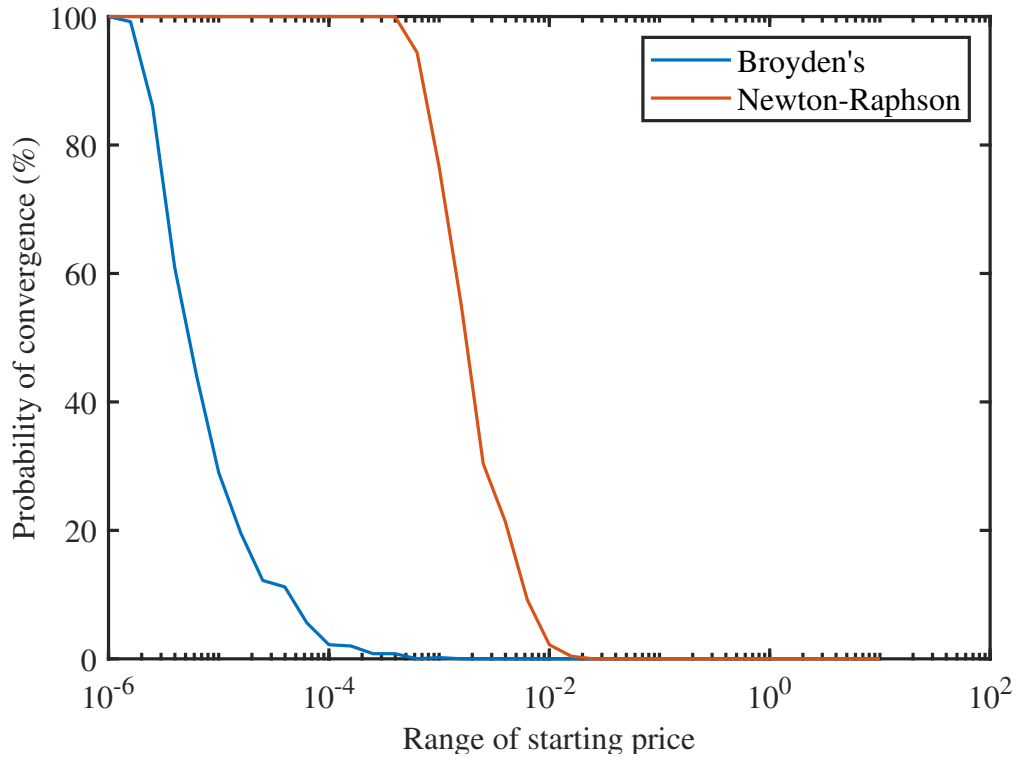


Figure 4: Price convergence probability for System 2 in Scenario 1 (Scarcity).



H

Figure 5: Price convergence probability for System 3 in Scenario 1 (Scarcity).

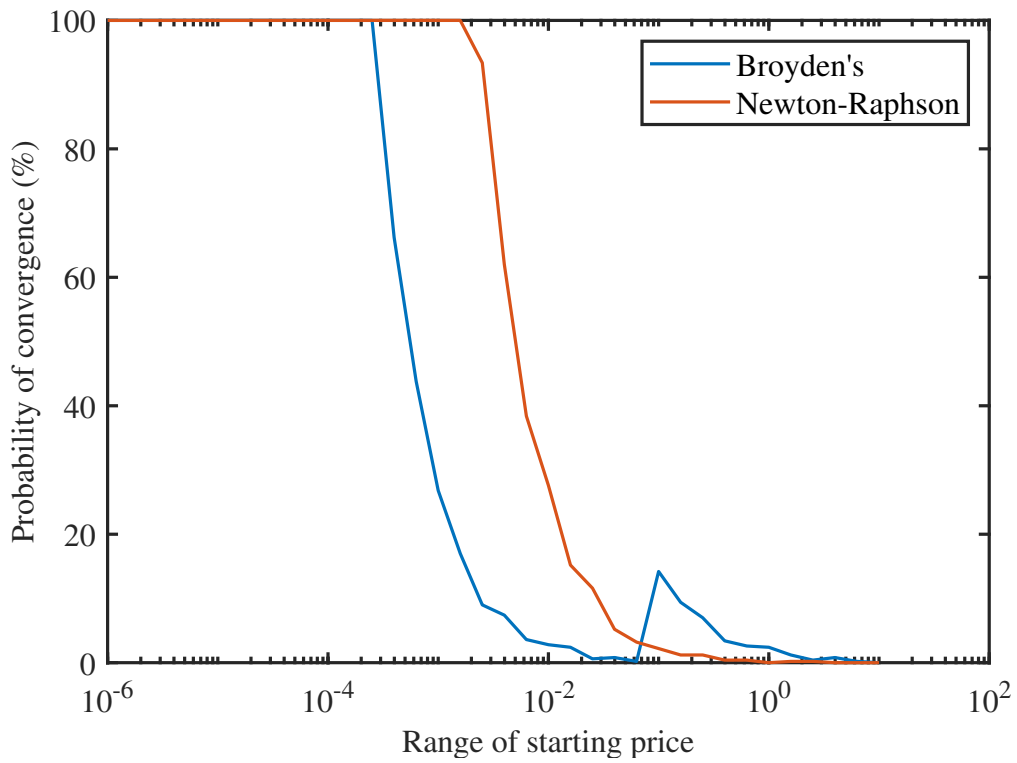


Figure 6: Price convergence probability for System 1 in Scenario 2 (Sufficiency).

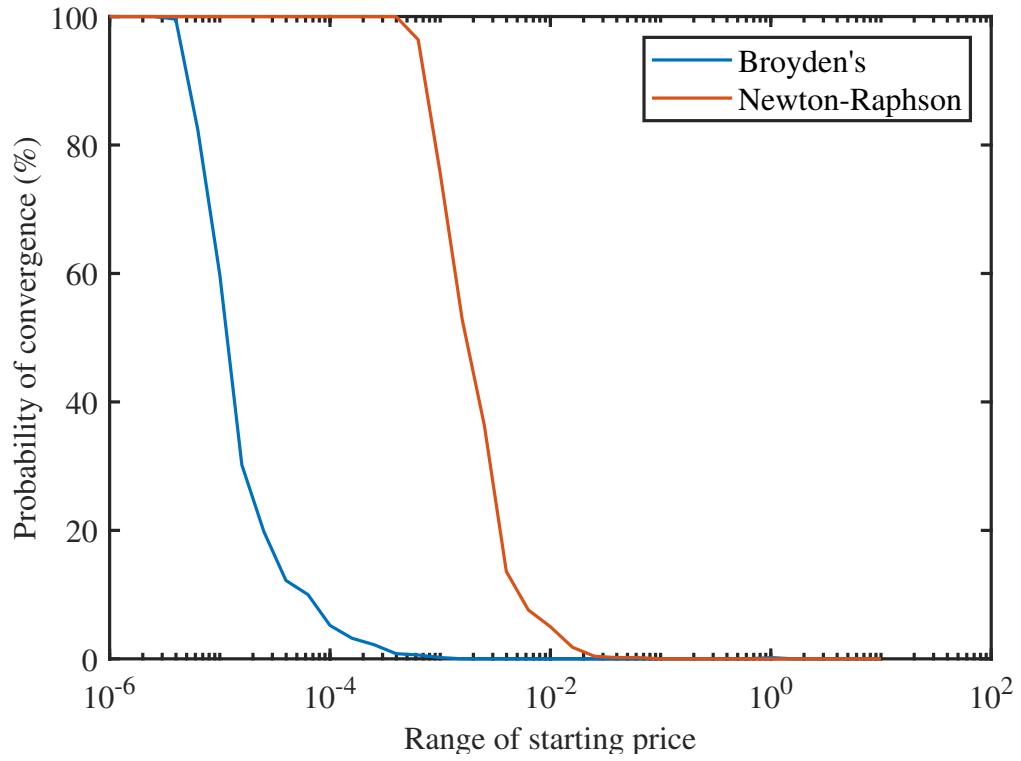


Figure 7: Price convergence probability for System 2 in Scenario 2 (Sufficiency).

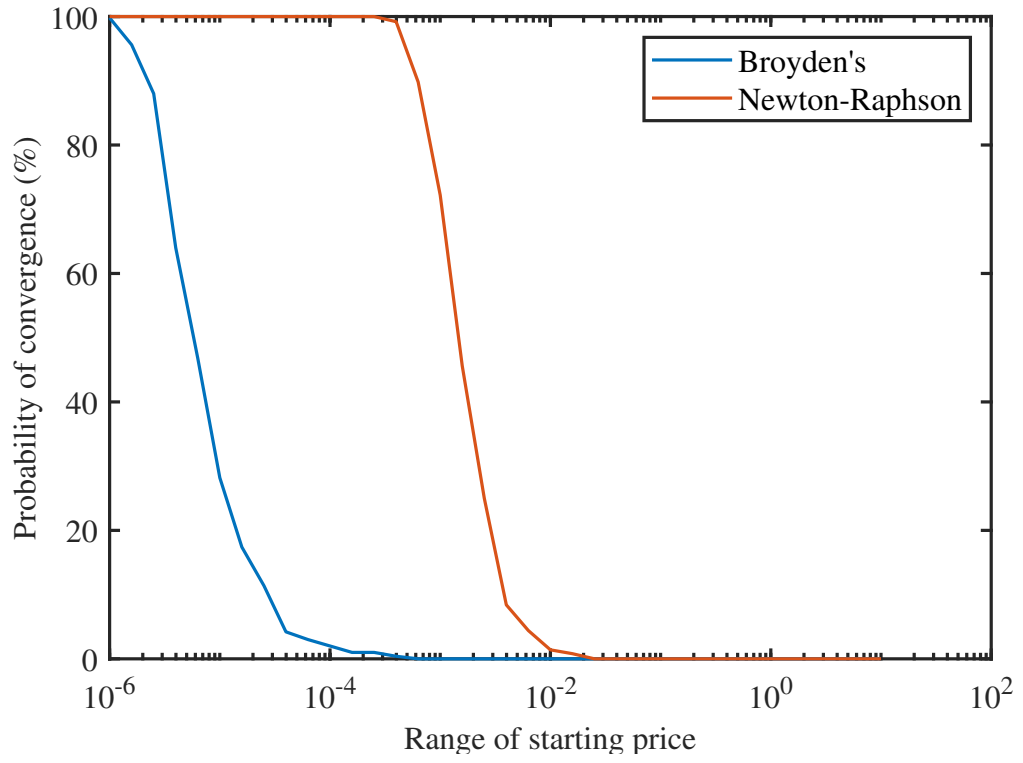


Figure 8: Price convergence probability for System 3 in Scenario 2 (Sufficiency).

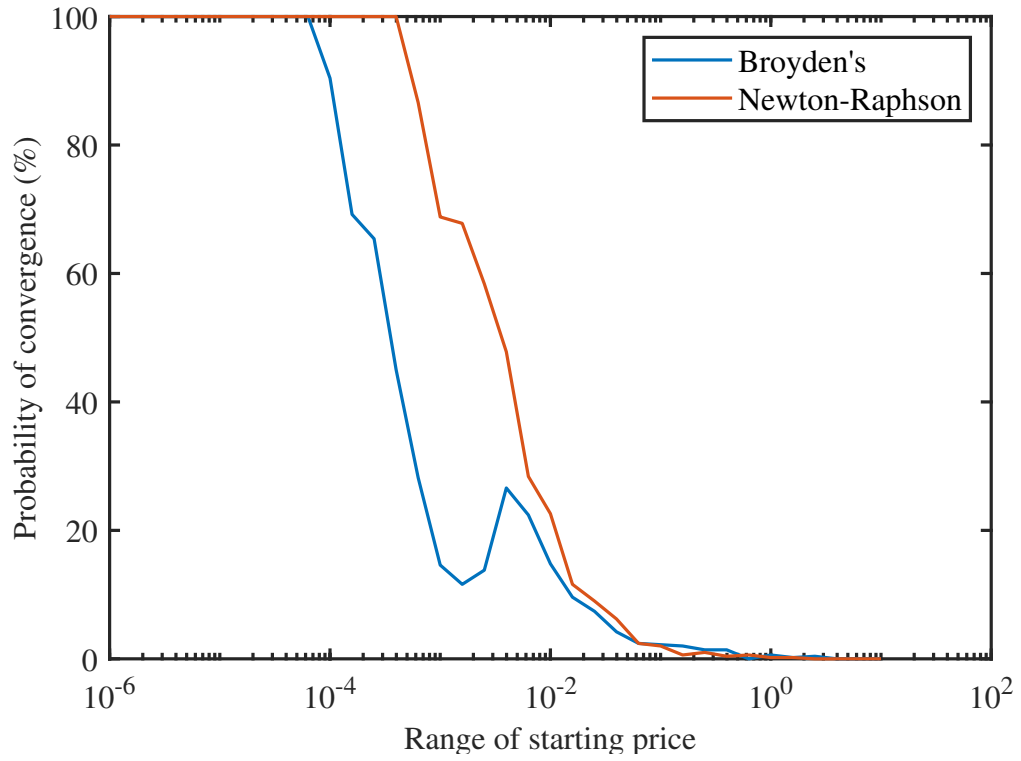


Figure 9: Price convergence probability for System 1 in Scenario 3 (Overabundance).

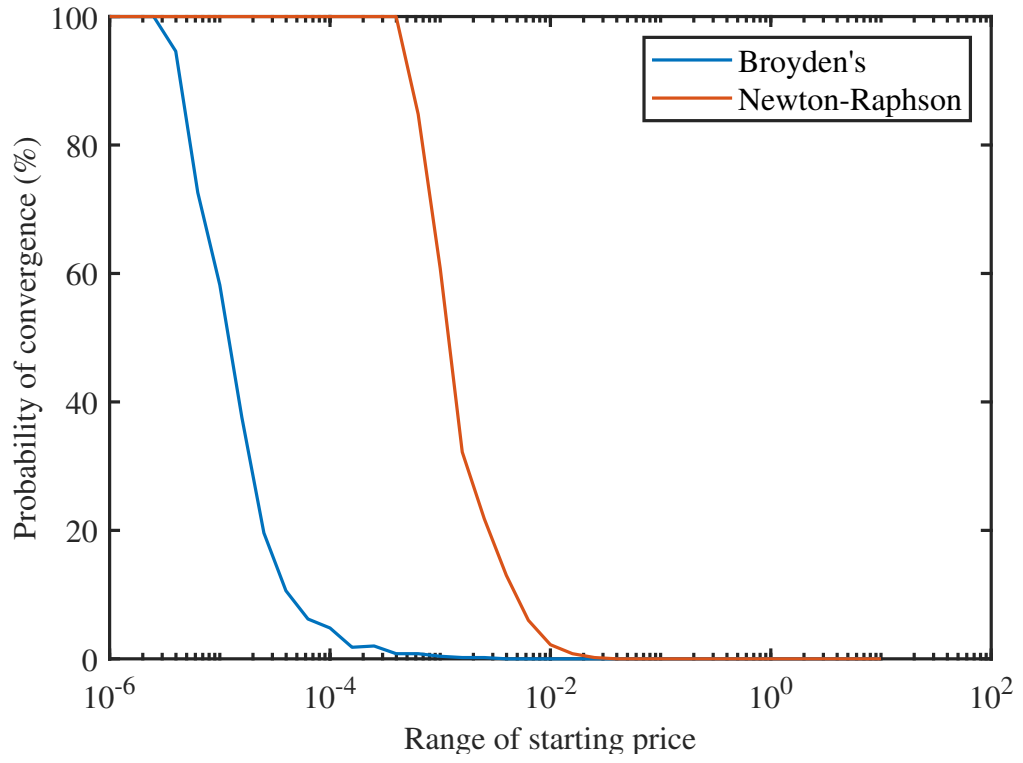


Figure 10: Price convergence probability for System 2 in Scenario 3 (Overabundance).



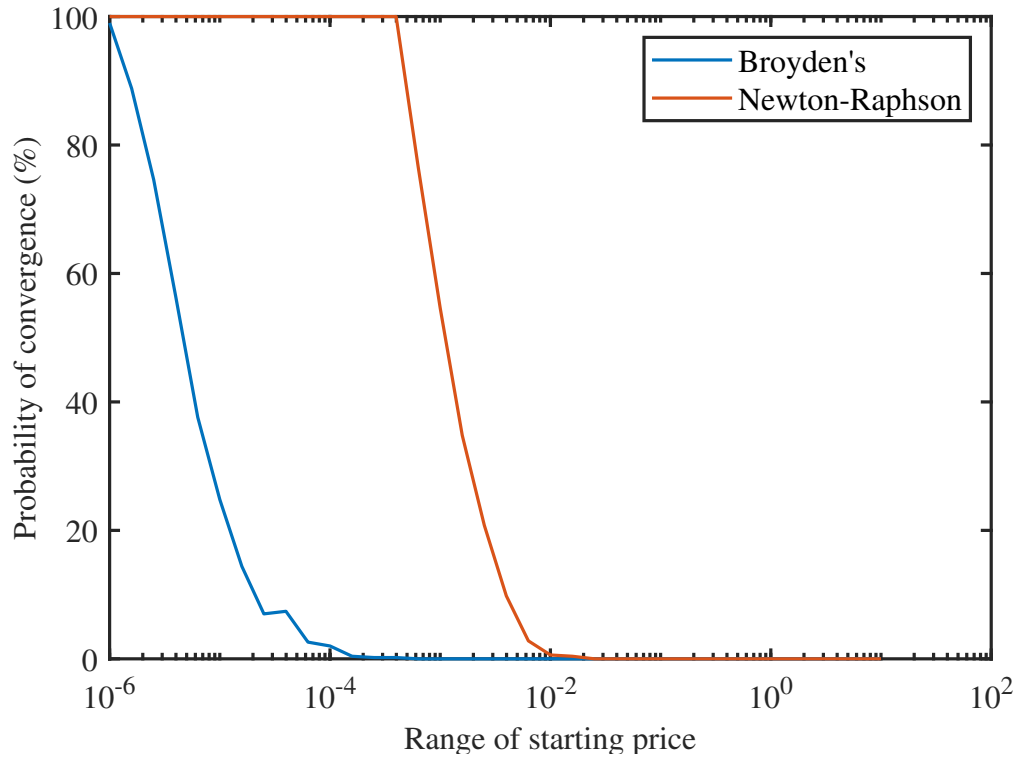


Figure 11: Price convergence probability for System 3 in Scenario 3 (Overabundance).

## Appendix C: Figures for Chapter 7

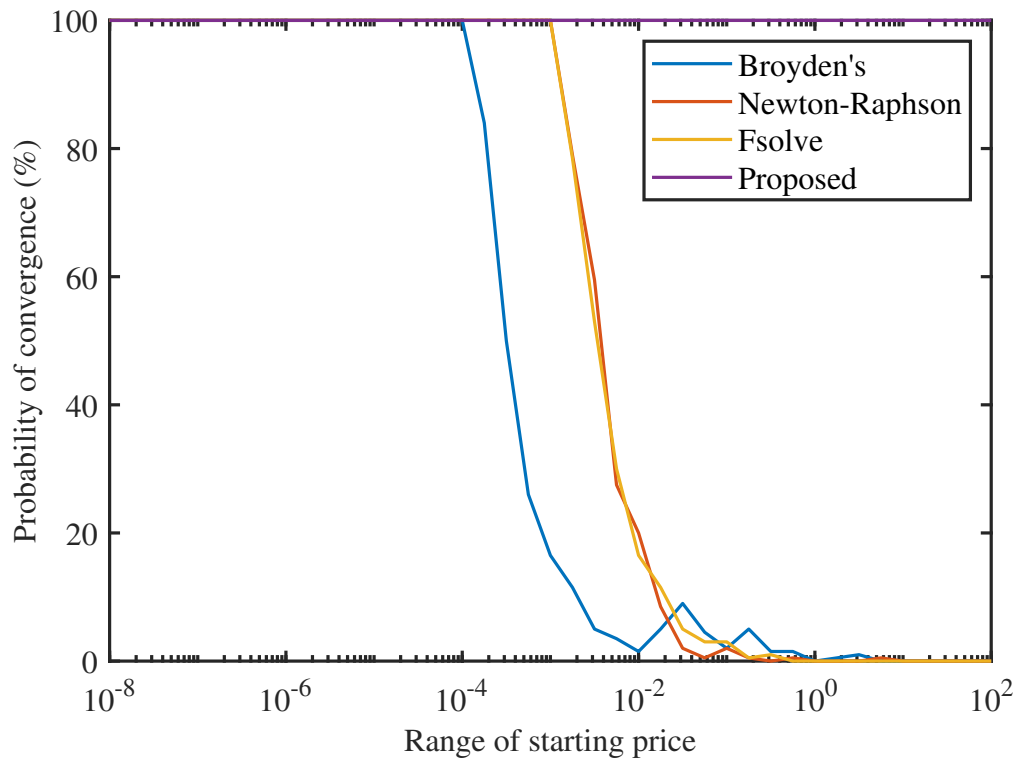


Figure 12: Price convergence probability for System 1 in Scenario 2 (Sufficiency).

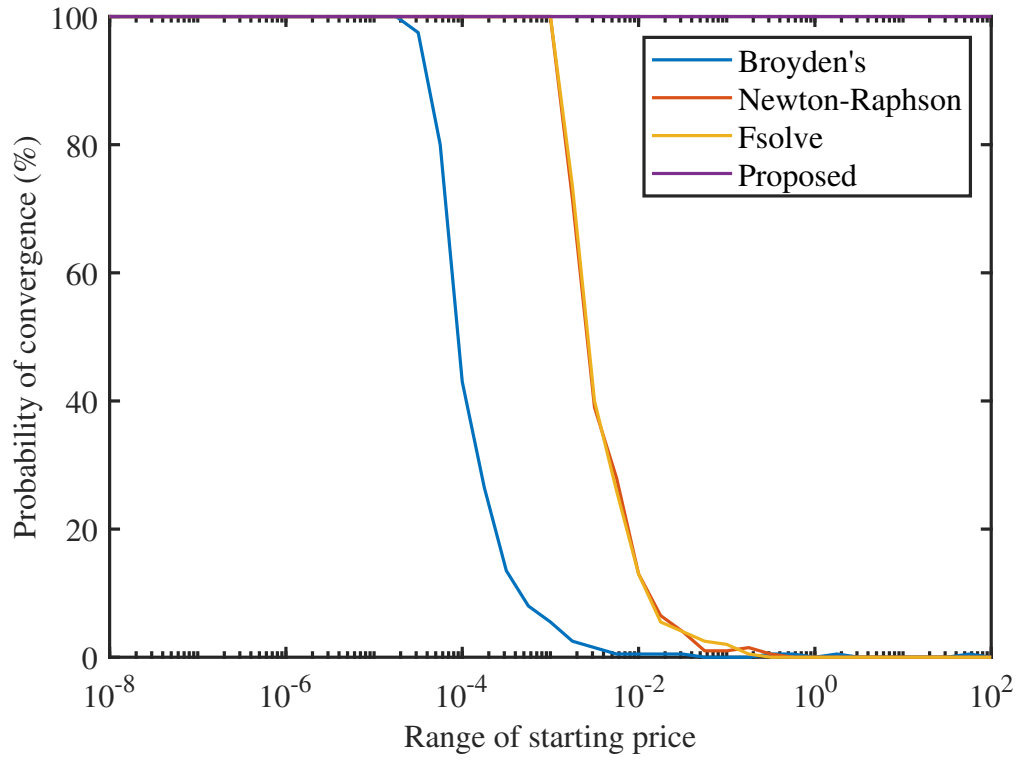


Figure 13: Price convergence probability for System 1 in Scenario 3 (Overabundance).

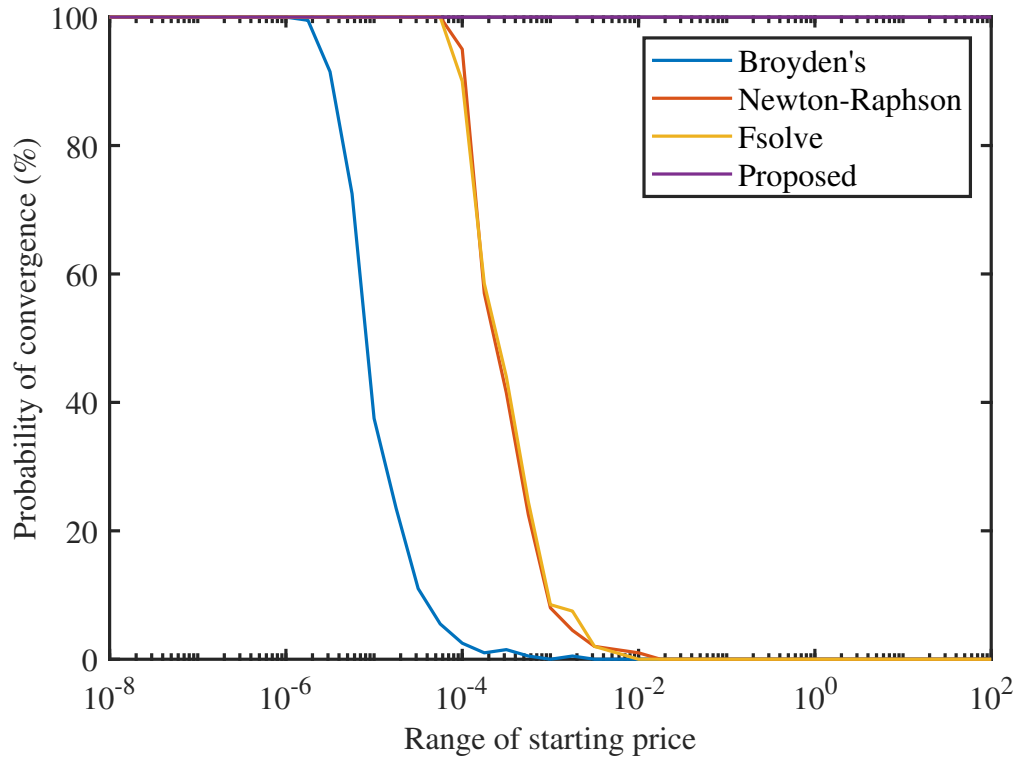


Figure 14: Price convergence probability for System 2 in Scenario 1 (Scarcity).

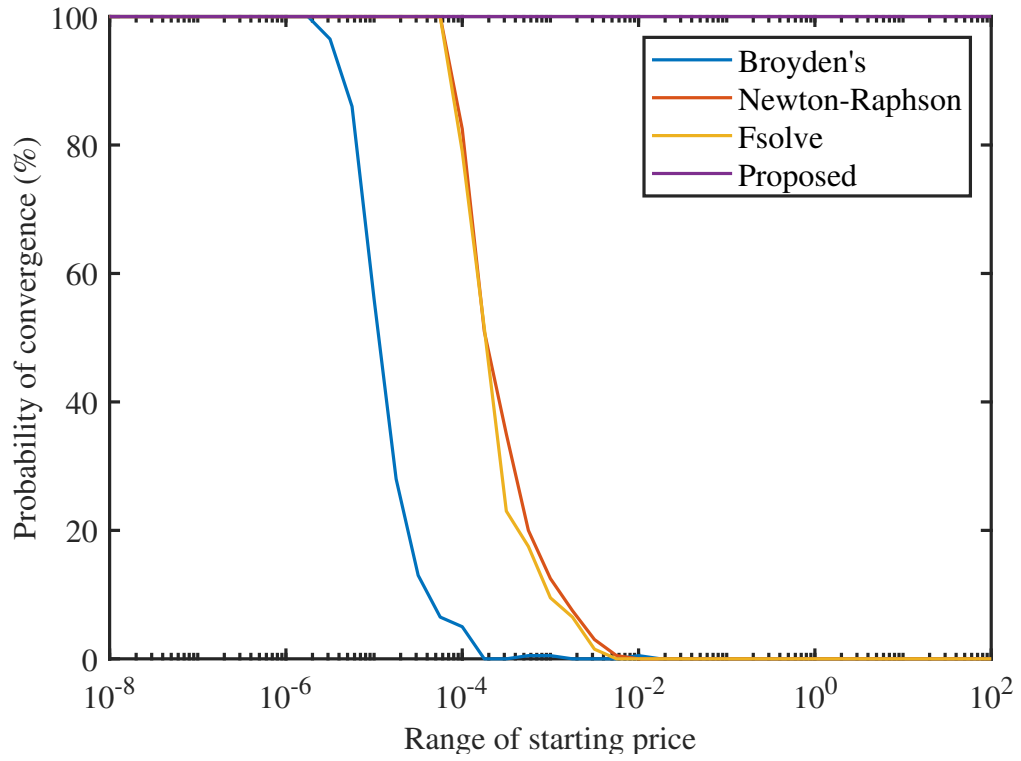


Figure 15: Price convergence probability for System 2 in Scenario 2 (Sufficiency).

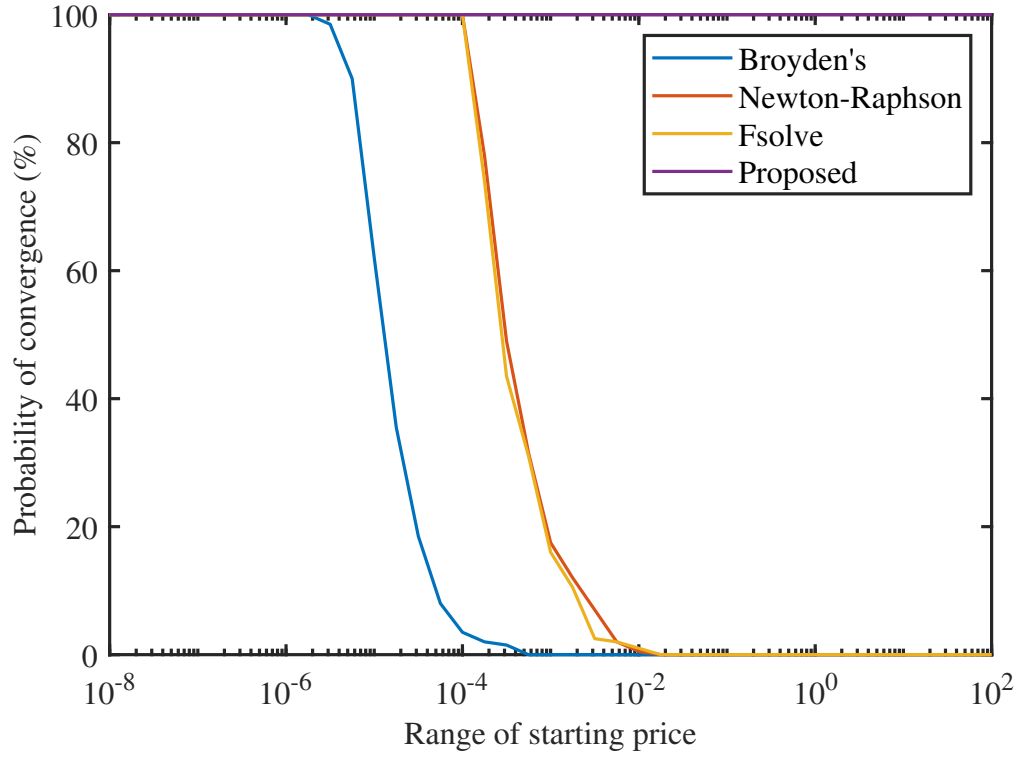


Figure 16: Price convergence probability for System 2 in Scenario 3 (Overabundance).

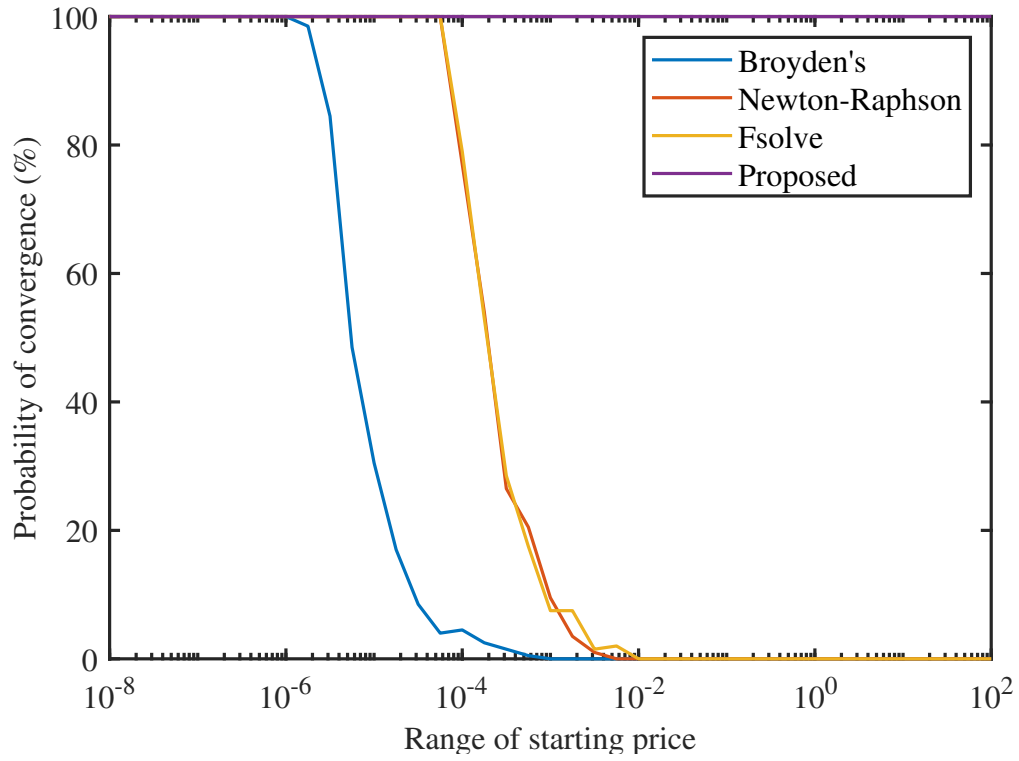


Figure 17: Price convergence probability for System 3 in Scenario 1 (Scarcity).

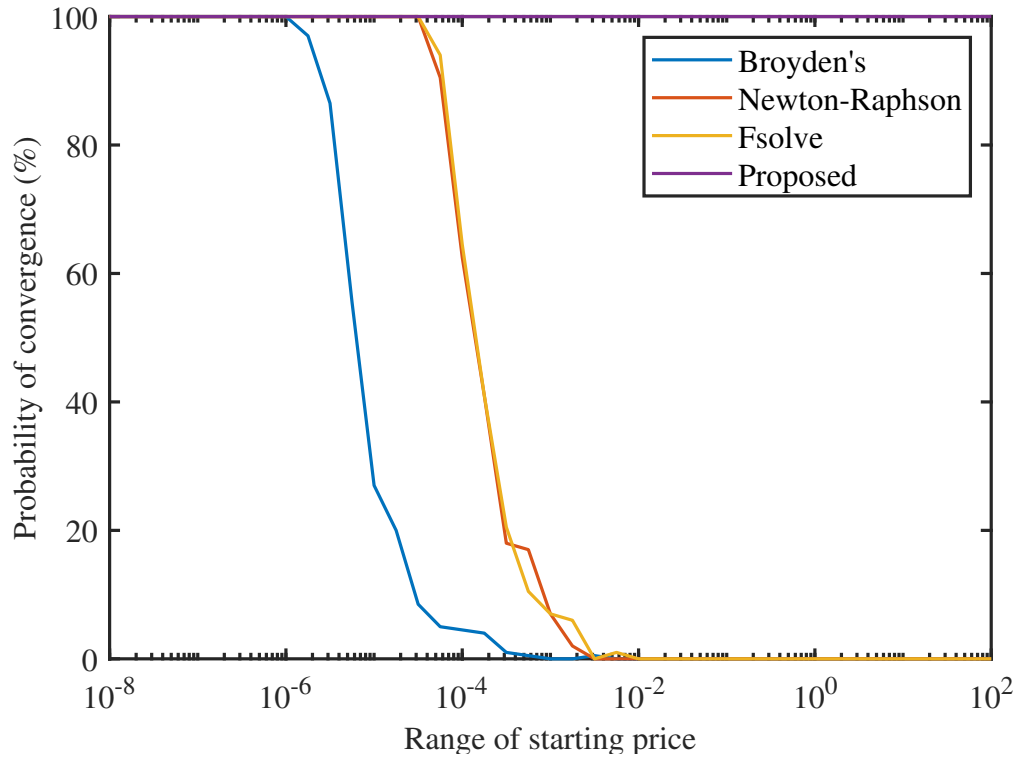


Figure 18: Price convergence probability for System 3 in Scenario 2 (Sufficiency).



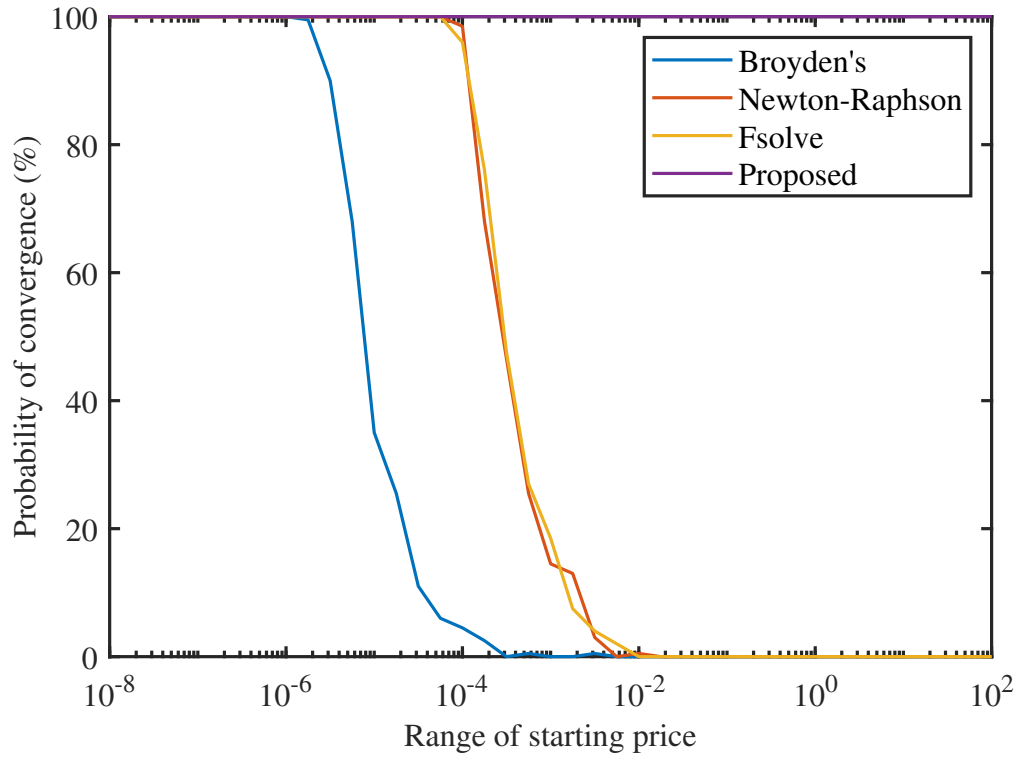


Figure 19: Price convergence probability for System 3 in Scenario 3 (Overabundance).

## Bibliography

- [1] A. M. Cramer, X. Liu, Y. Zhang, J. D. Stevens, and E. L. Zivi, “Early-stage shipboard power system simulation of operational vignettes for dependability assessment,” in *2015 IEEE Electric Ship Technologies Symposium (ESTS)*, pp. 382–387, 2015.
- [2] E. Oh, D. F. Opila, J. Stevens, E. Zivi, and A. Cramer, “Early stage design evaluation of shipboard power systems using multi-period power flow,” in *2017 IEEE Electric Ship Technologies Symposium (ESTS)*, pp. 225–231, 2017.
- [3] N. Zohrabi, J. Shi, and S. Abdelwahed, “An overview of design specifications and requirements for the MVDC shipboard power system,” *International Journal of Electrical Power & Energy Systems*, 2019.
- [4] A. W. Flath, A. M. Cramer, and J. E. Lumpp, “Mathematical programming based approach to modular electric power system design,” in *2019 IEEE Aerospace Conference*, pp. 1–8, 2019.
- [5] A. M. Madni, D. Erwin, and C. C. Madni, “Digital twin-enabled mbse testbed for prototyping and evaluating aerospace systems: Lessons learned,” in *2021 IEEE Aerospace Conference (50100)*, pp. 1–8, 2021.
- [6] A. Gong, J. L. Palmer, G. Brian, J. R. Harvey, and D. Verstraete, “Performance of a hybrid, fuel-cell-based power system during simulated small unmanned aircraft missions,” *International Journal of Hydrogen Energy*, vol. 41, pp. 11418–11426, 2016.
- [7] E. Frimann Løes Narum, R. Hann, and T. Arne Johansen, “Optimal mission planning for fixed-wing UAVs with electro-thermal icing protection and hybrid-electric power systems,” in *2020 International Conference on Unmanned Aircraft Systems (ICUAS)*, pp. 651–660, 2020.
- [8] S. Peyghami, H. Wang, P. Davari, and F. Blaabjerg, “Mission profile based power converter reliability analysis in a DC power electronic based power system,” in *2018 IEEE Energy Conversion Congress and Exposition (ECCE)*, pp. 4122–4128, 2018.
- [9] S. Peyghami, H. Wang, P. Davari, and F. Blaabjerg, “Mission-profile-based system-level reliability analysis in DC microgrids,” *IEEE Transactions on Industry Applications*, vol. 55, no. 5, pp. 5055–5067, 2019.
- [10] E. Zivi, “Integrated shipboard power and automation control challenge problem,” in *IEEE Power Engineering Society Summer Meeting*, vol. 1, pp. 325–330 vol.1, 2002.

- [11] E. L. Zivi, “Design of robust shipboard power automation systems,” *Annu. Rev. Control.*, vol. 29, pp. 261–272, 2005.
- [12] M. G. Richards, D. H. Rhodes, D. E. Hastings, and A. L. Weigel, “Defining survivability for engineering systems,” 2007.
- [13] A. M. Cramer, S. D. Sudhoff, and E. L. Zivi, “Performance metrics for electric warship integrated engineering plant battle damage response,” in *2007 IEEE Electric Ship Technologies Symposium*, pp. 22–29, 2007.
- [14] I. Gyparis, I. Hatzilau, J. Prousalidis, S. Perros, and A. Dalakos, “Perspectives of enhanced survivability on aes,” in *All Electric Ship (AES2003), International conference on*, pp. 13–14, 2003.
- [15] A. M. Cramer, S. D. Sudhoff, and E. L. Zivi, “Performance metrics for electric warship integrated engineering plant battle damage response,” *IEEE Transactions on Aerospace and Electronic Systems*, vol. 47, no. 1, pp. 634–646, 2011.
- [16] A. M. Cramer, J. D. Stevens, and I. Ojo, “Mission-based optimal control for the evaluation of power and energy system capability,” in *2019 IEEE Electric Ship Technologies Symposium (ESTS)*, pp. 311–316, 2019.
- [17] M. Sabah, I. T. Ojo, and A. M. Cramer, “Evolution of operability-based performance metrics for assessment of mission performance,” in *2021 IEEE Electric Ship Technologies Symposium (ESTS)*, pp. 1–6, 2021.
- [18] J. Cerminara and R. O. Kotacka, “Ship service electrical systems —designing for survivability,” *Naval Engineers Journal*, vol. 102, no. 5, pp. 32–36, 1990.
- [19] J. Famme and B. TAYLOR, “Integration of ship control systems for total ship survivability,” *Naval Engineers Journal*, vol. 104, pp. 210 – 218, 03 2009.
- [20] R. E. Ball and C. N. Calvano, “Establishing the fundamentals of a surface ship survivability design discipline,” *Naval Engineers Journal*, vol. 106, pp. 71–74, 1994.
- [21] J. Cerminara and R. O. Kotacka, “Ship service electrical systems —designing for survivability,” *Naval Engineers Journal*, vol. 102, no. 5, pp. 32–36, 1990.
- [22] N. Doerry and D. Clayton, “Shipboard electrical power quality of service,” in *IEEE Electric Ship Technologies Symposium, 2005.*, pp. 274–279, 2005.
- [23] A. Dubey and S. Santoso, “A two-level topology design framework for reliable shipboard power systems,” *Inventions*, vol. 1, 07 2016.
- [24] N. Doerry, “Zonal ship design,” *Naval Engineers Journal - NAV ENG J*, vol. 118, pp. 39–53, 12 2006.
- [25] N. Doerry, “Designing electrical power systems for survivability and quality of service,” *Naval Engineers Journal*, vol. 119, pp. 25 – 34, 11 2007.

- [26] A. M. Cramer, S. D. Sudhoff, and E. L. Zivi, "Metric optimization-based design of systems subject to hostile disruptions," *IEEE Transactions on Systems, Man, and Cybernetics - Part A: Systems and Humans*, vol. 41, no. 5, pp. 989–1000, 2011.
- [27] J. D. Stevens, D. F. Opila, A. M. Cramer, and E. L. Zivi, "Operational vignette-based electric warship load demand," in *2015 IEEE Electric Ship Technologies Symposium (ESTS)*, pp. 213–218, 2015.
- [28] A. W. Flath, A. M. Cramer, and X. Liu, "Control system modeling in early-stage simulation for cyber vulnerability assessment," in *2017 IEEE Electric Ship Technologies Symposium (ESTS)*, pp. 9–15, 2017.
- [29] J. Langston, M. Stanovich, K. Schoder, and M. Steurer, "Distributed energy storage allocation algorithm for early stage design," in *2017 IEEE Electric Ship Technologies Symposium (ESTS)*, pp. 345–351, 2017.
- [30] D. Opila, J. Stevens, and A. Cramer, "The role of future information in control system design for shipboard power systems," in *Proc. Int. Ship Control Syst. Symp. (iSCSS)*, 2018.
- [31] N. R. Council, *Evaluation of the National Aerospace Initiative*. Washington, DC: The National Academies Press, 2004.
- [32] C. Georgakis, D. Uztürk, S. Subramanian, and D. Vinson, "On the operability of continuous processes," *Control Engineering Practice*, vol. 11, pp. 859–869, 08 2003.
- [33] D. Uztürk and C. Georgakis, "Inherent dynamic operability of processes: General definitions and analysis of siso cases," *Industrial and Engineering Chemistry Research - IND ENG CHEM RES*, vol. 41, 10 2001.
- [34] Y. Lee, E. Zivi, J. Langston, M. Steurer, R. Dougal, Y. Zhang, J. Crider, S. Sudhoff, R. Hebner, and A. Ouroua, "Waveform-level time-domain simulation comparison study of three shipboard power system architectures," *CEM Publications*, 2012.
- [35] R. R. Chan, S. D. Sudhoff, and E. L. Zivi, "An approach to optimally allocate energy storage in naval electric ships," in *2011 IEEE Electric Ship Technologies Symposium*, pp. 402–405, 2011.
- [36] J. Neely, L. Rashkin, M. Cook, D. Wilson, and S. Glover, "Evaluation of power flow control for an all-electric warship power system with pulsed load applications," in *2016 IEEE Applied Power Electronics Conference and Exposition (APEC)*, pp. 3537–3544, 2016.
- [37] R. R. Chan, S. D. Sudhoff, Y. Lee, and E. L. Zivi, "A linear programming approach to shipboard electrical system modeling," in *2009 IEEE Electric Ship Technologies Symposium*, pp. 261–269, 2009.

- [38] J. D. Stevens, D. F. Opila, E. S. Oh, and E. L. Zivi, “All-electric warship load demand model for power and energy system analysis using exogenously initiated threats,” in *2017 IEEE Electric Ship Technologies Symposium (ESTS)*, pp. 486–492, 2017.
- [39] A. M. Cramer, F. Pan, H. Chen, and E. L. Zivi, “Modeling and simulation for early-stage quantitative assessment of medium-voltage dc power system protection schemes,” in *2014 Electric Machines Technologists Symposium*, 2014.
- [40] A. M. Cramer, E. Zivi, and J. Stevens, “Light-weight, early-stage power system model for time-domain simulation,” in *2016 Advanced Machinery Technology Symposium*, 2016.
- [41] T. V. Vu, D. Perkins, D. Gonsoulin, C. S. Edrington, B. Papari, K. Schoder, M. Stanovich, and M. Steurer, “Large-scale distributed control for MVDC ship power systems,” in *IECON 2018 - 44th Annual Conference of the IEEE Industrial Electronics Society*, pp. 3431–3436, 2018.
- [42] R. Serfozo, *Markov Chains*, pp. 1–98. Berlin, Heidelberg: Springer Berlin Heidelberg, 2009.
- [43] A. H. Sayed, *Markov Decision Processes*, p. 1807–1852. Cambridge University Press, 2022.
- [44] S. Keneally, M. Robbins, and B. Lunday, “A Markov decision process model for the optimal dispatch of military medical evacuation assets,” *Health Care Management Science*, vol. 19, pp. 111–129, 06 2016.
- [45] Y. Hao, M. Wang, and J. H. Chow, “Likelihood analysis of cyber data attacks to power systems with Markov decision processes,” *IEEE Transactions on Smart Grid*, vol. 9, no. 4, pp. 3191–3202, 2018.
- [46] M. Abdelmalak and M. Benidris, “A Markov decision process to enhance power system operation resilience during hurricanes,” in *2021 IEEE Power and Energy Society General Meeting (PESGM)*, pp. 01–05, 2021.
- [47] C. Wang, P. Ju, S. Lei, Z. Wang, F. Wu, and Y. Hou, “Markov decision process-based resilience enhancement for distribution systems: An approximate dynamic programming approach,” *IEEE Transactions on Smart Grid*, vol. 11, no. 3, pp. 2498–2510, 2020.
- [48] W. Wu, D. Wang, A. Arapostathis, and K. Davey, “Optimal power generation scheduling of a shipboard power system,” in *2007 IEEE Electric Ship Technologies Symposium*, pp. 519–522, 2007.
- [49] C. Wang, S. Lei, P. Ju, C. Chen, C. Peng, and Y. Hou, “MDP-based distribution network reconfiguration with renewable distributed generation: Approximate dynamic programming approach,” *IEEE Transactions on Smart Grid*, vol. 11, no. 4, pp. 3620–3631, 2020.

- [50] G. Li, Z. Yang, B. Li, and H. Bi, “Power allocation smoothing strategy for hybrid energy storage system based on Markov decision process,” *Applied Energy*, vol. 241, pp. 152–163, May 2019.
- [51] F. Bowman, “An integrated electric power system: The next step.” [http://www.public.navy.mil/subfor/underseawarfaremagazine/Issues/Archives/issue\\_09/power\\_system.html/](http://www.public.navy.mil/subfor/underseawarfaremagazine/Issues/Archives/issue_09/power_system.html/), 2000. *Undersea Warfare*, vol. 3, no. 1, Fall 2000.
- [52] N. Doerry, J. Amy, and C. Krolick, “History and the status of electric ship propulsion, integrated power systems, and future trends in the u.s. navy,” *Proceedings of the IEEE*, vol. 103, no. 12, pp. 2243–2251, 2015.
- [53] A. L. Gattozzi, J. D. Herbst, R. E. Hebner, J. A. Blau, K. R. Cohn, W. B. Colson, J. E. Sylvester, and M. A. Woehrman, “Power system and energy storage models for laser integration on naval platforms,” in *2015 IEEE Electric Ship Technologies Symposium (ESTS)*, pp. 173–180, 2015.
- [54] C. Dufour, Z. Soghomonian, and W. Li, “Hardware-in-the-loop testing of modern on-board power systems using digital twins,” in *2018 International Symposium on Power Electronics, Electrical Drives, Automation and Motion (SPEEDAM)*, pp. 118–123, 2018.
- [55] J. Langston, H. Ravindra, M. Steurer, T. Fikse, C. Schegan, and J. Borraccini, “Priority-based management of energy resources during power-constrained operation of shipboard power system,” in *2021 IEEE Electric Ship Technologies Symposium (ESTS)*, pp. 1–9, 2021.
- [56] M. Musallam, C. Yin, C. Bailey, and M. Johnson, “Mission profile-based reliability design and real-time life consumption estimation in power electronics,” *IEEE Transactions on Power Electronics*, vol. 30, no. 5, pp. 2601–2613, 2015.
- [57] D. Zhou, H. Wang, and F. Blaabjerg, “Mission profile based system-level reliability analysis of DC/DC converters for a backup power application,” *IEEE Transactions on Power Electronics*, vol. 33, no. 9, pp. 8030–8039, 2018.
- [58] Y. Zhang, H. Wang, Z. Wang, F. Blaabjerg, and M. Saeedifard, “Mission profile-based system-level reliability prediction method for modular multilevel converters,” *IEEE Transactions on Power Electronics*, vol. 35, no. 7, pp. 6916–6930, 2020.
- [59] M. Vasic, S. D. Round, J. Biela, and J. W. Kolar, “Mission profile based optimization of a synchronous-buck DC-DC converter for a wearable power system,” in *2009 IEEE 6th International Power Electronics and Motion Control Conference*, pp. 1384–1389, 2009.

- [60] Y. Yang, H. Wang, F. Blaabjerg, and K. Ma, "Mission profile based multi-disciplinary analysis of power modules in single-phase transformerless photovoltaic inverters," in *2013 15th European Conference on Power Electronics and Applications (EPE)*, pp. 1–10, 2013.
- [61] W. Zhu, J. Shi, P. Zhi, Y. Yang, X. Wei, and G. J. Lim, "Mission based re-configuration for hybrid shipboard power systems considering threats," in *2020 IEEE 18th International Conference on Industrial Informatics (INDIN)*, vol. 1, pp. 833–838, 2020.
- [62] S. Fish and T. Savoie, "Simulation-based optimal sizing of hybrid electric vehicle components for specific combat missions," *IEEE Transactions on Magnetics*, vol. 37, no. 1, pp. 485–488, 2001.
- [63] A. S. Prasetia, R.-J. Wai, Y.-L. Wen, and Y.-K. Wang, "Mission-based energy consumption prediction of multirotor UAV," *IEEE Access*, vol. 7, pp. 33055–33063, 2019.
- [64] S. Misra, A. Mondal, S. Banik, M. Khatua, S. Bera, and M. S. Obaidat, "Residential energy management in smart grid: A Markov decision process-based approach," in *2013 IEEE International Conference on Green Computing and Communications and IEEE Internet of Things and IEEE Cyber, Physical and Social Computing*, pp. 1152–1157, 2013.
- [65] G. D'Angelo, M. Tipaldi, L. Glielmo, and S. Rampone, "Spacecraft autonomy modeled via Markov decision process and associative rule-based machine learning," in *2017 IEEE International Workshop on Metrology for AeroSpace (MetroAeroSpace)*, pp. 324–329, 2017.
- [66] X. Yu, X. Zhou, and Y. Zhang, "Collision-free trajectory generation and tracking for UAVs using Markov decision process in a cluttered environment," *Journal of Intelligent and Robotic Systems*, vol. 93, 02 2019.
- [67] Y. Zhang, K. Yao, J. Zhang, F. Jiang, and M. Warren, "A new Markov decision process based behavioral prediction system for airborne crews," *IEEE Access*, vol. 8, pp. 28021–28032, 2020.
- [68] S. Ragi and E. Chong, "UAV path planning in a dynamic environment via partially observable Markov decision process," *Aerospace and Electronic Systems, IEEE Transactions on*, vol. 49, pp. 2397–2412, 10 2013.
- [69] X. C. Ding, A. Pinto, and A. Surana, "Strategic planning under uncertainties via constrained Markov decision processes," in *2013 IEEE International Conference on Robotics and Automation*, pp. 4568–4575, 2013.
- [70] S. Dimopoulou, A. Oppermann, E. Boggasch, and A. Rausch, "A Markov Decision Process for managing a Hybrid Energy Storage System," *Journal of Energy Storage*, vol. 19, pp. 160–169, Oct. 2018.

- [71] M. A. López, J. A. Aguado, S. de la Torre, and M. Figuerola, “Optimization-based market-clearing procedure with evs aggregator participation,” in *IEEE PES ISGT Europe 2013*, pp. 1–5, 2013.
- [72] Y. Zhang and G. B. Giannakis, “Distributed stochastic market clearing with high-penetration wind power,” *IEEE Transactions on Power Systems*, vol. 31, no. 2, pp. 895–906, 2016.
- [73] S. Peyghami, P. Pakensky, and F. Blaabjerg, “An overview on the reliability of modern power electronic based power systems,” *IEEE Open Journal of Power Electronics*, vol. PP, pp. 1–1, 02 2020.
- [74] F. D. Kanellos, A. Anvari-Moghaddam, and J. M. Guerrero, “A cost-effective and emission-aware power management system for ships with integrated full electric propulsion,” *Electric Power Systems Research*, vol. 150, no. C, pp. 63–75, 2017.
- [75] X. Wang, F. Blaabjerg, and W. Wu, “Modeling and analysis of harmonic stability in an ac power-electronics-based power system,” *IEEE Transactions on Power Electronics*, vol. 29, no. 12, pp. 6421–6432, 2014.
- [76] Y. Zhang and A. M. Cramer, “Market-based control of electric ship power systems,” in *2017 IEEE Electric Ship Technologies Symposium (ESTS)*, pp. 372–379, 2017.
- [77] E. F. Bompard and B. Han, “Market-based control in emerging distribution system operation,” *IEEE Transactions on Power Delivery*, vol. 28, no. 4, pp. 2373–2382, 2013.
- [78] K. Kok, G. Venekamp, and P. Macdougall, “Market-based control in decentralized electrical power systems,” in *First international workshop on agent technologies for energy systems, ATES2010, Toronto*, 2010.
- [79] M. Ashkaboosi, S. Nourani, P. Khazaei, M. Dabbaghjamanesh, and A. Moeini, “An optimization technique based on profit of investment and market clearing in wind power systems,” *American Journal of Electrical and Electronic Engineering*, vol. 4, pp. 85–91, 01 2016.
- [80] H. Chen, L. Fu, L. Bai, T. Jiang, Y. Xue, R. Zhang, B. Chowdhury, J. Stekli, and X. Li, “Distribution Market-Clearing and Pricing Considering Coordination of DSOs and ISO: An EPEC Approach,” *IEEE Transactions on Smart Grid*, vol. 12, no. 4, pp. 3150–3162, 2021.
- [81] J. Wang, Z. Wei, B. Yang, Y. Yong, M. Xue, G. Sun, H. Zang, and S. Chen, “Two-stage integrated electricity and heat market clearing with energy stations,” *IEEE Access*, vol. 7, pp. 44928–44938, 2019.
- [82] F. Bouffard, F. Galiana, and A. Conejo, “Market-clearing with stochastic security-part I: formulation,” *IEEE Transactions on Power Systems*, vol. 20, no. 4, pp. 1818–1826, 2005.



- [83] N. Amjady, J. Aghaei, and H. A. Shayanfar, “Stochastic multiobjective market clearing of joint energy and reserves auctions ensuring power system security,” *IEEE Transactions on Power Systems*, vol. 24, no. 4, pp. 1841–1854, 2009.
- [84] A. Rabiee, H. Shayanfar, and N. Amjady, “Coupled energy and reactive power market clearing considering power system security,” *Energy Conversion and Management - ENERG CONV MANAGE*, vol. 50, pp. 907–915, 04 2009.
- [85] J. Aghaei, H. Shayanfar, and N. Amjady, “Joint market clearing in a stochastic framework considering power system security,” *Applied Energy*, vol. 86, no. 9, pp. 1675–1682, 2009.
- [86] S. S. Reddy, A. R. Abhyankar, and P. R. Bijwe, “Market clearing for a wind-thermal power system incorporating wind generation and load forecast uncertainties,” in *2012 IEEE Power and Energy Society General Meeting*, pp. 1–8, 2012.
- [87] F. Gao, X. Guan, X.-R. Cao, and A. Papalexopoulos, “Forecasting power market clearing price and quantity using a neural network method,” in *2000 Power Engineering Society Summer Meeting (Cat. No.00CH37134)*, vol. 4, pp. 2183–2188 vol. 4, 2000.
- [88] S. Salkuti, P. Bijwe, and A. Abhyankar, “Multi-objective market clearing of electrical energy, spinning reserves and emission for wind-thermal power system,” *International Journal of Electrical Power and Energy Systems*, vol. 53, pp. 782–794, 12 2013.
- [89] A. Ramli, L. Abdullah, and M. Mamat, “Broyden’s method for solving fuzzy nonlinear equations,” *Adv. Fuzzy Systems*, vol. 2010, 01 2010.
- [90] M. Al-Baali, E. Spedicato, and F. Maggioni, “Broyden’s quasi-newton methods for a nonlinear system of equations and unconstrained optimization: a review and open problems,” *Optimization Methods and Software*, vol. 29, no. 5, pp. 937–954, 2014.
- [91] M. Sabah, A. M. Cramer, and I. T. Ojo, “Numerical challenges for market clearing in power electronics-based power distribution systems,” in *2023 IEEE Electric Ship Technologies Symposium (ESTS)*, pp. 458–463, 2023.
- [92] R. Yao, Y. Liu, K. Sun, F. Qiu, and J. Wang, “Efficient and robust dynamic simulation of power systems with holomorphic embedding,” *IEEE Transactions on Power Systems*, vol. 35, no. 2, pp. 938–949, 2020.
- [93] P. Aristidou, D. Fabozzi, and T. Van Cutsem, “Dynamic simulation of large-scale power systems using a parallel schur-complement-based decomposition method,” *IEEE Transactions on Parallel and Distributed Systems*, vol. 25, no. 10, pp. 2561–2570, 2014.

- [94] F. Alobaid, N. Mertens, R. Starkloff, T. Lanz, C. Heinze, and B. Epple, “Progress in dynamic simulation of thermal power plants,” *Progress in Energy and Combustion Science*, vol. 59, pp. 79–162, 2017.
- [95] H. Jain, A. Parchure, R. P. Broadwater, M. Dilek, and J. Woyak, “Three-phase dynamic simulation of power systems using combined transmission and distribution system models,” *IEEE Transactions on Power Systems*, vol. 31, no. 6, pp. 4517–4524, 2016.
- [96] A. Ramli, L. Abdullah, and M. Mamat, “Broyden’s method for solving fuzzy nonlinear equations,” *Adv. Fuzzy Systems*, vol. 2010, 01 2010.
- [97] M. Al-Baali, E. Spedicato, and F. Maggioni, “Broyden’s quasi-newton methods for a nonlinear system of equations and unconstrained optimization: a review and open problems,” *Optimization Methods and Software*, vol. 29, no. 5, pp. 937–954, 2014.

## Vita

### Personal Information

Name: Musharrat Sabah

Country of Origin: Bangladesh

### Educational Background

Bachelor of Science in Electrical and Electronic Engineering,  
Bangladesh University of Engineering and Technology (BUET), 2017

### Publications

1. M. Sabah, I. T. Ojo and A. M. Cramer, "Evolution of Operability-Based Performance Metrics for Assessment of Mission Performance," 2021 IEEE Electric Ship Technologies Symposium (ESTS), Arlington, VA, USA, 2021, pp. 1-6.
2. M. Sabah and A. M. Cramer, "Optimal-Control-Based Evaluation of Shipboard Power Systems with Energy Magazines," 2023 IEEE Electric Ship Technologies Symposium (ESTS), Alexandria, VA, USA, 2023, pp. 72-77.
3. M. Sabah, A. M. Cramer and I. T. Ojo, "Numerical Challenges for Market Clearing in Power Electronics-Based Power Distribution Systems," 2023 IEEE Electric Ship Technologies Symposium (ESTS), Alexandria, VA, USA, 2023, pp. 458-463.
4. M. Sabah and A. M. Cramer, "Optimal-Control-Based Evaluation of Mission-Oriented Power Systems," in IEEE Transactions on Aerospace and Electronic Systems, vol. 60, no. 2, pp. 2350-2363, April 2024.
5. M. Sabah and A. M. Cramer, Yuan Liao, "Numerical Algorithm for Solving Market-Clearing Problem in Power Electronics-Based Power Distribution Systems," submitted in IEEE Transactions on Power Systems, May 2024.